PALEOENVIRONMENTAL CHANGES ASSOCIATED WITH THE PALEOCENE-EOCENE THERMAL MAXIMUM, MILLVILLE (ODP LEG 174AX), NEW JERSEY COASTAL PLAIN

by

MARIA MAKAROVA

A thesis submitted to the

Graduate School-New Brunswick

Rutgers, The State University of New Jersey

in partial fulfillment of the requirements

for the degree of

Master of Science

Graduate Program in Geological Sciences

written under the direction of

Professor Kenneth G. Miller

and approved by

_____

_____

_____

New Brunswick, New Jersey

January, 2014

ABSTRACT OF THE THESIS

Paleoenvironmental changes associated with the Paleocene-Eocene thermal maximum, Millville (ODP Leg 174AX), New Jersey coastal plain

By MARIA MAKAROVA

Thesis Director:
Professor Kenneth G. Miller

The Paleocene-Eocene Thermal Maximum (PETM) was an abrupt warming of about 5°C that lasted ~170-220 kyr. The PETM is recognized by the Carbon Isotope Excursion (CIE), represented by a ~2.5-4‰ decrease in planktonic foraminiferal $\delta^{13}C$ values in open ocean cores (Kennett and Stott, 1991; Zachos et al., 2003). The New Jersey coastal plain contains thick (~15 m) sections recording the PETM. Kopp et al. (2009) proposed an enhanced hydrologic cycle to explain the widespread clay deposition on the mid-Atlantic continental shelf during the PETM, suggesting an Appalachian Amazon analog. An increased flux of fresh water to the shelf would have lowered salinities substantially. I tested this hypothesis by measuring changes in salinity in the PETM section in the Millville, New Jersey core (ODP Leg 174AX). I used two paleothermometers to constrain temperature changes associated with planktonic foraminiferal $\delta^{18}O$ variations, with the residual attributed to salinity-induced $\delta^{18}O_{water}$ changes. Using the TEX^{H}_{86} calibration of Kim et al. (2010), I compute a 5.5°C warming across the CIE at Millville from 30 to 35.5°C; using the TEX^{L}_{86} calibration, I compute a 7°C warming, but cooler temperatures (23-30°C).

Mg/Ca ratio of planktonic foraminifera shows less warming of ~5°C from 29.5 to 34.3°C. TEX_{86} shows a possible precursor warming at Wilson Lake and Bass River, NJ (Zachos et al., 2006; Sluijs et al., 2007). I compare TEX_{86} at Wilson Lake Hole A, Bass River, and Millville and conclude that the precursor warming may be spurious because it only occurs in TEX^{H}_{86} and not TEX^{L}_{86}. Intermediate dwelling (*Subbotina*) planktonic foraminifera show a large decrease in $\delta^{18}O$ values (~2.26‰) across the CIE. Use of the TEX^{H}_{86} calibration and Mg/Ca ratio calibration (Anand et al., 2003) requires unrealistic salinities exceeding 44 psu. The TEX^{L}_{86} calibration requires realistic salinity estimates and a ~4 psu salinity decrease associated with the CIE. This suggests a freshening of surface and intermediate waters during the CIE due to an enhanced hydrological cycle as proposed by Kopp et al. (2009). I attribute changes in surface to deep dwelling planktonic $\delta^{18}O$ values to a breakdown of the thermocline caused by increased storm intensity during the PETM.

ACKNOWLEDGEMENTS

First and foremost, I would like to thank Dr. Kenneth G. Miller for being such a one of a kind, energetic, supportive, and caring advisor. His constructive criticism and guiding has shaped up not only my research work but also my character.

I would like to thank my committee members, Dr. James D. Wright and Dr. Yair Rosenthal, for providing valuable comments and asking insightful questions. I would not have completed this piece of work without their expertise of stable isotope and trace metal analyses.

Also, my thank you goes to Tali Babila, a PhD student from Institute of marine and coastal sciences (IMSC), Rutgers, for her enthusiasm and encouragement, as well as tremendous help with trace metal analysis.

Thank you Dr. James V. Browning for providing corrections on my written works and for your honest opinions. Thanks to Dr. Richard K. Olsson for advice on foraminiferal taxonomy. My big gratitude is to Richard A. Mortlock and Nicole Abdul for help with stable isotope analyses; Chris Lombardi for his help at the core repository; Dr. Marie-Pierre Aubry and Selen Esmeray-Senlet for providing useful advices.

My acknowledgements go to Rutgers Graduate School New Brunswick for the research grant that made my trip to Brown University possible. I am grateful for the opportunity to work with Dr. Timothy D. Herbert from Geology department at Brown University and his talented research team, particularly Shuo Yang, Alexandrina Tzanova, and Rafael Tarozo. An important part of my research

including TEX_{86} and BIT analyses was done there and would not have been possible without their assistance.

I would also like to thank Dr. Elisabeth L. Sikes from IMCS, Rutgers, and her research team for their help with the alkenone analysis, as well as Charlotte Fuller for her assistance in sample preparation.

A special thanks goes to ExxonMobil Corporation for the unique opportunity to study at Rutgers University. I would like to specifically thank Bob Stewart and Brenda Roper for selecting me for the ExxonMobil Russian Scholar Program. I would like to thank Institute of international education (IIE) especially my advisor Enam Haddad for preparing all official documents that eased my moving and stay here.

Also, I would like to thank Geology department at Moscow State University for providing me with extensive geological education and scientific knowledge. I would like to thank all my professors that I had pleasure to learn from, and particularly Dr. Michael K. Ivanov for bringing me to Marine geology group, and believing in me as a specialist. I wish I had a chance to thank him in person.

Also, thanks go to Dr. Alina Stadnitskaia and biogeochemistry department at Royal Netherlands Institute for Sea Research (Royal NIOZ) for my first significant research project and introduction to the world of geoscience.

Last but not least, I would like to thank all professors and graduate students of Department of Earth and Planetary Sciences at Rutgers. And of course my very special thanks go to my lovely friends who made my stay in the US unforgettable. Thanks to my fellow graduate students at Rutgers for a great time in classes, in

Doolittle, and of course outside of the department. Thanks a lot for sharing morning coffee and occasional evening beer. Also, I would like to thank my new friends outside of the department. And finally my special thanks goes to my Russian friends from Moscow State University who have kept in touch with me within these 2.5 years. You all are the best! Thanks for your massive support during the last couple weeks before my thesis defense.

At the very end, I would like to thank my family, mom Elena, dad Alexander, and sister Irina, for their unconditional love, encouragement, and faith in me no matter where I am. I am very grateful and proud to have such an amazing family.

TABLE OF CONTENTS

LIST OF TABLES

LIST OF FIGURES

I. INTRODUCTION

The Paleocene-Eocene thermal maximum (PETM) was an abrupt warming event initiated at the beginning of the Eocene (dated as ~55.5±0.3 Ma (Storey et al., 2007) to 56.0 Ma (Gradstein et al., 2012) on different time scales) and was associated with a global temperature increase of about 5°C in the tropical ocean (Bralower et al., 1995; Thomas et al., 1999; Zachos et al., 2003; Tripati and Elderfield, 2004), 5 to 8°C in the middle and high latitude ocean surfaces (Kennett and Stott, 1991; Zachos et al., 2003, 2006; Sluijs et al., 2006), and 4 to 6°C in deep waters (Kennett and Stott, 1991; Bralower et al., 1995; Thomas and Shackleton, 1996; Tripati and Elderfield, 2005).

The PETM is also associated with the carbon isotope excursion (CIE) represented by a decrease in $\delta^{13}C$ values in both open ocean cores (~2-3‰ and ~2.5-4‰ in benthic and planktonic foraminifera, respectively; Kennett and Stott, 1991; Zachos et al., 2003; McInerney and Wing, 2011) and terrestrial sections (~2.5-6‰; Koch et al., 1992; Wing et al., 2005). Kennett and Stott (1991) constrained the onset of the CIE to less than 6 kyr based on magneto- and biostratigraphic studies. However, alternative age models provide different durations for the CIE onset, varying significantly from ~30 kyr based on extraterrestrial ^{3}He (Farley and Eltgroth, 2003; Murphy et al., 2010) to less than 750 yr using the orbital cyclostratigraphic chronology (Röhl et al., 2007) and even to less than a year based on rhythmic sedimentary couplets ascribed to seasonal insolation (Wright and Schaller, 2013). Nevertheless, though there is disagreement of the

rapidity of its initiation, most studies agree that the CIE/PETM persisted in total for about 170-220 kyr (Röhl et al., 2000, 2007; Murphy et al., 2010).

The magnitude of the CIE requires massive injection of isotopically depleted carbon in the form of greenhouse gases (methane [CH_4] and/or carbon dioxide [CO_2]) into the ocean-atmosphere system (Kennett and Stott, 1991; Dickens et al., 1995, 1997; Thomas and Shackleton, 1996; Zachos et al., 2005; Zeebe et al., 2009). However, the cause(s) of the PETM and exact carbon sources still remain unknown. Proposed hypotheses include various mechanisms for triggering the PETM: 1) CH_4 release via the destabilization of marine gas hydrates initiated by warming (Dickens et al., 1995, 1997; Thomas et al., 2002) or continental slope failure (Katz et al., 2001); 2) thermogenic CH_4 and CO_2 explosive emissions through the hydrothermal vent complexes caused by sill intrusion into carbon-rich strata in the northeast Atlantic (Svensen et al., 2004) or due to massive flood basalt volcanism during the final rifting stage between Greenland and Europe (Storey et al., 2007); 3) rapid burning of Paleocene terrestrial organic carbon reservoir (peatlands and coal) as a result of enhanced aridity (Kurtz et al., 2003); 4) input of extraterrestrial ^{12}C-enriched carbon from cometary impact (Kent et al., 2003; Cramer and Kent, 2005); 5) tectonically triggered isolation of a widespread epicontinental seaway followed by CO_2 injection from the desiccation and bacterial oxidation of organic-rich wetlands (Higgins and Schrag, 2006); 6) release of CO_2 from the orbitally triggered decomposition of soil organic carbon in thawing permafrost (DeConto et al., 2012); and 7) exsolved magmatic CO_2 release due to kimberlite pipes emplacement (Patterson and Francis, 2013).

Given the magnitude of the CIE and variety of carbon sources, carbon cycle models predict 1,200 to over 5,000 Gt of carbon injected into the ocean-atmosphere system. A 2.5‰ deep ocean CIE requires total carbon input of 1,200 to 2,000 Gt in the form of biogenic CH_4 ($\delta^{13}C_{CH4}$ = -60‰; Dickens et al., 1995, 1997; Svensen et al., 2004), 3,000 to 4,000 Gt as thermogenic CH_4 ($\delta^{13}C_{CH4}$ = -35 to -50‰; Svensen et al., 2004), or 4,500 to 5,000 Gt as ^{12}C-enriched CO_2 or sedimentary organic carbon ($\delta^{13}C_{org}$ = -20 to -30‰; Zachos et al., 2005; Higgins and Schrag, 2006). Using published records of the CIE magnitude and calcite compensation depth (CCD) shoaling (e.g., 2 km CCD shoaling in South Atlantic; Zachos et al., 2005), a recent model of Zeebe et al. (2009) constrains the initial carbon pulse to 3,000 Gt or less ($\delta^{13}C_{source}$ = -50‰).

The relationship of the CIE to global warming is also debatable. Most studies assume that a massive input of greenhouse gases initiated the temperature rise. In contrast, Sluijs et al. (2007) suggest a precursor warming based on the organic paleothermometer TEX_{86} record (Fig. 1) from New Jersey cores at Bass River and Wilson Lake (Fig. 2, 3). Using sediment accumulation rates, the authors estimate that surface water warming preceded the CIE by ~3,000 years. Their results are consistent with the warming-triggered gas hydrate dissociation hypothesis. Moreover, based on high-resolution stable isotope records of planktonic and benthic foraminifera, Thomas et al. (2002) likewise conclude that the warming may have commenced before the CIE. I propose to test the precursor warming hypothesis and results of Sluijs et al. (2007) using a temperature record across the PETM from the Millville, New Jersey core, derived from the organic paleothermometer TEX_{86}, trace

element (Mg/Ca) analysis of planktonic foraminifera, and stable isotopic ($\delta^{13}C$ and $\delta^{18}O$) analyses of planktonic foraminifera.

Other environmental perturbations across the PETM, such as changes in hydrology, also remain untested. The New Jersey coastal plain contains thick (~50 ft; 15 m) sections recording the PETM. The P/E boundary here is accompanied by a change in the sedimentary record from sandy silts of the Vincentown Formation to kaolinitic fine clayey silts of the Marlboro Formation (Gibson et al., 1993; Cramer et al., 1999; Sugarman, Miller, Browning, et al., 2005; Lombardi, 2013). Kopp et al. (2009) proposed an enhanced hydrologic cycle to explain the widespread clay/silt deposition on the mid-Atlantic continental shelf during the PETM. Based on the investigation of magnetofossils in the Marlboro Formation, they suggested the development of a river-dominated shelf providing an Appalachian Amazon analog to explain the expanded suboxic conditions favorable for the magnetic facies distribution. The authors also support their hypothesis with the evidence of abundant *Apectodinium* cysts, derived from an opportunistic (interpreted as low salinity) dinoflagellate (Fig. 1), reported in Bass River and Wilson Lake New Jersey cores by Sluijs et al. (2007). Moreover, implications of an active hydrologic cycle have been noted in other locations. Pagani et al. (2006) used stable hydrogen isotopes in *n*-alkanes extracted from the central Arctic Ocean sediments to suggest increased moisture transport from subtropics to the high latitudes that freshened surface water in the Arctic Ocean. John et al. (2008) explained increased sediment accumulation rates on the continental margins during the PETM mostly by an expanded flux of the fine sediment to shelves. The authors link this widespread

increase in sediment supply to increased weathering and erosion of Cretaceous outcrops induced by a stronger hydrologic cycle. Overall, the suggested enhanced hydrologic cycle would have caused an increased flux of fresh water to the shelf substantially lowering salinities. I propose to test this hypothesis by estimating changes in salinity in the PETM section at Millville, New Jersey. I use two paleothermometers (TEX_{86} and Mg/Ca ratio of planktonic foraminifera) to constrain temperature changes associated with planktonic foraminiferal $\delta^{18}O$ variations, with the residual attributed to salinity changes.

II. METHODS

2.1. Material.

I studied the uppermost Paleocene-lower Eocene section of the Ocean Drilling Program (ODP) Leg 174AX core drilled at Millville, NJ (39°24’16.67"N, 75°05’19.99"W; elevation = 89.7 ft; 27.16 m) (Fig. 2). Millville was the fifth site drilled as part of ODP Leg 174AX and the ninth site drilled as part of the Coastal Plain Drilling Project (CPDP) (Sugarman, Miller, Browning et al., 2005). The total length studied is 52.5 ft (16.0 m) (Fig. 4). The top (857.0-858.0 ft; 261.2-261.5 m) and bottom (899.4-909.5 ft; 274.1-277.2 m) parts of the interval comprise micaceous, glauconitic, quartzose, sandy clayey silts of the Vincentown Formation (Fig. 5). The intervening unit (858.0-899.4 ft; 261.5-274.1 m) contains laminated to massive greenish gray fine clayey silts of the Marlboro Formation. Clay mineralogy of this formation has not been studied at Millville; however, at Clayton, Wilson Lake, and Bass River (Fig. 2), the Marlboro Formation contains 40% kaolinite (Gibson et

al., 1993; Cramer et al., 1999; Lombardi, 2013). The lower contact between the Vincentown and Marlboro Formations appears to be conformable with a few burrows while the upper contact between these formations is disconformable (Fig. 6). The section is correlated to planktonic foraminiferal Zone P5 and calcareous nannoplankton Zone NP9b (Gibson et al., 1993; Cramer et al., 1999; Sugarman, Miller, Browning et al., 2005; Harris et al., 2010).

Table 1 lists the samples taken for both planktonic foraminiferal analyses (initial sampling) and organic geochemical proxies (additional sampling). The top (857.0-896.5 ft; 261.2-273.2 m) and bottom (901.2-909.5 ft; 274.7-277.2 m) parts of the core were sampled at interval of 2 ft (61 cm). The samples from the "critical" interval of the core (896.5-901.2 ft; 273.2-274.7 m) containing the initiation of the CIE were taken at sampling interval of 4-6 inches (10-15 cm).

For isotopic and trace metal analyses of planktonic foraminifera, the samples were dried in a 50°C oven and weighed dry (Table 2). To deflocculate clays, the samples were disaggregated in a sodium metaphosphate solution (5.5 g of sodium metaphosphate per liter) and then washed through a 63 μm sieve to remove the fine fraction (<63 μm). The sand fraction (>63 μm) was dried in a 50°C oven and weighed dry to compute the percentage of sand (Fig. 5; Table 2). Planktonic foraminifera >250 μm in size were picked and identified. For organic proxies (TEX_{86} and $U^{k'}_{37}$), the samples were frozen at -20°C, freeze-dried, and homogenized using a mortar and pestle.

2.2. Stable isotopes ($\delta^{18}O$ and $\delta^{13}C$) of planktonic foraminifera.

Planktonic foraminifera incorporate carbon and oxygen from the surrounding water to construct their calcium carbonate ($CaCO_3$) tests. The oxygen isotope ratio $^{18}O/^{16}O$ of planktonic foraminifera expressed as $\delta^{18}O$ is affected by the temperature and $\delta^{18}O$ of the surrounding water. The latter is affected by ice volume negligible at the late Paleocene - early Eocene and mixing between freshwater river runoff and marine waters (Urey, 1947; Epstein et al., 1951). The carbon isotope ratio $^{13}C/^{12}C$ of planktonic foraminifera expressed as $\delta^{13}C$ depends on $\delta^{13}C$ of the surrounding water affected by the photosynthesis. Organisms preferentially remove the lighter ^{12}C, leaving the ambient water enriched in ^{13}C. In addition, $\delta^{13}C$ variations reflect global carbon budget changes including input from different sources (e.g., biogenic methane has very low $\delta^{13}C$ values of -60‰, thermogenic methane has $\delta^{13}C$ values of -35 to -50‰, organic matter has $\delta^{13}C$ values of -20 to -30‰).

Analytical method. Specimens of *Morozovella aequa, Morozovella acuta, Morozovella velascoensis, Acarinina soldadoensis, Acarinina esnehensis, Subbotina roesnaesensis*, and *Subbotina triangularis* from the 250-300 μm, 300-350 μm, 350-400 μm, and >400 μm size fractions (Tables 4, 5, 6) were gently crushed, rinsed with milli-Q water, and loaded into reaction vials for the stable isotope analyses. All analyses were conducted on a Micromass Optima Mass Spectrometer with an attached multi-prep device. Carbonate samples were reacted in 100% phosphoric acid (H_3PO_4) at 90°C for 15 minutes and the evolved CO_2 gas was collected in a liquid nitrogen cold finger. Ratios are reported in standard delta notation in parts

per thousand (per mil, ‰) $\delta = [(R_{sample}/R_{standard}) - 1] \times 1000$ where $R = {}^{13}C/{}^{12}C$ or ${}^{18}O/{}^{16}O$, relative to Vienna-Pee Dee Belemnite ($\delta^{13}C_{VPDB}$ and $\delta^{18}O_{VPDB}$). Analytical errors are ±0.05‰ and ±0.08‰ for $\delta^{13}C$ and $\delta^{18}O$, respectively. Analyses of stable isotopes were performed at the Stable Isotope Laboratory supervised by Dr. James D. Wright at the Department of Earth and Planetary Sciences, Rutgers University.

2.3. Trace metal analysis (Mg/Ca ratio) of planktonic foraminifera.

Foraminiferal Mg/Ca thermometry is a useful paleoceanography proxy to determine past ocean temperatures (Lear et al., 2000; Billups and Schrag, 2002). The theoretical basis for the Mg/Ca proxy is the substitution of magnesium for calcium in the calcium carbonate ($CaCO_3$) foraminiferal tests (Katz, 1973; Hartley and Mucci, 1996). Mg/Ca in seawater is considered to be constant across the PETM given the oceanic residence times of these elements, 13 Myr for Mg and 1 Myr for Ca (Broecker and Peng, 1982). Coretops (Rosenthal et al., 1997; Elderfield and Ganssen, 2000; Lea et al., 2000; Lear et al., 2002), sediment traps (Anand et al., 2003), and cultures (Nürnberg et al., 1996; Lea et al., 1999) show a positive correlation between the magnesium incorporation into foraminiferal $CaCO_3$ and the temperature of the surrounding seawater at the estimated calcification depth. Therefore, as temperature increases, the Mg/Ca ratio also increases. However, the interpretation of foraminiferal Mg/Ca ratio primarily as a temperature proxy may be complicated by additional factors that affect the magnesium concentration in foraminiferal tests, such as: 1) variable habitat depth of individual planktonic foraminifera during their life cycle (Fairbanks et al., 1982); 2) post-depositional

dissolution of calcite (Rosenthal and Boyle, 1993); 3) influence of test size (Elderfield et al., 2002); and 4) secular variations in Mg/Ca in seawater (Stanley and Hardie, 1998; Wilkinson and Algeo, 1989; Coggon et al., 2010).

Anand et al. (2003) developed Mg/Ca calibrations for twelve modern species of planktonic foraminifera. Based of the narrow range of temperature sensitivities among species, Anand et al. (2003) compiled a multi-species calibration equation: Mg/Ca = 0.38 (±0.02) exp 0.09 (±0.003) T (r^2 = 0.93; the standard error in temperature estimate is ±1°C). The calibration is equivalent to a 9±0.3 % change in Mg/Ca per 1°C.

Analytical method. For each sample, 10-30 foraminifera tests of *Morozovella aequa, Morozovella acuta, Acarinina esnaensis, Acarinina soldadoensis*, *Acarinina angulosa*, *Subbotina roesnaesensis*, and *Subbotina velascoensis* were picked from size fractions 250-300 µm, 300-350 µm, and 350-400 µm to yield ~100-400 µg sample weight. To yield sufficient foraminiferal calcite ($CaCO_3$) for the analysis, a few species of the same genus were combined in single samples (Tables 7, 8, 9). Tests were gently crushed between two glass plates to open the chambers to facilitate cleaning following the protocol reported by Boyle and Keigwin (1985) later modified by Rosenthal et al. (1997). To remove fine clays, gently crushed samples were rinsed three times with Milli-Q water and glass-distilled methanol (MeOH). To remove metal oxides, samples were reductively cleaned using reducing cleaning solution: anhydrous hydrazine (NH_2NH_2), ammonium hydroxide (NH_4OH), and citric acid ($C_6H_8O_7$)/ammonia (NH_3) solution. To remove organic matter, samples were cleaned in oxidizing reagents: hydrogen peroxide (H_2O_2) and 0.1N sodium

hydroxide (NaOH). Samples were transferred into clean vials to avoid contaminations caused by adsorption during the cleaning stages. A final acid leach was done with 0.001N nitric acid (HNO_3) before completely dissolving the samples in 0.065N OPTIMA HNO_3.

Trace element analyses (B/Ca, Mg/Ca, Mn/Ca, Al/Ca, Sr/Ca, and Fe/Ca) were measured on a Thermo Finnigan Element XR Sector Field Inductively Coupled Plasma Mass Spectrometer (SF-ICP-MS) operated in low resolution ($m/\Delta m$ =300) and medium resolution ($m/\Delta m$ =4300) settings outlined in the protocol of Rosenthal et al. (1999). Samples were monitored for potential contamination from clay and metal oxides by measuring Mn/Ca, Al/Ca and Fe/Ca to monitor for diagenetic coatings. Elemental ratios were monitored and corrected for matrix effects for each analytical run by analyzing a suite of standards using an internal spiked gravimetric standard (SGS) with the same elemental ratios but varying [Ca] (1.5mmol/l to 8mmol/l) (Rosenthal et al., 1999). [Ca] concentrations in sample solutions were typically maintained in the range of 1.5 to 4mmol/l to minimize matrix effects on Mg/Ca. Trace metal analyses were performed at the Inorganic Chemistry Laboratory supervised by Dr. Yair Rosenthal at the Institute of Marine and Coastal Sciences (IMCS), Rutgers University.

2.4. TEX_{86} analysis.

TEX_{86} (TetraEther Index of lipids with 86 carbon atoms) is a paleothermometer based on the distribution of thaumarchaeotal membrane lipids (Schouten et al., 2002). Marine Thaumarchaeota is one of the most abundant

prokaryotic groups in the modern ocean that are ubiquitous throughout the water column with a maximum occurrence at depths less than 200 m (Karner et al., 2001; Schouten et al., 2013 and references therein). Membranes of such organisms contain glycerol dibiphytanyl glycerol tetraethers (GDGTs; Fig. 7) including in their structures zero to three cyclopentane rings (GDGT 0-3) and crenarchaeol with its regio-isomer including four cyclopentane rings and one cyclohexane ring (Schouten et al., 2000; Sinninghe Damsté et al., 2002). The composition of thaumarchaeotal membranes changes with the temperature they are grown in (i.e., higher temperatures cause increased amounts of GDGTs with two or more cyclopentane rings), but it does not depend on surface water salinity or nutrients (Schouten et al., 2002; Wuchter et al., 2004, Schouten et al., 2007). Regional core-top studies have shown that the distribution of GDGTs represented by TEX_{86} (TEX_{86} = ([III] +[IV] + [V'])/([II] + [III] + [IV] + [V']); see Fig. 7 for lipid's structures) corresponds with present-day mean annual sea surface temperature (SST) in the range of 5 to 30°C (Schouten et al., 2002; Kim et al., 2008). Although surface sediment studies show good correlation between TEX_{86} and mean annual SST, TEX_{86} values do not always indicate mean annual SST because the depth and season of maximum thaumarchaeotal abundance as well as its export to sediments may vary at different locations. Nevertheless, studies of surface sediment, sediment trap, and water column altogether revealed that TEX_{86} values reflect average water temperatures at the depth of 0 to 200 m and often correspond to the temperature of the subsurface layer (30-200 m) even better than to SST (Schouten et al., 2013 and references therein).

TEX_{86} values are convertible to SST using various calibrations. In this study, SSTs were reconstructed applying calibrations from Kim et al. (2010). They introduced new GDGT indices (TEX^H_{86} and TEX^L_{86}) and proposed two equations for high and low temperatures, suggesting use of the first one to calibrate Paleogene temperatures: SST = 68.4 × TEX^H_{86} + 38.6 (r^2 = 0.87; the standard error in temperature estimate is ±2.5°C), where TEX^H_{86} = logTEX_{86}. In contrast, Taylor et al. (2013) recommended using Kim's (2010) equation for low temperatures for Paleogene sediments due to its better correlation with inorganic paleothermometers: SST = 67.5 × TEX^L_{86} + 46.9 (r^2 = 0.86; the standard error in temperature estimate is ±4°C), where TEX^L_{86} = log ([III]/([II] + [III] + [IV])), see Fig. 7 for lipid's structures.

Analytical method. Powdered and freeze-dried sediments (~20 g dry mass) were extracted with a Dionex accelerated solvent extractor (ASE 200) using a 9:1 mixture (v:v) of dichloromethane (DCM) and methanol (MeOH) at a temperature of 150°C and a pressure of 1500 psi. GDGT C46 standard (0.0252 μg/μl) was added to each as an internal reference standard. The polar fraction containing the GDGTs was separated from the total lipid extract through the alumina column (Al_2O_3 was activated for 2 h at 150°C). Hexane:DCM (9:1 (v:v), 4 column volumes) mixture was used to elute the apolar fraction, hexane:DCM (1:1 (v:v), 3 column volumes) to improve the sample "cleanness", and DCM:MeOH (1:1 (v:v), 3 column volumes) to elute the polar fraction. After evaporation of the solvents, the polar fraction was redissolved in a 99:1 (v:v) mixture of hexane:isopropanol and filtered through a 0.4 mm PTFE filter. The GDGT analysis was performed by normal phase

chromatography on an Agilent 1100 series high-performance liquid chromatography (HPLC) using the Prevail Cyano column (3 mm, 150 × 2.1 mm). A 99:1 (v:v) mixture of hexane:isopropanol was used to elute GDGTs at a flow rate 0.2 ml/min and column temperature 30°C according to the Hopmans et al. (2000) and Schouten et al. (2007) methodology. Detection of GDGTs was accomplished via Single Ion Monitoring mode using Agilent OpenLAB Software. TEX_{86} analysis was performed at the Geochemical Laboratory supervised by Dr. Timothy D. Herbert at the Department of Geological Sciences at Brown University.

2.5. BIT analysis.

The BIT (Branched and Isoprenoid Tetraether) index is a recently proposed tracer for fluvial terrestrial input in sediments (Hopmans et al., 2004). It is based on the relative distribution of soil-derived branched non-isoprenoid tetraether lipids versus isoprenoid crenarchaeol synthesized by marine Thaumarchaeota: BIT = ([I + II + III)/([I + II + III] + [IV]); see Fig. 8 for lipid's structures). According to the BIT index equation, it can range from 0, indicating no terrestrial organic matter (OM) input, to 1, representing absence of crenarchaeol, the biomarker that is abundant in marine environment. Recently, Walsh et al. (2008) suggested that the BIT index is the tracer of soil- or peat-derived OM only rather than the indicator of total terrestrial input. They revealed the absence of branched GDGTs in terrestrial vegetation and showed that the BIT index doesn't agree with other measures of terrestrial OM ($\delta^{13}C_{org}$ and lignin phenols). Moreover, Weijers et al. (2006) detected small concentrations of crenarchaeol in soils that can probably bias the BIT values

and make the application of the BIT index slightly inaccurate. Nevertheless, the BIT values higher than 0.8 generally indicate a significant soil OM input, while values lower than 0.2 correspond to a low soil OM imprint (Fig. 9; Schouten et al., 2013).

Analytical method. GDGTs for the BIT index measurement were extracted and identified by high-performance liquid chromatography-mass spectrometry (HPLC-MS), described in TEX_{86} procedure section.

2.6. $U^{K'}_{37}$ analysis.

$U^{K'}_{37}$ index is a paleothermometer based on the distribution of the di-($C_{37:2}$) and tri-($C_{37:3}$) unsaturated ketones (alkenones). It was initially defined by Brassell et al. (1986) and then modified by Prahl and Wakeham (1987) through excluding tetra-($C_{37:4}$) unsaturated ketone from the original equation due to its rare occurrence in sediments. Alkenones are Haptophyceae biomarkers, synthesized in the modern ocean mostly by two species of coccolithophorids, *Emiliania huxleyi* and *Gephyrocapsa oceanica*. Initially, Marlowe et al. (1984 a) and Brassell et al. (1986) proposed that changes in alkenone unsaturation maintain membrane fluidity at various temperatures; however, the actual function of alkenones in Haptophyceae cells is still unclear. These organisms require sunlight and generally inhabit the mixed layer in the ocean regardless of the latitude and seasonality. The $U^{K'}_{37}$ method implies that the degree of alkenone unsaturation depends on the temperature of water and it is not affected by salinity or ice volume (Brassell et al., 1986; Prahl and Wakeham, 1987; Sikes et al., 1991; Müller et al., 1998).

The $U^{K'}_{37}$ index shows only the relative proportion of C_{37} alkenones: $U^{K'}_{37}$ = [$C_{37:2}$] / [$C_{37:2}$ + $C_{37:3}$]. It is calibrated to mean annual SSTs through the equation: $U^{K'}_{37}$ = 0.033 T + 0.044 (r^2 = 0.958; the standard error of estimate is ±0.050 $U^{K'}_{37}$ units or ±1.5°C) (Müller et al., 1998). According to the $U^{K'}_{37}$ index equation, it can vary between 0 and 1 corresponding to either cold or warm temperatures. Herbert (2003) suggested interpreting $U^{K'}_{37}$ index only for temperatures between 5°C and 27°C (0.20-0.96 $U^{K'}_{37}$ values, respectively).

Analytical method. Powdered and freeze-dried sediments (~ 10 g dry mass) were extracted with Dionex 2000 Accelerated Solvent Extractor (ASE) using a 4:1 (v:v) mixture of DCM and MeOH with the ASE programmed to 150°C and 2000 psi. Nonadecanone was added to each as an internal reference standard. Extracts were evaporated and redissolved in toluene and subsequently analyzed by capillary Gas Chromatography with a flame ionization detector (FID), using a Shimadzu GC-17A fitted with a 30 m JW Scientific DB-5 (0.32mm i.d.). Samples were injected on-column using hydrogen as a carrier gas and the temperature program was 50-150°C at 30°C min^{-1} and 150-325°C at 3°C min^{-1}, which ensured good separation of all major constituents. Compounds were integrated using Shimadzu-provided software. C_{37} alkenone analysis for $U^{K'}_{37}$- SST estimation was performed at the Geochemical Laboratory supervised by Dr. Elisabeth L. Sikes at the Institute of Marine and Coastal Sciences (IMCS), Rutgers University.

III. RESULTS

3.1. Bulk carbon isotopic and lithologic records.

Biostratigraphy (planktonic foraminiferal Zone P5 and calcareous nannoplankton Zone NP9b; Sugarman, Miller, Browning et al., 2005) and previous isotopic studies (Wright and Schaller, 2013) indicate that the Vincentown and Marlboro Formations at Millville span the Paleocene/Eocene boundary that includes the CIE (Fig. 5). Carbon isotope measurements of bulk carbonate (Wright and Schaller, 2013; this study) allow for the firm placement of the initiation of the CIE and the CIE "core" at Millville (Fig. 5; Table 1). Pre-CIE $\delta^{13}C_{bulk}$ values start decreasing from 2.3‰ at 905.62 ft (276.03 m) to 1.2‰ at 898.95 ft (274.00 m) and then abruptly decrease to -2‰ at 897.37 ft (273.52 m), marking the initiation of the CIE. The excursion from 1.2 to -2‰ occurs within a 1.58 ft (0.48 m) section of the core (Fig. 4; Fig. 5 inset). I place the initiation of the CIE at 898.82 ft (273.96 m), which is the average between 898.69 ft (273.92m) and 898.95 ft (274.00 m) (Fig. 5 inset). Wright and Schaller (2013) placed the CIE onset more precisely at 898.75 ft (273.94 m) that falls within my sampling resolution. Above the CIE onset, the bulk carbonate isotopic record reaches a minimum value of -3.4‰ at 889.18 ft (271.03 m), gradually increases to -2.5‰ at 879.20 ft (267.98 m), and remains constant up to 869.13 ft (264.91 m). There is a hint of recovery from -2.5 to -0.65‰ in the upper section from 857.00 to 869.13 ft (261.21-264.91 m). The isotopic record of bulk organic carbon (Harris et al., 2010) shows constant $\delta^{13}C_{org}$ values of - 2.5‰ within the CIE "core" and does not exhibit such pronounced recovery in the top core interval.

The maximum amplitude change in the bulk carbonate isotopic record is ~5.5‰, whereas the organic carbon isotopic record shows a smaller change of ~3.5‰. The large excursion of ~5.5‰ in $\delta^{13}C_{bulk}$ values is much greater than the ~2.5-3.0‰ change in $\delta^{13}C$ of deep-sea benthic foraminifera (Kennett and Stott, 1991; Zachos et al., 2003; McInerney and Wing, 2011). Likewise, Wright and Schaller (2013) reported high amplitudes of the CIE in bulk carbonate isotopic records from seven locations on the New Jersey coastal plain and observed an increase of CIE amplitudes in shallower water depth. They suggested that stronger isolation of shallower sites from the deep ocean and restricted mixing with the deep ocean carbon pool resulted in a greater proportion of the atmospheric carbon and consequently higher CIE amplitudes.

The percent sand dramatically decreases spanning the onset of the CIE at Millville. According to the site report (Sugarman, Miller, Browning et al., 2005), glauconitic micaceous sandy (~44 %) silts of the Vincentown Formation are overlain by the clayey silts of the Marlboro Formation at 899.4 ft (273.83 m). A decrease in sand begins at 903.74 ft (275.46 m), 5 ft (1.5 m) below the CIE onset at 898.82 ft (273.96 m) and, with one exception, percent sand monotonically decreases to ~3% at 897.05 ft (273.42 m) and to ~1% above 893.10 ft (272.22 m). This is consistent with the observation that rhythmic bedding begins below the CIE at Millville (Wright and Schaller, 2013) and implies that the paleoenvironmental changes associated with the lithologic and bedding changes preceded the CIE onset at Millville.

3.2. Stable isotopes ($\delta^{18}O$ and $\delta^{13}C$) of planktonic foraminifera.

Stable isotopic analyses of planktonic foraminifera delineate intermediate dwellers (*Subbotina*) and mixed layer dwellers (*Acarinina* and *Morozovella*). Deep dwelling *Subbotina* are marked by high $\delta^{18}O$ values reflecting calcification in the deep layer that is seasonally stratified, while mixed layer dwellers have low $\delta^{18}O$ values, reflecting calcification in the surface mixed layer (Fig. 3). *Acarinina* varies between $\delta^{18}O$ values closer to *Subbotina* in the lower part of the record and values closer to *Morozovella* in the upper part, and could be classified as lower mixed layer or upper thermocline dwellers. Seasonal stratification results in a deep chlorophyll maximum (DCM) at the base of the mixed layer, ~30-50 m (Glenn et al., 2008). The DCM and intermediate layer have low $\delta^{13}C$ values, recorded by *Subbotina*. However, *Acarinina* has high $\delta^{13}C$ values, suggesting that it lived in the deep mixed layer above the top of the DCM.

To avoid species bias, most of the samples analyzed consisted of single species of one size fraction (Tables 2, 3, 4). Stable isotopic values of planktonic foraminifera were plotted based on genus (Fig. 10). Samples from the pre-CIE interval contain very few planktonic foraminifera. From the pre-CIE section, only genus *Subbotina* had sufficient number of specimens for analyses providing the only complete isotopic record (857.05-903.74 ft; 261.23-275.46 m). *Acarinina* spp. isotopic records include a single data point below the CIE onset (857.05-899.18 ft; 261.23-274.07 m). *Morozovella* spp. isotopic records were obtained only above the CIE onset (857.05-895.14 ft; 261.23-272.84 m).

3.2.1. Oxygen isotopes ($\delta^{18}O$) of planktonic foraminifera.

Subbotina spp. $\delta^{18}O$ values record a large decrease (~2.3‰) across the CIE onset from -1.2 to -3.5‰, indicating warming (Fig. 10). Above the CIE onset, $\delta^{18}O$ values slightly increase from -3.5‰ at 893.10 ft (272.22 m) to -2.8‰ at 863.08 ft (263.07 m). Towards the top of the section, $\delta^{18}O$ values increase from -2.8‰ at 863.08 ft (263.07 m) to -1.8‰ at 857.05 ft (261.23 m), returning to pre-CIE values. Interestingly, *Subbotina* spp. $\delta^{18}O$ values perfectly coincide with $\delta^{18}O$ record of bulk carbonate, suggesting similar temperatures and $\delta^{18}O_{water}$ in the absence of vital effects. Since *Subbotina* spp. are intermediate dwellers living in the seasonal thermocline to deep layer, $\delta^{18}O$ of bulk carbonate should reflect thermocline temperatures as well. Moreover, if the $\delta^{18}O$ signal of bulk carbonate comes from the thermocline, then bulk carbonate should be dominated mostly by calcareous nannoplankton thriving on the top of the thermocline.

The *Morozovella* $\delta^{18}O$ record shows lower values corresponding to their shallower habitat (Fig. 10). The *Morozovella* $\delta^{18}O$ record shows an increasing trend in $\delta^{18}O$ values from -3.9‰ at 895.14 ft (272.84 m) to -3.1‰ at 857.05 ft (261.23 m). The *Acarinina* $\delta^{18}O$ record exhibits intermediate $\delta^{18}O$ values between *Subbotina* and *Morozovella* records (Fig. 10). Within the 873.08 to 899.18 ft (266.11-274.07 m) interval, $\delta^{18}O$ values of *Acarinina* spp. are similar to those of *Subbotina* spp. and bulk carbonate. In the top 857.05-873.08 ft (261.23-266.11 m) interval, the *Acarinina* $\delta^{18}O$ record has significant variability, represented by two prominent spikes in $\delta^{18}O$ values from -2.8 to -3.6‰ similar to those of *Morozovella* spp.

3.2.2. Carbon isotopes ($\delta^{13}C$) of planktonic foraminifera.

The carbon isotopic record of *Subbotina* spp. shows a ~3.3‰ decrease in $\delta^{13}C$ values from 1.0 to -2.3‰ across the CIE onset (Fig. 10). Above the CIE onset, $\delta^{13}C$ values gradually increase from -2.3‰ at 893.10 ft (272.22 m) to -0.2‰ at 857.05 ft (261.23 m) and do not return to pre-CIE values. The carbon isotopic record of *Subbotina* spp. is consistent with the $\delta^{13}C_{bulk}$ record below the CIE onset; however, within the CIE "core", it records ~1‰ higher values than $\delta^{13}C_{bulk}$.

The carbon isotopic record of *Acarinina* spp. shows a larger decrease in $\delta^{13}C$ values of ~4‰ from 3.6 to -0.4‰ across the CIE onset (Fig. 10). Above the CIE onset, values are consistently around 0‰. At the top of the section (857.05-867.08 ft; 261.23-264.28 m), it exhibits a gradual increase in $\delta^{13}C$ values from -0.3 to 1.6‰. The carbon isotopic record of *Morozovella* spp. above the CIE shows similar $\delta^{13}C$ trends as *Acarinina* spp. (Fig. 10). Within the CIE "core", it shows constant values about 0.5‰. At the top of the section (857.05-865.14 ft; 261.23-263.69 m), $\delta^{13}C$ values show a significant increase from 0.7 to 4‰.

3.3. Trace metal analysis (Mg/Ca ratio) of planktonic foraminifera.

Trace element to calcium analyses (Mg/Ca) were performed on planktonic foraminifera using intermediate (*Subbotina*) and mixed-layer dwelling planktonic foraminifera (*Acarinina* and *Morozovella*) (Fig. 11; Tables 7, 8, 9). Specimens of planktonic foraminifera were picked from core samples and analyzed for both stable isotopes ($\delta^{13}C$ and $\delta^{18}O$) and trace metals (Mg/Ca). Thus, almost each planktonic foraminifera sample reflects paired measurements of $\delta^{13}C$, $\delta^{18}O$, and Mg/Ca. To

avoid species and size related (D'Hondt et al., 1994; Elderfield et al., 2002) bias, most samples analyzed for trace metals consisted of single species and were from a narrow size fraction range (Tables 7, 8, 9). Values of Mg/Ca in planktonic foraminifera were plotted based on their genus (Fig. 11). Samples with calcium elemental ratios less than the smallest calcium elemental ratio in the matrix standard (1.5 mmol/l) were rejected (Fig. 11; Table 8). Samples with Fe/Ca greater than 4000 μmol/mol were also excluded (Tables 7, 8, 9). Elevated Fe/Ca ratios most probably indicate contaminations of the foraminifera tests. Interestingly, samples with high Fe/Ca ratios belong to the same depth interval (Fig. 11) probably corresponding to lithological changes. Additionally, samples with low B/Ca, Sr/Ca, Li/Ca, and high Mg/Ca were considered as possibly altered due to diagenesis, and thus also rejected from the reconstructions (Fig. 11; Tables 7, 9).

Even with elimination of possibly contaminated samples, I was able to generate a complete Mg/Ca record of *Subbotina* spp. (861.15-900.21 ft; 262.48-274.38 m). *Morozovella* spp. Mg/Ca values comprise a complete record in the upper part of the section (857.05-881.15 ft; 261.23-268.57 m), and Mg/Ca values of *Acarinina* spp. are scattered throughout (859.00-896.49 ft; 261.82-273.25 m). The *Subbotina* record has the lowest Mg/Ca values, whereas, the *Morozovella* record shows highest values. This implies higher temperatures for the mixed-layer dweller *Morozovella* and lower temperatures for the intermediate layer dweller *Subbotina*, consistent with observations from $\delta^{18}O$ records of these genera from proximal New Jersey core sites (John et al., 2008; Zachos et al., 2006; this study Figure 10).

The total change in Mg/Ca ratio of *Subbotina* spp. across the CIE onset is 1.34 mmol/mol (from 2.46 to 3.8 mmol/mol) (Fig. 11). Above the CIE onset, values remain constant at an average value of 3.6 mmol/mol and show a gradual decrease of 1.4 mmol/mol from 3.6 mmol/mol at 881.15 ft (268.57 m) to 2.2 mmol/mol at 861.15 ft (262.48 m), returning to pre-CIE values (Fig. 11).

The *Morozovella* Mg/Ca record in general shows higher values than the *Subbotina* record, but does not indicate any trend in values. Comparison of the two records indicates that *Morozovella* spp. Mg/Ca values are 0-1.5 mmol/mol higher than those of *Subbotina* spp. (with the exception of one sample where Mg/Ca ratio in *Morozovella* spp. is 0.5 mmol/mol lower than in *Subbotina* spp.). Excluding this point, the average difference between Mg/Ca values of *Morozovella* and *Subbotina* spp. is 0.7 mmol/mol.

It is difficult to discern any significant trend in the *Acarinina* Mg/Ca record due to the lower resolution of the data. However, in the lower part (890.96-896.49 ft; 271.56-273.25 m), the *Acarinina* Mg/Ca record shows values even lower than in the *Subbotina* record, implying lower temperatures indicated by *Acarinina* spp. In contrast, Mg/Ca values of *Acarinina* spp. from the upper part of the core coincide better with *Morozovella* spp. values. This observation is consistent with oxygen isotopic records that show that $\delta^{18}O$ values of *Acarinina* and *Subbotina* spp. are similar in the lower part of the core, and $\delta^{18}O$ values of *Acarinina* spp. correspond better to *Morozovella* spp. $\delta^{18}O$ values in the upper section (Fig. 10).

3.4. TEX_{86} analysis.

Lipid biomarker analysis of the Millville core revealed the set of isoprenoid glycerol dibiphytanyl glycerol tetraethers (GDGTs), expressed in the TEX_{86} index values (Fig. 12; Table 10). The original TEX_{86} introduced by Schouten et al. (2002) comprises GDGT-1 [II], GDGT-2 [III], GDGT-3 [IV], and crenarchaeol regio-isomer [V'] in its ratio: TEX_{86} = ([III] + [IV] + [V']) / ([II] + [III] + [IV] + [V']), see Fig. 7 for lipid's structures. The authors excluded more abundant GDGT-0 [I] and creanarchaeol [V] from the ratio since their very high concentrations can diminish the overprint of the other GDGTs on TEX_{86} and thus yield to weaker correlation of the index with SST. Moreover, GDGT-0 is a membrane lipid that is also synthesized by methanogenic and methanotrophic Archea; therefore, the additional input of GDGT-0 from other Archaea may bias the TEX_{86} values.

Reassessement of the correlation between the GDGT distribution and SST using extended core-top dataset provided new indices. Kim et al. (2010) modified the original TEX_{86} index including the data from (sub)polar core-tops and excluded Red Sea data from the global dataset due to its distinct water chemistry. Computing all possible combinations of GDGT ratios, the authors presented a new index that shows the best correlation with SST: TEX^{L}_{86} = log ([III] / ([II] + [III] + [IV])), see Fig. 7 for lipid's structures. Additionally, to correlate GDGT distribution with much warmer past SSTs, such as in the Cretaceous greenhouse world, they excluded the data from the (sub)polar ocean and evaluated an index that correlates best with temperatures above 20°C: TEX^{H}_{86}= log (([III] + [IV] + [V']) / ([II] + [III] + [IV] + [V'])), see Fig. 7 for lipid's structures. Interestingly, the GDGT ratio in TEX^{H}_{86} represents

the original TEX_{86} itself, and thus TEX^{H}_{86} can be simply defined as $logTEX_{86}$. TEX^{H}_{86} differs from TEX^{L}_{86} by crenarchaeol regio-isomer [V'], which correlates well with high SST but has poorer correlation with low SST. According to this relation, Kim et al. (2010) highlighted GDGT indices by letters H and L that stand for high and low temperatures, respectively, and suggested use of TEX^{H}_{86} for sub(tropical) oceans and TEX^{L}_{86} for sub(polar) oceans. Taylor et al. (2013) suggested that the TEX^{L}_{86} was most appropriate for the warm Paleogene, a suggestion corroborated here (see Discussion).

Based on the assumption that indices evaluated by Kim et al. (2010) represent the best correlation with SSTs, I calculated TEX^{H}_{86} and TEX^{L}_{86} (Fig. 12). Both indices reveal similar trends in values; however, they slightly differ across the CIE onset and within the CIE "core". TEX^{L}_{86} shows almost constant values of -0.36 in the pre-CIE interval. There is a sharp increase of 0.06 associated with the CIE onset from -0.35 at 899.30 ft (274.11 m) to -0.29 at 898.47 ft (273.27 m). Above this, four samples revealed the same TEX^{L}_{86} values of -0.29 within the 896.54-898.47 ft (273.27-273.85 m) interval. A second increase of 0.04 occurs at 896.54 ft (273.27 m), yielding a total change of 0.1 from 899.30 ft (274.11 m) to 896.30 ft (273.19 m). Within the CIE "core", TEX^{L}_{86} shows average values of -0.26 with a pronounced decrease of 0.1 from -0.24 to -0.34 in the upper part of the core (857.00-865.17 ft; 261.21-263.70 m).

TEX^{H}_{86} reveals trend similar to TEX^{L}_{86}. TEX^{H}_{86} shows constant values of -0.13 in the pre-CIE interval and a 0.1 increase from -0.15 at 900.29 ft (274.41 m) to -0.05 at 896.30 ft (273.19 m). Interestingly, the amplitude change of TEX^{H}_{86} values

across the CIE is the same as in TEX^{L}_{86}; however, values of the indices begin to increase at different depths. The increase of TEX^{H}_{86} appears 1.5 ft (45 cm) below the CIE onset and 1 ft (30 cm) lower than in TEX^{L}_{86}. Moreover, the TEX^{H}_{86} increase happens in three steps. The first increase of 0.03 from -0.15 to -0.12 occurs from 898.95 ft to 900.29 ft (274.00-274.41 m). The second increase of 0.04 associated with the CIE onset appears exactly at the same depth as the initial increase in the TEX^{L}_{86} values, i.e. from 898.47 ft to 898.30 ft (273.27-274.11 m). A third increase of 0.3 occurs from 896.30 ft to 896.54 ft (273.19-273.27 m). Also, it is harder to delineate the initiation of the TEX^{H}_{86} increase. Only two data points define it, and if we exclude them, the onset of the TEX^{H}_{86} increase appears at exactly the same depth as TEX^{L}_{86} and the CIE onset, but comprise a lower amplitude change of 0.6 than in TEX^{L}_{86}. Within the CIE "core", TEX^{H}_{86} shows constant values of -0.05 from 896.30 ft (273.19 m) up to 881.20 ft (268.59 m) and regular decrease of 0.07 in the upper section from 881.20 ft (268.59 m) up to 857.00 ft (261.21 m). In comparison with the TEX^{L}_{86} values, the gradual decrease trend of TEX^{H}_{86} starts lower and has a lower amplitude change. Finally, since TEX^{H}_{86} is a logarithmic function of the original TEX_{86}, their trends are almost identical (Fig. 13).

3.5. BIT analysis.

The relative distribution of branched non-isoprenoid tetraether lipids versus isoprenoid crenarchaeol revealed the BIT values ranging from 0.06 to 0.15 at Millville (Fig. 13; Table 11). Such low values of the BIT index reflect the dominance of marine-derived crenarchaeol versus soil-derived non-isoprenoid GDGTs.

Schouten et al. (2013) compared BIT values from both marine sediments and soil samples and observed that the BIT index in marine sediments is generally less than 0.2 corresponding to a low soil or peat imprint, whereas the BIT index in soils tends to be higher than 0.8 (Fig. 9). The BIT index at Millville samples corresponds to values obtained from marine sediments (<0.2), thus indicating that lipid biomarkers are mainly marine- rather than soil-derived.

3.6. $U^{K'}_{37}$ analysis.

For the $U^{K'}_{37}$ proxy, I analyzed six samples across the PETM section, i.e. from 857.00 ft (261.21 m), 883.14 ft (269.18 m), 897.10 ft (273.44 m), 899.81 ft (274.26 m), 907.60 ft (276.64 m), and 909.44 ft (277.26 m) depths. In comparison with the alkenone standard, the obtained chromatograms revealed either no alkenone signal or a very small bump in the alkenone appearance area (Fig. 14). Farrimond et al. (1986) discovered alkenones in the Cenomanian and mid-Albian shales from Blake-Bahama Basin, western North Atlantic, thus extending the geological appearance of alkenones to the Cretaceous and verifying their resistance to breakdown in sediments (i.e., Marlowe et al., 1984 b). The unusual lipid distribution in analyzed shales included only di-unsaturated ketones significantly differing from the previously reported studies. The authors asserted that the source of the alkenones is unknown and speculated that it is probably an earlier genus of the family *Gephyrocapsaceae*. In this case, an absence of alkenones in the PETM samples can be an outcome of the early diagenesis processes and biodegradation of organic matter. However, genetic and micropaleontological studies suggest an absence of alkenone

producers at the late Paleocene - early Eocene. The extinct genus *Reticulofenestra* from the family *Gephyrocapsaceae*, considered being the earliest potential source of alkenones, evolved only in the early Eocene (Marlowe et al., 1990). Thus, an alkenone signal in the PETM samples is unlikely.

IV. DISCUSSION

4.1. Temperature reconstructions of the PETM at Millville, NJ.

To reconstruct temperatures during the PETM at Millville, NJ, I calibrated records obtained from the organic paleothermometer TEX_{86} and trace metal analyses (Mg/Ca ratio) of planktonic foraminifera. I estimated both absolute values for temperature and relative change (delta) temperature. Oxygen isotope records of planktonic foraminifera also place constraints on paleotemperatures.

4.1.2. TEX_{86} analysis.

I used TEX^{H}_{86} and TEX^{L}_{86} indices from Kim et al. (2010) to calibrate temperatures at the uppermost Paleocene-lower Eocene section at Millvile, NJ (Fig. 15). Currently, these calibrations represent the best relationships between the relative distribution of GDGTs and temperature in (sub)polar (TEX^{L}_{86} for temperatures <15°C) and (sub)tropic (TEX^{H}_{86} for temperatures >15°C) regions. TEX^{H}_{86} and TEX^{L}_{86} have a good correlation with present-day SSTs at temperatures higher than 15°C; thus, both can be used to reconstruct greenhouse world SSTs. Since the Paleogene temperatures were higher than 15°C, Kim et al. (2010) suggested use of TEX^{H}_{86} to compute temperature for the PETM sections due to its

smaller error (±2.5°C versus ±4°C for TEX^{H}_{86} and TEX^{L}_{86}, respectively). Moreover, the authors compared temperature records obtained from both indices at Wilson Lake, NJ, (Fig. 2) that showed similar temperature amplitudes during the PETM but different absolute values (Fig. 16). Kim et al. (2010) preferred use of TEX^{H}_{86} because it indicates higher temperatures (28-36°C) that are more expected to be during the PETM and rejected application of TEX^{L}_{86} due to its low background temperature (21°C) at the CIE onset (Fig. 16). The authors considered 21°C being too low for the PETM when CO_2 levels may have reached 3000 ppmv.

In contrast, Taylor et al. (2013) suggested that the TEX^{L}_{86} calibration was most appropriate for the warm Paleogene. Both TEX^{H}_{86} and TEX^{L}_{86} indicate similar SSTs above 15°C in the modern ocean; therefore, application of these indices for the Paleogene sediments should also yield similar SSTs. However, temperature records obtained from TEX^{H}_{86} and TEX^{L}_{86} at different locations reveal a large offset (ΔH-L) of 3.5-9°C in absolute temperatures for the Paleogene. Taylor et al. (2013) examined the relationship between ΔH-L and raw GDGT ratios in TEX^{H}_{86} and TEX^{L}_{86} indices and found that ΔH-L depends only on the GDGT-2/GDGT-3 ratio ([III]/[IV], see Fig. 7 for lipid's structures) that greatly varies with depth. Thus, in locations where water depths are greater than 1,000 m, ΔH–L values are low and GDGT-2/GDGT-3 ratio is high; whereas, at shallower depths (<1,000 m) both ΔH–L and GDGT-2/GDGT-3 ratio have a wide range. Since the coretop dataset for the TEX^{H}_{86} calibration is mostly derived from the deep-water settings (>1,000 m), the authors suggested use of the TEX^{L}_{86} calibration for "shallow" depths (<1,000 m). Moreover, Taylor et al. (2013) showed that the deep water thaumarchaeotal community produces different

proportions of GDGTs that can bias the surface GDGT distribution exported to sediments. Because most of the Paleogene datasets are from shallow depths, and particularly Millville core samples (Fig. 3), use of the TEX^{L}_{86} calibration should be more applicable for the PETM.

Application of the TEX^{H}_{86} calibration at Millville reveals a 5.5°C warming across the CIE onset (Fig. 15). Temperature increases from pre-CIE (899.30-909.44 ft; 274.11-277.20 m) values of ~30°C to ~35.5°C above the CIE onset (881.20-896.30 ft; 268.59-273.19 m). The warming occurs in two steps separated by a ~2 ft (59 cm) interval within which temperatures are about 33.5°C. The first step of 3.5°C is from ~30°C at 899.30 ft (274.11 m) to ~33.5°C at 898.47 ft (273.85 m) and the second step of 2°C is from ~33.5°C at 896.54 ft (273.27 m) to ~35.5°C at 896.30 ft (273.19 m). Within the CIE "core", temperatures remain constant at ~35.5°C in average and show a gradual 4.5°C decrease to 30.7°C towards the top of the core (857.00-881.20 ft; 261.21-268.59 m).

The TEX^{L}_{86} calibration at Millville implies a 7°C warming across the CIE onset (Fig. 15). Temperature increases from pre-CIE (899.30-909.44 ft; 274.11-277.20 m) values of ~23°C to ~30°C above the CIE onset (881.20-896.30 ft; 268.59-273.19 m). Similarly to TEX^{H}_{86}, TEX^{L}_{86} reveals that the warming occurred in two steps separated by a ~2 ft (59 cm) interval within which temperatures are about 27°C. The first step of 4°C is from ~23°C at 899.30 ft (274.11 m) to ~27°C at 898.47 ft (273.85 m) and the second step of 3°C is from ~27°C at 896.54 ft (273.27 m) to ~30°C at 896.30 ft (273.19 m). Within the CIE "core", temperature remains high and then decreases gradually within the 865.17-883.14 ft (263.70-269.18 m)

interval and more abruptly to almost pre-CIE values of 24°C at the upper section of the core (857.00-865.17 ft; 261.21-263.70 m).

Comparing two calibrations, both TEX^{H}_{86} and TEX^{L}_{86} exhibit warming across the CIE onset but different absolute temperatures values (ΔH-L varies between 1.9°C and 7.4°C, Fig. 15). TEX^{L}_{86} shows cooler temperatures and higher amplitude of warming. The calibrations show little precursor warming prior to the CIE onset, i.e., 1°C based on the TEX^{L}_{86} calibration and 1.5°C based on the TEX^{H}_{86} calibration). Moreover, they indicate that warming occurred in two steps with a more pronounced initial temperature increase of 3.5-4°C and the second temperature increase of 2-3°C. Within the CIE "core", both calibrations reveal constant temperatures that gradually decrease to almost pre-CIE values in the upper section of the core.

The identification of the warming onset, however, is arguable. To compute the amount of warming across the CIE onset, I used average base temperatures in the pre-CIE interval (dashed lines on Fig. 15). The purported precursors of 1.5°C and 1°C are within the errors on the TEX_{86} temperature estimates. Errors of 2.5°C and 4°C for TEX^{H}_{86} and TEX^{L}_{86}, respectively, are much higher than the estimated precursor warming (Fig. 15). Therefore, such slight precursors are negligible and both TEX^{H}_{86} and TEX^{L}_{86} records suggest no precursor warming at Millville. However, use of the absolute temperature values in the pre-CIE interval yields to different estimates, i.e. the TEX^{L}_{86} calibration still shows a very small or no precursor warming, whereas the TEX^{H}_{86} calibration indicates a 2.5°C pre-CIE

warming similar to what is observed at Bass River and Wilson Lake (Zachos et al., 2006; Sluijs et al., 2007).

Thereby, the criteria used to oppose the precursor warming are 1) large calibration errors in both TEX^{H}_{86} and TEX^{L}_{86} indices and 2) the choice of base temperatures for warming estimates. However, raw ratios of GTGTs that show only relative lipid distribution also indicate some differences in two records (Fig. 16). In this case only instrument error should be counted, which is very small for the liquid chromatography. Interestingly, raw GDGT ratio-1 (TEX^{L}_{86}) shows smaller amplitude change than GDGT ratio-2 (TEX^{H}_{86}) (Fig. 18). However, when calculating TEX_{86} indices (logarithmic functions of GDGT ratios) and calibrating them to temperatures, TEX^{L}_{86} indicates temperature change larger than TEX^{H}_{86} (Fig. 15). Moreover, similarly to calibrated TEX^{H}_{86} and TEX^{L}_{86} temperature records (Fig. 15), GDGT ratio-1 shows almost no change before the CIE onset, whereas GDGT-2 indicates a slight change in values prior to the CIE onset (Fig. 18). The GDGT ratios are different only by one component according to their formulas. Thus, inclusion of the extra component crenarchaeol in the formula and GDGT-3 and GDGT-4 in numerator (see Fig. 7 for lipid's structures) yields changes in relative lipid distribution before the CIE onset and thus in two GDGT ratios.

Previously published TEX_{86} temperature calibrations shows a possible precursor warming at Wilson Lake (Zachos et al., 2006; Sluijs et al., 2007) and Bass River, NJ (Sluijs et al., 2007). I compare temperature records at Wilson Lake Hole A, Bass River, and Millville applying TEX^{H}_{86} and TEX^{L}_{86} calibrations (Kim et al., 2010) and conclude that the precursor warming may be spurious depending on the

calibration (Fig. 16, 17). Comparison of Wilson Lake and Millville (Fig. 16) shows that there is a little to no precursor warming using TEX^{L}_{86}, whereas TEX^{H}_{86} shows some precursor. Sluijs et al. (2007) used a calibration similar to TEX^{H}_{86}, therefore they also indicated some precursor warming. Comparison of Bass River and Millville (Fig. 17), shows a possible small precursor warming of less than 2°C using TEX^{L}_{86} calibration and the precursor warming of 4°C applying TEX^{H}_{86} calibration. Thus, evidence for the precursor warming is equivocal because it only occurs in TEX^{H}_{86} and not TEX^{L}_{86}.

4.1.2. Mg/Ca ratio of planktonic foraminifera.

Integrating Mg/Ca records with stable isotope data indicates a pattern of warming coincident with the CIE. The sampling resolution for the analyses of trace metals in planktonic foraminifera is too low due to a lack of foraminifera in the pre-CIE interval and across the CIE onset. Therefore, the Mg/Ca record cannot provide information about the warming initiation in relation to the CIE onset, but it can give more reliable amplitude of temperature change across the CIE due to smaller error in temperature calibration (1°C in Mg/Ca analysis versus 2.5°C and 4°C in TEX^{H}_{86} and TEX^{L}_{86}).

I used the equation of Anand et al. (2003): Mg/Ca (PF) = f * 0.38 * exp(0.09T), where f = Mg/Ca (PETM water) / 5.2. Assuming that the Mg/Ca ratio of the seawater was 2.5 mmol/mol during the PETM (Cramer et al., 2011), temperatures in the intermediate layer (*Subbotina* Mg/Ca) increased from 29.5 to 34.3°C with an amplitude change of ~5°C (Fig. 19). Use of 1.5 mmol/mol for the Mg/Ca ratio of

seawater yields unrealistic temperatures changing from 35 to 40°C across the CIE onset (Fig. 19). Use of 3.5 mmol/mol for the Mg/Ca ratio of seawater yields temperature change from 26 to 31°C across the CIE onset similar in absolute temperature values calibrated by TEX^{L}_{86} (Fig. 19).

In summary, both trace metal and TEX_{86} proxies yield various absolute temperature values. Five different calibrations indicate a wide range of temperatures (23 to 40°C) across the CIE onset (Fig. 20). Among them, TEX^{L}_{86} and Mg/Ca ratio (Mg/Ca_{sw} = 3.5 mmol/mol) show the lowest absolute temperatures that look more realistic than indicated by other calibrations. Nevertheless, while the applied calibrations indicate different absolute temperatures, all of them show warming of 5 to 7°C across the CIE onset at Millville (Fig. 20).

4.2. Salinity estimates at Millville, NJ, during the PETM.

Salinity and $\delta^{18}O_{water}$ are linked through the mixing of river runoff and marine waters. Today, the mid-Atlantic river runoff has an average $\delta^{18}O_{water}$ value of ~-6‰. Assuming that the paleolatitude of Millville, NJ, during the PETM was similar to the modern latitude and the slope of the $\delta^{18}O_{water}$/salinity was also similar to the present day relationship, I used the equation to link absolute values of salinity and $\delta^{18}O_{water}$: $\delta^{18}O_{water}$ = 0.14 Salinity - 5.

To estimate $\delta^{18}O_{water}$, I applied the paleotemperature equation from O'Neil et al. (1969): $T = 16.9 - 4.38(\delta^{18}O_{calcite} - \delta^{18}O_{water}) + 0.1(\delta^{18}O_{calcite} - \delta^{18}O_{water})^2$ (eq. 1), where $\delta^{18}O_{calcite}$ is $\delta^{18}O$ of planktonic foraminifera (*Morozovella* spp. and *Subbotina*

spp.) and T is the water temperature calibrated from two paleothermometers, the TEX_{86} index and Mg/Ca ratio of planktonic foraminifera (*Morozovella* spp. and *Subbotina* spp.).

Use of *Morozovella* spp. and *Subbotina* spp. provides salinity estimates for the mixed layer and intermediate layer, respectively. Temperatures were derived from the same species using the Mg/Ca ratio (Anand et al. (2003) multispecies equation). I interpreted TEX_{86}-derived temperatures as the mixed-layer temperatures because both TEX^{H}_{86} and TEX^{L}_{86} indices are calibrated to SSTs (Kim et al, 2010). In order to define TEX_{86}-derived temperatures for the intermediate layer, I used the temperature difference between *Morozovella* spp. (mixed layer dwellers) and *Subbotina* spp. (intermediate dwellers). Mg/Ca ratios indicate ~2.5°C average difference between them; thus, the temperature of the intermediate layer can be calculated as: T_{int} = T (TEX_{86}) - 2.5°C. I excluded from the salinity estimate the *Acarinina* spp. data because: 1) I was not able to obtain a complete record due to rare occurrence; 2) apparent scatter in Mg/Ca values obtained from *Acarinina* spp. due to the incomplete record; 3) difficulty in constraining TEX_{86}-derived temperatures for *Acarinina* spp. due to the sparsely sampled Mg/Ca record; and 4) the *Acarinina* $\delta^{18}O$ record shows similarities with both *Morozovella* and *Subbotina* $\delta^{18}O$ records, indicating uncertainty in interpretation of the depth habitat of *Acarinina* spp.

The TEX^{H}_{86} calibration requires unrealistic salinities to satisfy the paleotemperature equation (eq. 1) (Fig. 21). For example, the 35°C temperatures predicted by the TEX^{H}_{86} calibration would require salinities on the order of 44 psu

for the pre-CIE interval while they should be similar to the present day salinities in the mid-Atlantic shelf, i.e. 31-35 psu (Geiger et al., 2011; Glenn et al., 2004). The TEX^{L}_{86} calibration yields realistic salinity estimates (33-34 psu for the pre-CIE interval) and a ~4 psu salinity decrease associated with the CIE onset (Fig. 21). It also indicates similar salinities for mixed and intermediate layers above the CIE onset. However, in the top section above 865.00 ft (263.65 m), salinity of the mixed layer is ~4 psu lower than in the intermediate layer (Fig. 21).

Use of temperature records derived from the Mg/Ca ratio of *Morozovella* spp. and *Subbotina* spp. required three scenarios for the salinity change that assume different values for long-term changes in the Mg/Ca ratio of seawater, which is 5.2 mmol/mol today but was lower in the past (Cramer et al., 2011; Fig. 21). Assuming the Mg/Ca ratio of seawater of 1.5 and 2.5 mmol/mol before the CIE onset (Cramer et al., 2011) yields salinities 48 and 56 psu, respectively. These salinity estimates are unrealistic. Use of 3.5 mmol/mol for the Mg/Ca ratio of the seawater yields realistic salinities of 32-35 psu above the CIE onset but indicates higher salinity of 40-43 psu for the pre-CIE interval. Also, the salinity change across the CIE onset is 5-6 psu; this is higher than the change from TEX_{86}-based salinity estimates. Such a difference is explained by different temperature increases across the CIE onset indicated by TEX^{L}_{86} and trace metal analyses (i.e. 7°C and 5°C warming, respectively).

The TEX^{L}_{86} calibration with a 23°C sea surface temperature in the pre-CIE interval and peak temperature of 30°C provides the most realistic salinities. Despite various absolute values, all salinity estimates require freshening of surface and

intermediate waters at the CIE onset in agreement with Kopp et al. (2009)'s hypothesis of an enhanced hydrological cycle. If I consider that Mg/Ca-derived temperature record is more accurate due to its smaller error than the TEX_{86} calibration, then there was a 5-6 psu freshening across the CIE onset.

Based on compilation (Fig. 22) of oxygen isotope records of planktonic foraminifera and temperatures obtained from TEX_{86} and trace metal analyses, I divided the Millville PETM section into 3 intervals (Fig. 23). The lower interval (stage 1, Fig. 23) reflects marine conditions on the Mid-Atlantic shelf before the CIE onset, i.e. pre-PETM. *Acarinina* spp. and *Subbotina* spp. $\delta^{18}O$ values differ by 1‰ that indicates mixed layer and intermediate layer habitats of these species, respectively. However, above the CIE onset, *Acarinina* spp. and *Subbotina* spp. $\delta^{18}O$ values are similar values suggesting similar temperatures in the mixed and intermediate layers. Also within this interval (stage 2, Fig. 23), Mg/Ca ratios of analyzed planktonic foraminifera species are similar and the most complete TEX_{86}-derived temperature record indicates high and stable temperatures. I link these observations to suggest a breakdown of the thermocline caused by increased storm activity that would have mixed surface and intermediate waters leading to diminished differences in temperatures and salinities. Salinity estimates also support this assumption displaying similar and constant values for mixed and intermediate layers above the CIE onset (Fig. 21). Finally, the upper section (stage 3, Fig. 23) shows a decrease in temperature as defined by TEX_{86}, Mg/Ca ratio and oxygen isotopes of planktonic foraminifera. *Acarinina* spp. and *Subbotina* spp. oxygen records once again have a 1‰ difference in $\delta^{18}O$ values that implies their

different depth habitats and redevelopment of the thermocline. Salinity estimates also show ~4 psu difference between mixed and intermediate layers also suggesting water stratification.

V. CONCLUSIONS

Using independent temperature proxies, I estimated the amount of warming and salinity change across the CIE and the Paleocene/Eocene boundary at Millville, NJ:

- The Mg/Ca ratio of planktonic foraminifera reveals a ~5°C warming from 29.5 to 34.3°C across the Paleocene/Eocene boundary.
- Organic paleothermometer TEX_{86} shows greater warming. Applying two different calibrations, I computed a 5.5°C warming from 30 to 35.5°C using the TEX^{H}_{86} calibration (Kim et al., 2010) and a 7°C warming from 23 to 30°C using the TEX^{L}_{86} calibration (Kim et al., 2010).
- Calibrations of TEX^{H}_{86} and Mg/Ca (Mg/Ca_{sw} = 1.5 and 2.5 mmol/mol) reveal very high temperatures, thus TEX^{L}_{86} and Mg/Ca (Mg/Ca_{sw} = 3.5 mmol/mol) show the best absolute values during the PETM.
- Calibration of temperatures yields a broad range of absolute values, thus it is more reliable to look at the amplitude of temperature change across the CIE onset. Due to smaller error in temperature calibration (1°C in Mg/Ca analysis versus 2.5°C and 4°C in TEX^{H}_{86} and TEX^{L}_{86}), Mg/Ca ratio of planktonic foraminifera provides the best estimate for warming across the CIE onset of ~5°C.

- Comparison of TEX_{86} data from Millville (this study) and two proximal New Jersey core sites Wilson Lake and Bass River (Zachos et al., 2006; Sluijs et al., 2007) indicates that the precursor warming before the CIE onset proposed by Sluijs et al. (2007) may be spurious because it only occurs in TEX^{H}_{86} and not TEX^{L}_{86}.
- Salinity estimates using temperatures from TEX^{H}_{86} calibration (Kim et al., 2010) and Mg/Ca ratio from planktonic foraminifera (Anand et al. (2003) equation and Mg/Ca_{sw} = 1.5 and 2.5 mmol/mol) yield unrealistic values exceeding 44 psu.
- The temperature calibration from TEX^{L}_{86} yields realistic salinity estimates. It suggests that temperatures calibrated with TEX^{L}_{86} represent the best absolute values.
- Use of all temperature calibrations requires a ~4-6 psu salinity decrease associated with the CIE onset. It implies freshening of surface and intermediate waters during the CIE onset due to an enhanced hydrologic cycle proposed by Kopp et al. (2009).
- The evidence of the water freshening across the CIE onset is consistent with the proposed thermocline breakdown caused by increased storm intensity during the PETM.

REFERENCES

Anand, P., H. Elderfield, and M.H. Conte (2003). Calibration of Mg/Ca thermometry in planktonic foraminifera from a sediment trap time series. *Paleoceanography*, Vol. 18, No. 2, pp. 1-15, doi:10.1029/2002PA000846

Billups, K. and D.P. Schrag (2002). Paleotemperatures and ice volume of the past 27 Myr revisited with paired Mg/Ca and $^{18}O/^{16}O$ measurements on benthic foraminifera. *Paleoceanography*, Vol. 17, No. 1, pp. 1-11

Bralower, T.J., J.C. Zachos, E. Thomas, M. Parrow, C.K. Paull, D.C. Kelly, I. Premoli Silva, W.V. Sliter, and K.C. Lohmann (1995). Late Paleocene to Eocene paleoceanography of the equatorial Pacific Ocean: stable isotopes recorded at Ocean Drilling Program Site 865, Allison Guyot. *Paleoceanography*, Vol. 10, pp. 841-865

Broecker, W.S. and T.-H. Peng (1987). The role of $CaCO_3$ compensation in the glacial to interglacial atmospheric CO_2 change. *Global Biogeochemical Cycles*, Vol. 1, No. 1, pp. 15-29

Boyle, E.A. and L.D. Keigwin (1985). Comparison of Atlantic and Pacific paleochemical records for the last 215,000 years: changes in deep ocean circulation and chemical inventories. *Earth and Planetary Science Letters*, Vol. 76, pp. 135-150

Brassell, S.C., G. Eglinton, I.T. Marlowe, U. Pflaumann, and M. Sarnthein (1986). Molecular stratigraphy: a new tool for climatic assessment. *Nature*, Vol. 320, pp. 129-133

Coggon, R., D. Teagle, C. Smith-Duque, J. Alt, and M. Cooper (2010). Reconstructing past seawater Mg/Ca and Sr/Ca from mid-ocean ridge flank calcium carbonate veins. *Science*, Vol. 327, pp. 1114-1117

Cramer, B.S., M.-P. Aubry, K.G. Miller, R.K. Olsson, J.D. Wright, and D.V. Kent (1999). An exceptional chronologic, isotopic, and clay mineralogic record at the latest Paleocene thermal maximum, Bass River, NJ, ODP 174AX. *Bulletin de la Société géologique de France*, Vol. 170, No. 6, pp. 883-897

Cramer, B.S. and D.V. Kent (2005). Bolide summer: The Paleocene/Eocene thermal maximum as a response to an extraterrestrial trigger. *Palaeogeography, Palaeoclimatology, Palaeoecology*, Vol. 224, pp. 144-166

Cramer, B.S., K.G. Miller, P.J. Barrett, and J.D. Wright (2011). Late Cretaceous–Neogene trends in deep ocean temperature and continental ice volume: Reconciling records of benthic foraminiferal geochemistry ($\delta^{18}O$ and Mg/Ca) with sea level history. *Journal of Geophysical Research*, Vol. 116, pp. 1-23, doi:10.1029/2011JC007255

DeConto, R.M., S. Galeotti, M. Pagani, D. Tracy, K. Schaefer, T. Zhang, D. Pollard, and D.J. Beerling (2012). Past extreme warming events linked to massive carbon release from thawing permafrost. *Nature*, Vol. 484, pp. 87-91

D'Hondt, S., J. Zachos, and G. Schultz (1994). Stable isotopic signals and photosymbiosis in late Paleocene planktic foraminifera. *Paleobiology*, Vol. 20, pp. 391-406

Dickens, G.R., J.R. O'Neil, D.K. Rea, and R.M. Owen (1995). Dissociation of oceanic methane hydrate as a cause of the carbon isotope excursion at the end of the Paleocene. *Paleoceanography*, Vol. 10, No. 6, pp. 965-971

Dickens, G.R., M.M. Castillo, and J.C.G. Walker (1997). A blast of gas in the latest Paleocene: Simulating first-order effects of massive dissociation of oceanic methane hydrate. *Geology*, Vol. 25, No. 3, pp. 259-262

Elderfield, H., and G. Ganssen (2000). Past temperature and $\delta^{18}O$ of surface ocean waters inferred from foraminiferal Mg/Ca ratios. *Nature*, Vol. 405, pp. 442-445

Elderfield, H., M. Vautravers, and M. Cooper (2002). The relationship between shell size and Mg/Ca, Sr/Ca, $\delta^{18}O$, and $\delta^{13}C$ of species of planktonic foraminifera. *Geochemistry Geophysics Geosystems*, Vol. 3, No. 8, pp. 1-13

Epstein, S., R. Buchsbaum, H. Lowenstam, and H.C. Urey (1951). Carbonate-water temperature scale. *Bulletin of the Geological Society of America*, Vol. 62, pp. 417-426

Esmeray-Senlet, S., J.D. Wright, R.K. Olsson, K.G. Miller, and J.V. Browning (2013). Evidence of the Living Ocean following the Creatceous/Paleogene Mass Extinction (in review)

Fairbanks R.G., M. Sverdlove, R. Free, P.H. Wiebe, and A.W.H. Bé (1982). Vertical distribution and isotopic fractionation of living planktonic foraminifera in the Panama Basin. *Nature*, Vol. 298, pp. 841-844

Farley, K.A. and S.F. Eltgroth (2003). An alternative age model for the Paleocene-Eocene thermal maximum using extraterrestrial ^{3}He. *Earth and Planetary Science Letters*, Vol. 208, pp. 135-148

Farrimond, P., G. Eglinton, and S.C. Brassell (1986). Alkenones in Cretaceous black shales, Blake-Bahama Basin, western North Atlantic. *Organic Geochemistry*, Vol. 10, pp. 897-903

Geiger, E.F., M.D. Grossi, A.C. Trembanis, J.T. Kohut, M.J. Oliver (2011). Satellite-derived coastal ocean and estuarine salinity in the Mid-Atlantic. Continental Shelf Research, Vol. 63, pp. 235–242, doi:10.1016/j.csr.2011.12.001

Gibson, T.G., L.M. Bybell, and J.P. Owens (1993). Latest Paleocene lithologic and biotic events in neritic deposits of southwestern New Jersey. *Paleoceanography*, Vol. 8, No. 4, pp. 495-514

Glenn, S., R. Arnone, T. Bergmann, W.P. Bissett, M. Crowley, J. Cullen, J. Gryzmski, D. Haidvogel, J. Kohut, M. Moline, M. Oliver, C. Orrico, R. Sherrell, T. Song, A. Weidemann, R. Chant, and O. Schofield (2004). Biogeochemical impact of summertime coastal upwelling on the New Jersey Shelf. *Journal of Geophysical Research*, Vol. 109, pp. 1-15, doi:10.1029/2003JC002265

Glenn, S.M., C. Jones, M. Twardowski, L. Bowers, J. Kerfoot, D. Webb, and O. Schofield (2008). Glider observations of sediment resuspension in a Middle Atlantic Bight fall transition storm. *Limnology and Oceanography*, Vol. 53, pp. 2180-2196

Gradstein, F.M., J.G. Ogg, M.D. Schmitz, and G.M. Ogg (2012). The geologic time scale 2012 2-Volume Set. Published by *Elsevier BV*, 1176 p.

Harris, A.D., K.G. Miller, J.V. Browning, P.J. Sugarman, R.K. Olsson, B.S. Cramer, and J.D. Wright (2010). Integrated stratigraphic studies of Paleocene-lowermost Eocene sequences, New Jersey Coastal Plain: Evidence for glacioeustatic control. *Paleoceanography*, Vol. 25, pp. 1-18, doi:10.1029/2009PA001800

Hartley, G. and A. Mucci (1996). The influence of P_{CO2} on the partitioning of magnesium in calcite overgrowths precipitated from artificial seawater at 25° and 1 atm total pressure. *Geochimica et Cosmochimica Acta*, Vol. 60, No. 2, pp. 315-324

Herbert, T.D. (2003). Alkenones as paleotemperature indicators. *Treatise on Geochemistry*, Vol. 6, pp. 391-432

Higgins, J.A. and D.P. Schrag (2006). Beyond methane: Towards a theory for the Paleocene-Eocene Thermal Maximum. *Earth and Planetary Science Letters*, Vol. 245, pp. 523-537

Hopmans, E.C., S. Schouten, R.D. Pancost, M.T.J. van der Meer, and J.S. Sinninghe Damsté (2000). Analysis of intact tetraether lipids in archaeal cell material and sediments using high performance liquid chromatography/atmospheric pressure ionization mass spectrometry. *Rapid Communications in Mass Spectrometry*, Vol. 14, pp. 585-589

Hopmans, E.C., J.W.H. Weijers, E. Schefuβ, L. Herfort, J.S. Sinninghe Damsté, and S. Schouten (2004). A novel proxy for terrestrial organic matter in sediments based on branched and isoprenoid tetraether lipids. *Earth and Planetary Science Letters*, Vol. 224, pp. 107-116

John, C.M., S.M. Bohaty, J.C. Zachos, A. Sluijs, S. Gibbs, H. Brinkhuis, and T.J. Bralower (2008). North American continental margin records of the Paleocene-Eocene thermal maximum: Implications for global carbon and hydrological cycling. *Paleoceanography*, Vol. 23, pp. 1-20, doi:10.1029/2007PA001465

Karner, M.B., E.F. DeLong, and D.M. Karl (2001). Archaeal dominance in the Mesopelagic zone of the Pacific Ocean. *Nature*, Vol. 409, pp. 507-510

Katz, A. (1973). The interaction of magnesium with calcite during crystal growth at 25-90°C and one atmosphere. *Geochimica et Cosmochimica Acta*, Vol. 37, pp. 1563-1586

Katz, M.E., B.S. Cramer, G.S. Mountain, S. Katz, and K.G. Miller (2001). Uncorking the bottle: What triggered the Paleocene/Eocene thermal maximum methane release? *Paleoceanography*, Vol. 16, No. 6, pp. 549-562

Kennett, J.P. and L.D. Stott (1991). Abrupt deep-sea warming, palaeoceanographic changes and benthic extinctions at the end of the Palaeocene. *Nature*, Vol. 353, pp. 225-229

Kent, D.V., B.S. Cramer, L. Lanci, D. Wang, J.D. Wright, and R. Van der Voo (2003). A case for a comet impact trigger for the Paleocene/Eocene thermal maximum and carbon isotope excursion. *Earth and Planetary Science Letters*, Vol. 211, pp. 13-26

Kim, J.-H., S. Schouten, E.C. Hopmans, B. Donner, and J.S. Sinninghe Damsté (2008). Global sediment core-top calibration of the TEX_{86} paleothermometer in the ocean. *Geochimica et Cosmochimica Acta*, Vol. 72, pp. 1154-1173

Kim, J.-H., J. van der Meer, S. Schouten, P. Helmke, V. Willmott, F. Sangiorgi, N. Koc, E.C. Hopmans, and J.S. Sinninghe Damsté (2010). New indices and calibrations derived from the distribution of crenarchaeal isoprenoid tetraether lipids: implications for past sea surface temperature reconstructions. *Geochimica et Cosmochimica Acta*, Vol. 74, pp. 4639-4654

Koch, P.L., J.C. Zachos, and P.D. Gingerich (1992). Correlation between isotope records in marine and continental carbon reservoirs near the Palaeocene/Eocene boundary. *Nature*, Vol. 358, pp. 319-322

Kopp, R.E., D. Schumann, T.D. Raub, D.S. Powars, L.V. Godfrey, N.L. Swanson-Hysell, A.C. Maloof, and H. Vali (2009). An Appalachian Amazon? Magnetofossil evidence for the development of a tropical river-like system in the mid-Atlantic United States during the Paleocene-Eocene thermal maximum. *Paleoceanography*, Vol. 24, pp. 1-17, doi:10.1029/2009PA001783

Kurtz, A.C., L.R. Kump, M.A. Arthur, J.C. Zachos, and A. Paytan (2003). Early Cenozoic decoupling of the global carbon and sulfur cycles. *Paleoceanography*, Vol. 18, No. 4, pp. 1-14, doi:10.1029/2003PA000908

Lea, D.W., T.A. Mashiotta, and H.J. Spero (1999). Controls on magnesium and strontium uptake in planktonic foraminifera determined by live culturing, *Geochimica et Cosmochimica Acta*, Vol. 63, No. 16, pp. 2369-2379

Lea, D.W., D.K. Pak, and H.J. Spero (2000). Climate impact of late Quaternary equatorial Pacific sea surface temperature variations. *Science*, Vol. 289, pp. 1719-1724

Lear, C.H., Y. Rosenthal, and N. Slowey (2002). Benthic foraminiferal Mg/Ca-paleothermometry: A revised core-top calibration. *Geochimica et Cosmochimica Acta*, Vol. 66, No. 19, pp. 3375-3387

Lombardi, C.J. (2013) Lithostratigraphy and clay mineralogy of Paleocene-Eocene thermal maximum sediments at Wilson Lake, NJ. M.Sc. Thesis, Rutgers University, 94 p.

Marlowe, I.T., J.C. Green, A.C. Neal, S.C. Brassell, G. Eglinton, and P.A. Course (1984 a). Long chain (n-C_{37}-C_{39}) alkenones in the Prymnesiophyceae. Distribution of alkenones and other lipids and their taxonomic significance. *British Phycological Journal*, Vol. 19, pp. 203-216

Marlowe, I.T., S.C. Brassell, G. Eglinton, and J.C. Green (1984 b). Long chain unsaturated ketones and esters in living algae and marine sediments. *Organic Geochemistry*, Vol. 6, pp. 135-141

Marlowe, I.T., S.C. Brassell, G. Eglinton, and J.C. Green (1990). Long-chain alkenones and alkyl alkenoates and the fossil coccolith record of marine sediments. *Chemical Geology*, Vol. 88, pp. 349-375

McInerney, F.A. and S.L. Wing (2011). The Paleocene-Eocene thermal maximum: a perturbation of carbon cycle, climate, and biosphere with implications for the future. *Annual Review of Earth and Planetary Sciences*, Vol. 39, pp. 489-516

Miller, K.G., P.J. Sugarman, J.V. Browning, M.-P. Aubry, G.J. Brenner, G.III Cobbs, L. de Romero, M.D. Feigenson, A. Harris, M.E. Katz, A. Kulpecz, P.P.Jr. McLaughlin, S. Misintseva, D.H. Monteverde, R.K. Olsson, L. Patrick, S.J. Pekar, and J. Uptegrove (2005). Millville site, *in* K.G. Miller, P.J. Sugarman, J.V. Browning et al., Proceedings of the Ocean Drilling Program, Scientific results, Volume 174AX (supplement): College Station, Texas, Ocean Drilling Program, pp. 1-95

Murphy, B.H., K.A. Farley, and J.C. Zachos (2010). An extraterrestrial ^{3}He-based timescale for the Paleocene-Eocene thermal maximum (PETM) from Walvis

Ridge, IODP Site 1266. *Geochimica et Cosmochimica Acta*, Vol. 74, pp. 5098-5108

Müller P.J., G. Kirst, G. Ruhland, I. von Storch, and A. Rosell-Mele (1998). Calibration of the alkenone paleotemperature index $U^{K'}_{37}$ based on core-tops from the eastern South Atlantic and the global ocean (60°N–60°S). *Geochimica at Cosmochimica Acta*, Vol. 62, No. 10, pp. 1757-1772

Nürnberg, D., J. Bijma, and C. Hemleben (1996). Assessing the reliability of magnesium in foraminiferal calcite as a proxy for water mass temperatures. *Geochimica at Cosmochimica Acta*, Vol. 60, No. 5, pp. 803-814

O'Neil, J.R., R.N. Clayton, and T.K. Mayeda (1969). Oxygen isotope fractionation in divalent metal carbonates. *Journal of Chemical Physics*, Vol. 51, No. 12, pp. 5547-5558

Pagani, M., N. Pedentchouk, M. Huber, A. Sluijs, S. Schouten, H. Brinkhuis, J.S. Sinninghe Damsté, G.R. Dickens, and the Expedition 302 Scientists (2006). Arctic hydrology during global warming at the Palaeocene/Eocene thermal maximum. *Nature*, Vol. 442, pp. 671-675

Patterson, M.V. and D. Francis (2013). Kimberlite eruptions as triggers for early Cenozoic hyperthermals. *Geochemistry Geophysics Geosystems*, Vol. 14, No. 2, pp. 448-456

Prahl, F.G. and S.G. Wakeham (1967). Calibration of unsaturation patterns in long-chain ketone compositions for palaeotemperature assessment. *Nature*, Vol. 330, pp. 367-369

Röhl, U., T. Westerhold, T.J. Bralower, and J.C. Zachos (2007). On the duration of the Paleocene-Eocene thermal maximum (PETM). *Geochemistry Geophysics Geosystems*, Vol. 8, No. 12, pp. 1-13

Rosenthal, Y. and E.A. Boyle (1993). Factors controlling the fluoride content of planktonic foraminifera: An evaluation of its paleoceanographic applicability. *Geochimica at Cosmochimica Acta*, Vol. 57, No. 2, pp. 335‑346

Rosenthal, Y., E.A. Boyle, and N. Slowey (1997). Temperature control on the incorporation of magnesium, strontium, fluorine, and cadmium into benthic foraminiferal shells from Little Bahama Bank: Prospects for thermocline paleoceanography. *Geochimica at Cosmochimica Acta*, Vol. 61, No. 17, pp. 3633-3643

Rosenthal, Y., M.P. Field, and R.M. Sherrell (1999). Precise Determination of Element/Calcium Ratios in Calcareous Samples Using Sector Field Inductively Coupled Plasma Mass Spectrometry. *Analytical Chemistry*, Vol. 71, pp. 3248-3253

Schouten, S., E.C. Hopmans, E. Schefuβ, and J.S. Sinninghe Damsté (2002). Distributional variations in marine crenarchaeotal membrane lipids: a new tool for reconstructing ancient sea water temperatures? *Earth and Planetary Science Letters*, Vol. 204, pp. 265-274

Schouten, S., C. Huguet, E.C. Hopmans, M.V.M. Kienhuis, and J.S. Sinninghe Damsté (2007). Analytical methodology for TEX_{86} paleothermometry by High-Performance Liquid Chromatography/Atmospheric Pressure Chemical Ionization-Mass Spectrometry. *Analytical Chemistry*, Vol. 79, pp. 2940-2944

Schouten, S., E.C. Hopmans, and J.S. Sinninghe Damsté (2013). The organic geochemistry of glycerol dialkyl glycerol tetraether lipids: A review. *Organic Geochemistry*, Vol. 54, pp. 19-61

Sikes E.L., J.W. Farrington, and L.D. Keigwin (1991). Use of the alkenone unsaturation ratio U^{K}_{37} to determine past sea surface temperatures: core-top SST calibrations and methodology considerations. *Earth and Planetary Science Letters*, Vol. 104, pp. 36-47

Sinninghe Damsté, J.S., S. Schouten, E.C. Hopmans, A.C.T. van Duin, and J.A.J. Geenevasen (2002). Crenarchaeol: the characteristic core glycerol dibiphytanyl glycerol tetraether membrane lipid of cosmopolitan pelagic crenarchaeota. *Journal of Lipid Research*, Vol. 43, pp. 1641-1651

Sluijs, A., S. Schouten, M. Pagani, M. Woltering, H. Brinkhuis, J.S. Sinninghe Damsté, G.R. Dickens, M. Huber, G.-J. Reichart, R. Stein, J. Matthiessen, L.J. Lourens, N. Pedentchouk, J. Backman, K. Moran, and the Expedition 302 Scientists (2006). Subtropical Arctic Ocean temperatures during the Palaeocene/Eocene thermal maximum. *Nature*, Vol. 441, pp. 610-613

Sluijs, A., H. Brinkhuis, S. Schouten, S.M. Bohaty, C.M. John, J.C. Zachos, G.-J. Reichart, J.S. Sinninghe Damste, E.M. Crouch, and G.R. Dickens (2007). Environmental precursors to rapid light carbon injection at the Palaeocene/Eocene boundary. *Nature*, Vol. 450, pp. 1218-1222

Stanley, S.M. and L.A. Hardie (1998). Secular oscillations in the carbonate mineralogy of reef-building and sediment-producing organisms driven by tectonically forced shifts in seawater chemistry. *Palaeogeography, Palaeoclimatology, Palaeoecology*, Vol. 144, pp. 3-19

Steckler, M.S., G.S. Mountain, K.G. Miller, and N. Christie-Blick (1999). Reconstruction of Tertiary progradation and clinoform development on the New Jersey passive margin by 2-D backstripping. *Marine Geology*, Vol. 154, pp. 399-420

Storey, M., R.A. Duncan, and C.C. Swisher III (2007). Paleocene-Eocene thermal maximum and the opening of the Northeast Atlantic. *Science*, Vol. 316, pp. 587-589

Svensen, H., S. Planke, A. Malthe-Sørenssen, B. Jamtveit, R. Myklebust, T. Rasmussen Eidem, and S.S. Rey (2004). Release of methane from a volcanic basin as a mechanism for initial Eocene global warming. *Nature*, Vol. 429, pp. 542-545

Taylor, K.W.R., M. Huber, C.J. Hollis, M.T. Hernandez-Sanchez, and R.D. Pancost (2013). Re-evaluating modern and Palaeogene GDGT distributions: Implications for SST reconstructions. *Global and Planetary Change*, Vol. 108, pp. 158-174

Thomas, E. and N.J. Shackleton (1996). The Palaeocene-Eocene benthic foraminiferal extinction and stable isotope anomalies. In: R.W.O.B. Knox, R.M. Corfield and R.E. Dunay (Editors) Correlation of the Early Paleogene in Northwestern Europe, Geological Society London Special Publication. *Geological Society, London, Special Publications*, Vol. 101, pp. 401-441

Thomas, D.J., T.J. Bralower, and J.C. Zachos (1999). New evidence for subtropical warming during the late Paleocene thermal maximum: Stable isotopes from Deep Sea Drilling Project Site 527, Walvis Ridge. *Paleoceanography*, Vol. 14, No. 5, pp. 561-570

Thomas, D.J., J.C. Zachos, T.M. Bralower, E. Thomas, and S. Bohaty (2002). Warming the fuel for the fire: Evidence for the thermal dissociation of methane hydrate during the Paleocene-Eocene thermal maximum. *Geology*, Vol. 30, No. 12, pp. 1067-1070

Tripati, A.K. and H. Elderfield (2004). Abrupt hydrographic changes in the equatorial Pacific and subtropical Atlantic from foraminiferal Mg/Ca indicate greenhouse origin for the thermal maximum at the Paleocene-Eocene Boundary. *Geochemistry Geophysics Geosystems*, Vol. 5, No. 2, pp. 1-11, doi:10.1029/2003GC000631

Tripati, A.K. and H. Elderfield (2005). Deep-Sea Temperature and Circulation Changes at the Paleocene-Eocene Thermal Maximum. *Science*, Vol. 308, pp. 1894-1898

Urey, H.C. (1947). The thermodynamic properties of isotopic substances. *Journal of the Chemical Society*, pp. 562-581

Walsh, E.M., A.E. Ingalls, and R.G. Keil (2008). Sources and transport of terrestrial organic matter in Vancouver Island fjords and the Vancouver-Washington Margin: a multiproxy approach using $\delta^{13}C_{org}$, lignin phenols, and the ether lipid BIT index. *Limnology and Oceanography*, Vol. 53, pp. 1054-1063

Weijers, J.W.H., S. Schouten, O.C. Spaargaren, and J.S. Sinninghe Damsté (2006). Occurrence and distribution of tetraether membrane in soils: implications for the use of the BIT index and the TEX_{86} SST proxy. *Organic Geochemistry*, Vol. 37, pp. 1680-1693

Wilkinson, B.H. and T.J. Algeo (1989). Sedimentary carbonate record of calcium-magnesium cycling. *American Journal of Science*, Vol. 289, pp. 1158-1194

Wing, S.L., G.J. Harrington, F.A. Smith, J.I. Bloch, D.M. Boyer, and K.H. Freeman (2005). Transient floral change and rapid global warming at the Paleocene-Eocene boundary. *Science*, Vol. 310, pp. 993-996

Wright, J.D. and M.F. Schaller (2013). Evidence for a rapid release of carbon at the Paleocene-Eocene thermal maximum. *Proceedings of the National Academy of Sciences of the United States of America*, Vol. 110, No. 40, pp. 15908-15913

Wuchter, C., S. Schouten, M.J.L. Coolen, and J.S. Sinninghe Damsté (2004). Temperature-dependent variation in the distribution of tetraether membrane lipids of marine Crenarchaeota: Implications for TEX_{86} paleothermometry. *Paleoceanography*, Vol. 19, pp. 1-10, PA4028, doi:10.1029/2004PA001041

Zachos, J. C., M.W. Wara, S.M. Bohaty, M.L. Delaney, M. Rose-Petrizzo, A. Brill, T.J. Bralower, and I. Premoli-Silva (2003). A transient rise in tropical sea surface temperature during the Paleocene-Eocene thermal maximum. *Science*, Vol. 302, pp. 1551-1554

Zachos, J.C., U. Röhl, S.A. Schellenberg, A. Sluijs, D.A. Hodell, D.C. Kelly, E. Thomas, M. Nicolo, I. Raffi, L.J. Lourens, H. McCarren, and D. Kroon (2005). Rapid acidification of the ocean during the Paleocene-Eocene thermal maximum. *Science*, Vol. 308, pp. 1611-1615

Zachos, J.C., S. Schouten, S. Bohaty, T. Quattlebaum, A. Sluijs, H. Brinkhuis, S.J. Gibbs, and T.J. Bralower (2006). Extreme warming of mid-latitude coastal ocean during the Paleocene-Eocene Thermal Maximum: Inferences from TEX_{86} and isotope data. *Geology*, Vol. 34, No. 9, pp. 737-740

Zeebe, R.E., J.C. Zachos, and G.R. Dickens (2009). Carbon dioxide forcing alone insufficient to explain Palaeocene-Eocene Thermal Maximum warming. *Nature Geoscience*, Vol. 2, pp. 576-580

TABLE CAPTIONS

1. List of the samples from the uppermost Paleocene-lower Eocene section of the ODP Leg 174AX core located at Millville, NJ. Yellow color specifies the "critical" part across the CIE with high-resolution sampling interval of 4-6 ft (10-15 cm). Quotation marks indicate parts of the core with uncertain sampling depths due to core expansion or shift in a tray.

2. General information about the analyzed samples: sample weight, moisture loss, and percentage of sand fraction (>63 μm).

3. Stable isotopes ($\delta^{13}C$ and $\delta^{18}O$) of bulk carbonate and percent carbonate ($CaCO_3$).

4. Stable isotopes ($\delta^{13}C$ and $\delta^{18}O$) of *Morozovella* spp.

5. Stable isotopes ($\delta^{13}C$ and $\delta^{18}O$) of *Acarinina* spp.

6. Stable isotopes ($\delta^{13}C$ and $\delta^{18}O$) of *Subbotina* spp.

7. Mg/Ca ratio of *Morozovella* spp.; R stands for rejected samples due to possible diagenesis (D?) or high concentrations of iron (high Fe).

8. Mg/Ca ratio of *Acarinina* spp.; R stands for rejected samples due to low calcium concentrations (low Ca) or high concentrations of iron (high Fe).

9. Mg/Ca ratio of *Subbotina* spp.; R stands for rejected samples due to possible diagenesis (D?) or high concentrations of iron (high Fe).

10. TEX_{86} results: peak areas of GDGTs, values of the TEX^{H}_{86} and TEX^{L}_{86} indices, and calibrated temperatures using equations from Kim et al. (2010).

11. BIT index values.

12. Calibrated temperatures from Mg/Ca ratio of planktonic foraminifera using a multi-species equation of Anand et al. (2003).

13. Paleosalinity estimations using calibrated temperatures from TEX^{H}_{86} and TEX^{L}_{86} indices (Kim et al., 2010) and oxygen isotopic records of planktonic foraminifera *Morozovella* spp. (mixed layer dwellers).

14. Paleosalinity estimations using calibrated temperatures from TEX^{H}_{86} and TEX^{L}_{86} indices (Kim et al., 2010) and oxygen isotopic records of planktonic foraminifera *Subbotina* spp. (intermediate layer dwellers).

15. Paleosalinity estimations using calibrated temperatures from Mg/Ca ratio (multi-species equation of Anand et al. (2003)) and oxygen isotopic records of planktonic foraminifera *Morozovella* spp., *Acarinina* spp., and *Subbotina* spp.

Table 1

Initial sampling

Sample #	Depth interval, ft		Mean depth, ft	Mean depth, m
	top	bottom		
1	857.00	857.10	857.05	261.23
2	858.92	859.07	859.00	261.82
3	861.10	861.20	861.15	262.48
4	"863.00"	"863.15"	"863.08"	"263.07"
5	865.10	865.18	865.14	263.69
6	867.00	867.15	867.08	264.28
7	869.00	869.10	869.05	264.89
8	870.88	871.00	870.94	265.46
9	873.02	873.13	873.08	266.11
10	875.00	875.10	875.05	266.72
11	876.95	877.06	877.01	267.31
12	879.07	879.20	879.14	267.96
13	881.10	881.20	881.15	268.57
14	883.05	883.16	883.11	269.17
15	885.06	885.17	885.12	269.78
16	886.99	887.10	887.05	270.37
17	889.08	889.20	889.14	271.01
18	890.90	891.02	890.96	271.56
19	893.04	893.16	893.10	272.22
20	895.09	895.19	895.14	272.84

shifted in tray

Additional sampling

Sample #	Depth interval, ft		Mean depth, ft	Mean depth, m
	top	bottom		
1	856.90	857.00	856.95	261.20
2	858.88	858.95	858.92	261.80
3	861.20	861.30	861.25	262.51
4	"863.15"	"863.20"	"863.18"	"263.10"
5	865.18	865.24	865.21	263.72
6	867.15	867.25	867.20	264.32
7	869.10	869.25	869.18	264.93
8	870.82	870.88	870.85	265.44
9	872.94	873.02	872.98	266.08
10	875.10	875.20	875.15	266.75
11	877.06	877.20	877.13	267.35
12	879.20	879.32	879.26	268.00
13	881.20	881.30	881.25	268.61
14	883.16	883.23	883.20	269.20
15	885.17	885.25	885.21	269.81
16	887.10	887.20	887.15	270.40
17	889.20	889.30	889.25	271.04
18	891.02	891.06	891.04	271.59
19	893.16	893.26	893.21	272.25
20	895.19	895.30	895.25	272.87

Table 1 cont.

21	896.44	896.54	896.49	273.25		21	896.25	896.35	896.30	273.19
22	896.98	897.11	897.05	273.42		22	896.54	896.64	896.59	273.28
23	897.31	897.43	897.37	273.52		23	897.11	897.22	897.17	273.46
24	897.66	897.72	897.69	273.62		24	897.78	897.90	897.84	273.66
25	"898.16"	"898.23"	"898.20"	"273.77"	shifted in tray	25	"898.45"	"898.60"	"898.53"	"273.87"
26	898.34	898.45	898.40	273.83		26	898.80	898.90	898.85	273.97
27	898.64	898.74	898.69	273.92		27	899.05	899.20	899.13	274.05
28	898.94	899.09	899.02	274.02		28	899.31	899.40	899.36	274.12
29	899.20	899.31	899.26	274.09		29	899.65	899.70	899.68	274.22
30	899.73	899.82	899.78	274.25		30	899.82	899.88	899.85	274.27
31	"900.16"	"900.29"	"900.23"	"274.39"	core expansion	31	"900.07"	"900.16"	"900.12"	"274.36"
32	900.18	900.30	900.24	274.39		32	900.30	900.40	900.35	274.43
33	901.12	901.30	901.21	274.69		33	900.95	901.05	900.00	274.32
34	901.87	902.00	901.94	274.91		34	901.81	901.87	901.84	274.88
35	903.67	903.80	903.74	275.46		35	903.42	903.52	903.47	275.38
36	905.66	905.74	905.70	276.06		36	905.50	905.56	905.53	276.01
37	907.63	907.75	907.69	276.66		37	907.45	907.55	907.50	276.61
38	909.36	909.45	909.41	277.19		38	909.45	909.52	909.49	277.21

Table 2

Depth interval, ft		Mean depth, ft	Mean depth, m	Weight, g	Dry weight, g	Moisture loss, g	Moisture loss, %	Fraction > 63 µm, g	Fraction > 63 µm, %
top	bottom								
857.00	857.10	857.05	261.23	44.26	41.42	2.84	6.4	3.80	9.2
858.92	859.07	859.00	261.82	67.12	62.36	4.76	7.1	3.14	5.0
861.10	861.20	861.15	262.48	37.42	35.52	1.90	5.1	0.56	1.6
863.00	863.15	863.08	263.07	47.76	46.00	1.76	3.7	0.50	1.1
865.10	865.18	865.14	263.69	25.30	23.58	1.72	6.8	0.22	0.9
867.00	867.15	867.08	264.28	70.40	65.92	4.48	6.4	0.42	0.6
869.00	869.10	869.05	264.89	23.62	22.58	1.04	4.4	0.24	1.1
870.88	871.00	870.94	265.46	49.64	46.76	2.88	5.8	0.36	0.8
873.02	873.13	873.08	266.11	34.74	32.54	2.20	6.3	0.30	0.9
875.00	875.10	875.05	266.72	30.82	28.64	2.18	7.1	0.60	2.1
876.95	877.06	877.01	267.31	45.22	41.54	3.68	8.1	0.34	0.8
879.07	879.20	879.14	267.96	44.36	40.78	3.58	8.1	0.48	1.2
881.10	881.20	881.15	268.57	42.92	41.62	1.30	3.0	0.44	1.1
883.05	883.16	883.11	267.17	50.10	47.68	2.42	4.8	0.50	1.0
885.06	885.17	885.12	269.78	52.32	50.82	1.50	2.9	0.26	0.5
886.99	887.10	887.05	270.37	33.88	32.52	1.36	4.0	0.32	1.0
889.08	889.20	889.14	271.01	51.28	48.66	2.62	5.1	0.58	1.2
890.90	891.02	890.96	271.56	51.96	50.28	1.68	3.2	0.42	0.8
893.04	893.16	893.10	272.22	26.92	25.74	1.18	4.4	0.30	1.2
895.09	895.19	895.14	272.84	28.26	27.28	0.98	3.5	0.38	1.4
896.44	896.54	896.49	273.25	25.38	24.38	1.00	3.9	0.44	1.8
896.98	897.11	897.05	273.42	28.00	26.96	1.04	3.7	0.90	3.3
897.31	897.43	897.37	273.52	26.98	26.08	0.90	3.3	1.28	4.9
897.66	897.72	897.69	273.62	17.50	16.96	0.54	3.1	0.80	4.7
898.16	898.23	898.20	273.77	25.10	24.00	1.10	4.4	2.00	8.3
898.34	898.45	898.40	273.83	39.66	38.12	1.54	3.9	4.54	11.9
898.64	898.74	898.69	273.92	30.18	28.96	1.22	4.0	3.86	13.3
898.94	899.09	899.02	274.02	27.20	26.12	1.08	4.0	3.74	14.3
899.20	899.31	899.26	274.09	25.96	24.82	1.14	4.4	4.66	18.8
899.73	899.82	899.78	274.25	35.90	34.42	1.48	4.1	6.70	19.5
900.16	900.29	900.23	274.39	71.46	69.22	2.24	3.1	24.32	35.1
900.18	900.30	900.24	274.39	65.54	62.94	2.60	4.0	16.58	26.3
901.12	901.30	901.21	274.69	64.88	62.28	2.60	4.0	20.06	32.2
901.87	902.00	901.94	274.91	67.20	64.24	2.96	4.4	22.84	35.6
903.67	903.80	903.74	275.46	50.24	48.18	2.06	4.1	21.62	44.9
905.66	905.74	905.70	276.06	44.26	42.12	2.14	4.8	19.00	45.1
907.63	907.75	907.69	276.66	58.04	55.60	2.44	4.2	23.58	42.4
909.36	909.45	909.41	277.19	54.76	52.50	2.26	4.1	18.16	34.6

Table 3

Mean depth, ft	Mean depth, m	$\delta^{13}C$ PDB, ‰	$\delta^{18}O$ PDB, ‰	% $CaCO_3$
857.00	261.21	-0.65	-1.63	2.81
858.98	261.82	-1.03	-2.04	2.62
861.20	262.49	-1.42	-2.60	3.58
863.10	263.07	-1.69	-2.83	3.73
865.17	267.70	-2.02	-2.87	2.73
867.13	264.30	-2.28	-2.82	2.92
869.13	264.91	-2.48	-2.75	3.07
870.91	265.45	-2.56	-2.83	3.47
873.04	266.10	-2.48	-2.99	3.28
875.10	266.73	-2.23	-3.21	3.05
877.08	267.33	-2.55	-2.94	2.87
879.20	267.98	-2.46	-3.01	2.53
881.20	268.59	-2.81	-3.12	2.94
883.14	269.18	-2.71	-3.00	2.96
885.16	269.80	-3.08	-2.97	2.45
887.10	270.39	-2.78	-3.24	2.42
889.19	271.03	-3.37	-3.03	3.50
890.98	271.57	-3.08	-3.08	3.07
893.15	272.23	-2.88	-3.47	3.75
895.20	272.86	-2.54	-3.39	3.75
896.54	273.27	-2.33	-3.23	2.71
897.37	273.52	-1.99	-2.78	0.45
898.20	273.77	-0.68	-1.84	0.69
898.47	273.85	-0.26	-1.91	0.25
898.69	273.92	-0.17	-2.02	0.34
898.95	274.00	1.21	-1.77	3.03
899.30	274.11	1.01	-1.71	2.87
899.68	274.22	0.93	-1.63	2.63
899.81	274.26	0.94	-1.93	2.00
900.18	274.37	1.18	-1.50	2.41
900.29	274.41	1.34	-1.48	2.35
901.13	274.66	1.88	-1.35	2.97
901.91	274.90	1.71	-1.40	2.53
903.61	275.42	2.08	-1.20	1.90
905.62	276.03	2.30	-1.19	1.80
907.60	276.64	2.26	-1.12	2.15
909.44	277.20	2.20	-1.58	1.75

Table 4

Mean depth, ft	Mean depth, m	*Morozovella:* Species name	Weight, µg ($CaCO_3$)	Size, µm	Number of individuals	$\delta^{13}C$ PDB, ‰	$\delta^{18}O$ PDB, ‰
857.05	261.23	*aequa*	100	> 400	5	4.01	-3.11
859.00	261.82	*aequa*	-	> 400	5	2.80	-3.21
861.15	262.48	*aequa*	-	> 400	5	2.18	-3.63
865.14	263.69	*aequa*	-	> 400	5	0.73	-3.79
867.08	264.28	*aequa*	58	400	4	0.75	-3.30
870.94	265.46	*aequa*	-	≥ 400	5	0.48	-3.32
873.08	266.11	*aequa*	-	> 400	6	0.83	-3.50
877.06	267.33	*aequa*	-	400	5	0.35	-3.43
881.15	268.57	*acuta*	42	350	6	0.38	-3.98
883.11	269.17	*acuta/velascoensis*	68	300-400	7	-0.42	-3.56
885.12	269.78	*acuta*	-	350-400	6	0.21	-3.76
887.05	270.37	*acuta*	-	300-400	7	0.25	-3.67
889.14	271.01	*acuta*	-	300-400	8	0.67	-3.94
890.96	271.56	*acuta*	-	350-400	8	0.13	-3.69
895.14	272.84	*acuta*	-	400	9	0.93	-3.89

Table 5

Mean depth, ft	Mean depth, m	*Acarinina:* Species name	Weight, µg ($CaCO_3$)	Size, µm	Number of individuals	$\delta^{13}C$ PDB, ‰	$\delta^{18}O$ PDB, ‰
857.05	261.23	*esnehensis*	-	300-400	6	1.64	-2.83
859.00	261.82	*esnehensis*	-	300-400	7	1.11	-2.68
861.15	262.48	*esnehensis*	-	350-400	6	1.36	-3.73
*861.15	262.48	*soldadoensis/angulosa*	-	300-350	6	0.51	-3.02
865.14	263.69	*esnehensis*	-	300-350	7	0.41	-3.26
*865.14	263.69	*soldadaensis/angulosa/ esnehensis/coaliningensis*	-	300-350	5	0.65	-3.98
867.08	264.28	*esnehensis*	-	300-350	7	-0.33	-2.83
869.08	264.89	*esnehensis*	-	350	6	0.06	-2.85
870.94	265.46	*esnehensis*	-	350-400	3	-0.26	-3.50
*870.94	265.46	*coalingensis/esnehensis*		300-350	6	0.13	-3.76
873.08	266.11	*esnehensis*	-	350-400	7	-0.43	-2.86
875.08	266.72	*esnehensis*	-	300-350	5	-0.63	-3.02
877.06	267.33	*esnehensis*	-	350-400	6	-0.28	-3.21
879.14	267.96	*esnehensis*	-	350-400	6	-0.35	-3.03
881.15	268.57	*soldadoensis*	-	350-400	5	0.19	-3.33
883.11	269.17	*soldadoensis*	-	350-400	5	-0.48	-3.19
885.12	269.78	*soldadoensis*	-	350-400	5	0.40	-3.30
887.05	270.37	*soldadoensis*	-	350-400	5	0.10	-3.16
889.14	271.01	*soldadoensis*	-	400	5	0.24	-3.29
890.96	271.56	*soldadoensis*	-	400	5	0.02	-3.14
893.10	272.22	*soldadoensis*	-	400	5	-0.38	-3.53
896.49	273.25	*esnehensis*	-	300-350	7	0.33	-3.39
897.05	273.42	*soldadoensis*	42	300-350	3	0.66	-2.87
899.18	274.07	*soldadoensis*	-	300-350	4	3.61	-2.74

Table 6

Mean depth, ft	Mean depth, m	*Subbotina:* Species name	Weight, µg ($CaCO_3$)	Size, µm	Number of individuals	$\delta^{13}C$ PDB, ‰	$\delta^{18}O$ PDB, ‰
857.05	261.23	*roesnaesensis*	-	400	10	-0.18	-1.78
859.00	261.82	*roesnaesensis*	172	400	10	-0.56	-2.34
861.15	262.48	*roesnaesensis*	-	350-400	10	-1.01	-2.50
863.08	263.07	*roesnaesensis*	-	350-400	10	-1.32	-2.80
865.14	263.69	*roesnaesensis*	-	400	10	-1.33	-2.78
867.08	264.28	*roesnaesensis*	-	350-400	10	-1.61	-2.79
869.08	264.89	*roesnaesensis*	-	350-400	10	-1.78	-2.49
870.94	265.46	*roesnaesensis*	-	350-400	10	-1.49	-2.77
873.08	266.11	*roesnaesensis*	-	350-400	10	-1.43	-2.97
875.08	266.72	*roesnaesensis*	-	400	8	-1.65	-3.06
877.06	267.33	*roesnaesensis*	-	350-400	10	-1.68	-2.94
879.14	267.96	*roesnaesensis*	-	350-400	10	-1.86	-2.97
881.15	268.57	*roesnaesensis*	-	350-400	10	-1.89	-3.20
883.11	269.17	*roesnaesensis*	-	350-400	10	-1.71	-3.39
885.12	269.78	*roesnaesensis*	-	350-400	10	-2.11	-2.98
887.05	270.37	*roesnaesensis*	-	350-400	10	-1.93	-3.33
889.14	271.01	*roesnaesensis*	-	350-400	10	-1.99	-3.07
890.96	271.56	*roesnaesensis*	-	350-400	10	-2.04	-3.11
893.10	272.22	*triangularis*	-	250-300	7	-2.26	-3.45
899.26	274.09	*roesnaesensis*	-	300-400	5	1.01	-1.95
901.56	274.80	*roesnaesensis*	-	250-300	4	1.60	-1.19
903.74	275.46	*triangularis*	-	300	3	1.87	-1.28

Table 7

Mean depth, ft	Mean depth, m	*Morozovella:* Species name	Weight, µg ($CaCO_3$)	Size, µm	Number of individuals	Mg25/Ca43, mmol/mol	Rejected samples
857.05	261.23	*aequa*	214	300-400	21	3.30	
859.00	261.82	*aequa*	354	300-400	30	3.22	
861.15	262.48	*aequa*	148	300-400	16	3.64	
863.08	263.07	*aequa*	118	300-400	10	2.73	
865.14	263.69	*aequa*	154	300-400	14	3.18	
867.08	264.28	*aequa*	158	300-400	14	3.39	
869.05	264.89	*aequa*	204	300-400	21	3.12	
873.08	266.11	*aequa*	200	300-400	20	3.92	
875.05	266.72	*aequa*	150	300-400	12	4.36	
877.06	267.33	*aequa*	278	300-400	25	3.48	
881.15	268.57	*aequa*	134	300-400	11	3.08	
885.12	269.78	*acuta*	118	300-400	12	5.03	R (high Fe)
889.14	271.01	*acuta*	216	300-400	28	1.38	R (D?)
890.96	271.56	*acuta*	206	300-400	25	1.09	R (D?)
893.10	272.22	*acuta*	94	300-400	13	1.26	R (D?)
895.14	272.84	*acuta*	200	300-400	30	1.35	R (D?)

Table 8

Mean depth, ft	Mean depth, m	*Acarinina:* Species name	Weight, µg ($CaCO_3$)	Size, µm	Number of individuals	Mg25/Ca43, mmol/mol	Rejected samples
859.00	261.82	*esnaensis*	264	300-350	20	3.49	
865.14	263.69	*esnaensis*	158	300-350	15	2.68	R (low Ca)
867.08	264.28	*esnaensis*	142	300-400	15	2.95	R (low Ca)
870.94	265.46	*esnaensis/angulosa/ soldadoensis*	120	300-350	14	3.56	R (low Ca)
873.08	266.11	*soldadoensis*	172	350-400	14	3.48	
877.06	267.33	*soldadoensis*	154	300-350	15	4.76	R (high Fe)
879.14	267.96	*soldadoensis*	248	300-350	20	3.39	R (high Fe)
881.15	268.57	*soldadoensis*	224	300-350	20	3.63	
883.11	269.17	*soldadoensis*	240	300-350	20	3.76	R (high Fe)
885.12	269.78	*soldadoensis*	240	300-350	20	4.52	R (high Fe)
887.05	270.37	*soldadoensis*	252	300	20	4.58	R (high Fe)
889.14	271.01	*soldadoensis*	240	300-350	20	4.03	R (high Fe)
890.96	271.56	*soldadoensis*	238	300-350	20	3.24	
893.10	272.22	*soldadoensis*	176	300-350	15	2.79	
895.14	272.84	*soldadoensis*	248	300-350	20	2.76	
896.49	273.25	*soldadoensis*	142	300-400	12	2.77	

Table 9

Mean depth, ft	Mean depth, m	*Subbotina:* Species name	Weight, µg ($CaCO_3$)	Size, µm	Number of individuals	Mg25/Ca43, mmol/mol	Rejected samples
857.05	261.23	roesnaesensis	414	300-350	30	1.49	R (D?)
859.00	261.82	roesnaesensis	392	300-350	30	2.19	R (D?)
861.15	262.48	*roesnaesensis*	300	300-400	29	2.17	
863.08	263.07	*roesnaesensis*	326	300-350	29	2.54	
865.14	263.69	*roesnaesensis*	352	300-350	30	2.84	
867.08	264.28	*roesnaesensis*	330	300-350	28	2.88	
870.94	265.46	*roesnaesensis*	368	300-350	30	2.86	
873.08	266.11	*roesnaesensis*	396	300-350	31	3.04	
875.08	266.72	*roesnaesensis*	216	300-350	20	3.02	
877.06	267.33	*roesnaesensis*	352	300-350	30	3.47	
879.14	267.96	*roesnaesensis*	376	300-350	30	3.11	
881.15	268.57	*roesnaesensis*	438	300-350	30	3.56	
883.11	269.17	*roesnaesensis*	320	300-350	25	3.56	
885.12	269.78	*roesnaesensis*	302	300-350	30	4.54	R (high Fe)
887.05	270.37	*roesnaesensis*	254	300-350	30	4.66	R (high Fe)
889.14	271.01	*roesnaesensis*	354	300-350	30	4.20	R (high Fe)
890.96	271.56	*roesnaesensis*	304	300-350	30	3.87	
893.10	272.22	*roesnaesensis*	166	300-350	18	3.57	
895.14	272.84	*roesnaesensis*	310	250-350	35	3.80	
898.99	274.01	*roesnaesensis/ velascoensis*	138	250-350	15	2.89	
900.21	274.38	*roesnaesensis/ velascoensis*	142	250-350	12	2.46	

Table 10

Mean depth, ft	Mean depth, m	GDGT peak areas					Original TEX_{86}				
		m/z 1300	m/z 1298	m/z 1296	m/z 1292'	GDGT ratio-1	GDGT ratio-2	TEX^{H}_{86}	T^{H}, °C	TEX^{L}_{86}	T^{L}, °C
857.00	261.21	466325	653633	309982	560445	0.46	0.77	-0.12	30.7	-0.34	24.0
858.96	261.81	395340	623617	285317	560805	0.48	0.79	-0.10	31.5	-0.32	25.3
861.20	262.49	112068	202713	87573	263003	0.50	0.83	-0.08	33.1	-0.30	26.8
863.10	263.07	43340	85436	29040	94521	0.54	0.83	-0.08	33.0	-0.27	28.9
865.17	263.70	57236	124989	33084	110017	0.58	0.82	-0.08	32.9	-0.24	31.0
867.13	264.30	104850	186989	60022	199741	0.53	0.81	-0.09	32.3	-0.27	28.4
869.13	264.91	49835	101984	39810	130638	0.53	0.85	-0.07	33.6	-0.27	28.4
870.91	265.45	54609	80068	26125	86512	0.50	0.78	-0.11	31.2	-0.30	26.5
873.04	266.10	59570	102424	29775	108586	0.53	0.80	-0.10	32.0	-0.27	28.5
875.10	266.73	56955	111386	45081	181751	0.52	0.86	-0.07	34.0	-0.28	27.8
877.08	267.33	93501	193946	61381	235958	0.56	0.84	-0.08	33.4	-0.25	29.7
879.20	267.98	118693	247236	98446	466256	0.53	0.87	-0.06	34.5	-0.27	28.4
881.20	268.59	73629	171705	78182	330938	0.53	0.89	-0.05	35.1	-0.28	28.3
883.14	269.18	72714	174121	64189	299406	0.56	0.88	-0.06	34.8	-0.25	29.9
885.16	269.80	91501	243123	102260	463824	0.56	0.90	-0.05	35.4	-0.25	29.7
887.10	270.39	34626	82908	34380	160291	0.55	0.89	-0.05	35.1	-0.26	29.1
889.19	271.03	32065	85493	36921	194813	0.55	0.91	-0.04	35.7	-0.26	29.6
890.98	271.57	53167	129311	50242	225913	0.56	0.88	-0.05	34.9	-0.26	29.7
893.15	272.23	64659	160617	69650	362381	0.54	0.90	-0.04	35.5	-0.26	29.1
895.20	272.86	109203	262773	93201	572069	0.56	0.89	-0.05	35.3	-0.25	30.2
896.30	273.19	76661	190026	70399	361499	0.56	0.89	-0.05	35.1	-0.25	30.1
896.54	273.27	9044	15973	6063	22559	0.51	0.83	-0.08	33.1	-0.29	27.4
897.10	273.44	193057	394436	182203	509701	0.51	0.85	-0.07	33.7	-0.29	27.3
897.78	273.64	123030	255642	119682	308081	0.51	0.85	-0.07	33.7	-0.29	27.3

Table 10 cont.

898.47	273.85	83251	162991	73447	184332	0.51	0.83	-0.08	33.2	-0.29	27.2
898.95	274.00	125719	179270	86212	177464	0.46	0.78	-0.11	31.2	-0.34	24.0
899.30	274.11	174945	225370	108353	197533	0.44	0.75	-0.12	30.1	-0.35	23.0
899.68	274.22	8882	12285	5414	12131	0.46	0.77	-0.11	30.9	-0.34	24.3
899.81	274.26	169610	239257	115996	228621	0.46	0.77	-0.11	31.0	-0.34	23.9
900.18	274.37	116142	138812	59633	103890	0.44	0.72	-0.14	28.9	-0.36	22.9
900.29	274.41	189676	217021	92795	164730	0.43	0.71	-0.15	28.6	-0.36	22.5
901.13	274.66	124147	168085	70257	121503	0.46	0.74	-0.13	29.8	-0.33	24.4
901.91	274.90	119220	148307	71845	116607	0.44	0.74	-0.13	29.6	-0.36	22.6
903.61	275.42	115572	143996	72980	114725	0.43	0.74	-0.13	29.7	-0.36	22.4
905.62	276.03	136075	169529	85202	130541	0.43	0.74	-0.13	29.6	-0.36	22.4
907.60	276.64	14899	17619	8808	11892	0.43	0.72	-0.14	28.8	-0.37	21.9
909.44	277.20	120329	155415	73490	115964	0.45	0.74	-0.13	29.7	-0.35	23.2

Table 11

Mean depth, ft	Mean depth, m	GDGT peak areas				BIT
		m/z 1292	m/z 1050	m/z 1036	m/z 1022	
857.00	261.21	5921114	44881	357360	370843	0.12
858.96	261.81	5269858	30018	297012	333751	0.11
861.20	262.49	1763461	10380	121037	161364	0.14
863.10	263.07	654761	4246	38336	53250	0.13
865.17	263.70	684958	3748	35130	53998	0.12
867.13	264.30	1277956	5609	65933	101418	0.12
869.13	264.91	876081	4406	39246	56311	0.10
870.91	265.45	597682	5626	30757	43902	0.12
873.04	266.10	677609	5319	31599	45381	0.11
875.10	266.73	1204090	6160	50573	73546	0.10
877.08	267.33	1541796	7420	50954	78415	0.08
879.20	267.98	2664074	16052	83227	115891	0.07
881.20	268.59	2085924	8376	61709	92297	0.07
883.14	269.18	1840454	5458	52641	76538	0.07
885.16	269.80	3010298	11070	81443	123023	0.07
887.10	270.39	979729	2326	26459	38963	0.06
889.19	271.03	1102632	3237	27525	42803	0.06
890.98	271.57	1385388	3733	46399	72795	0.08
893.15	272.23	2070419	4036	55128	82347	0.06
895.20	272.86	3257431	5715	87423	135049	0.07
896.30	273.19	2210298	3581	63314	97016	0.07
896.54	273.27	155422	352	4546	6501	0.07
897.10	273.44	4331714	11529	125681	163756	0.06
897.78	273.64	2623008	7799	83856	114614	0.07
898.47	273.85	1499069	5164	56866	79209	0.09
898.95	274.00	1655160	8076	78592	92917	0.10
899.30	274.11	2064158	9890	80291	85092	0.08
899.68	274.22	100430	357	2662	3023	0.06
899.81	274.26	2242602	9266	81470	90948	0.07
900.18	274.37	1049804	6696	58852	66061	0.11
900.29	274.41	1704168	11624	97274	108445	0.11
901.13	274.66	1215816	8985	96772	107376	0.15
901.91	274.90	1229323	8632	77969	87286	0.12
903.61	275.42	1284453	9463	75745	81241	0.11
905.62	276.03	1514842	9502	93334	101840	0.12
907.60	276.64	132365	852	5811	5924	0.09
909.44	277.20	1256378	6810	72015	79296	0.11

Table 12

Mean depth, ft	Mean depth, m	Mg25/Ca43, mmol/mol	T, °C Mg/Ca sw = 1.5 mmol/mol	T, °C Mg/Ca sw = 2.5 mmol/mol	ΔT, °C
			Morozovella spp.		
857.05	261.23	3.3	38.5	32.8	0.8
859.00	261.82	3.2	38.2	32.5	0.5
861.15	262.48	3.6	39.6	33.9	1.9
863.08	263.07	2.7	36.3	30.6	-1.4
865.14	263.69	3.2	38.0	32.3	0.4
867.08	264.28	3.4	38.8	33.1	1.1
869.05	264.89	3.1	37.8	32.1	0.1
873.08	266.11	3.9	40.4	34.7	2.7
875.05	266.72	4.4	41.6	35.9	3.9
877.06	267.33	3.5	39.0	33.4	1.4
881.15	268.57	3.1	37.7	32.0	0.0
			Acarinina spp.		
859.00	261.82	3.5	39.1	33.4	2.6
873.08	266.11	3.5	39.0	33.3	2.5
881.15	268.57	3.6	39.5	33.8	3.0
890.96	271.56	3.2	38.3	32.6	1.8
893.10	272.22	2.8	36.6	30.9	0.1
895.14	272.84	2.8	36.5	30.8	0.0
896.49	273.25	2.8	36.5	30.8	0.0
			*Subbotin*a spp.		
861.15	262.48	2.2	33.8	28.1	-1.4
863.08	263.07	2.5	35.5	29.8	0.3
865.14	263.69	2.8	36.8	31.1	1.6
867.08	264.28	2.9	36.9	31.3	1.8
870.94	265.46	2.9	36.9	31.2	1.7
873.08	266.11	3.0	37.6	31.9	2.4
875.08	266.72	3.0	37.5	31.8	2.3
877.06	267.33	3.5	39.0	33.3	3.8
879.14	267.96	3.1	37.8	32.1	2.6
881.15	268.57	3.6	39.3	33.6	4.1
883.11	269.17	3.6	39.3	33.6	4.1
890.96	271.56	3.9	40.2	3.1	5.0
893.10	272.22	3.6	39.3	3.0	4.2
895.14	272.84	3.8	40.0	3.1	4.8
898.99	274.01	2.9	37.0	2.8	1.8
900.21	274.38	2.5	35.2	2.7	0.0

Table 13

Mean depth, ft	Mean depth, m	*Morozovella* spp. $\delta^{18}O$ PDB, ‰	Using temperatures from TEX^{H}_{86} + 2.5°C T, °C	$\delta^{18}O_{water}$ PDB, ‰	$\delta^{18}O_{water}$ SMOW, ‰	Salinity, psu	Using temperatures from TEX^{L}_{86} + 2.5°C T, °C	$\delta^{18}O_{water}$ PDB, ‰	$\delta^{18}O_{water}$ SMOW, ‰	Salinity, psu
857.05	261.23	-3.11	33.2	0.34	0.62	40.2	26.5	-1.03	-0.75	30.4
859.00	261.82	-3.21	34.0	0.40	0.68	40.6	27.8	-0.85	-0.57	31.6
861.15	262.48	-3.63	35.6	0.29	0.57	39.8	29.3	-0.96	-0.68	30.9
865.14	263.69	-3.79	35.4	0.09	0.37	38.4	33.5	-0.29	-0.01	35.7
867.08	264.28	-3.30	34.8	0.46	0.74	41.0	30.9	-0.32	-0.04	35.4
870.94	265.46	-3.32	33.7	0.23	0.51	39.3	29.0	-0.72	-0.44	32.6
873.08	266.11	-3.50	34.5	0.20	0.48	39.2	31.0	-0.49	-0.21	34.2
877.01	267.31	-3.43	35.9	0.54	0.82	41.6	32.2	-0.18	0.10	36.4
881.15	268.57	-3.98	37.6	0.32	0.60	40.0	30.8	-1.00	-0.72	30.5
883.11	269.17	-3.56	37.3	0.68	0.96	42.6	32.4	-0.27	0.01	35.8
885.12	269.78	-3.76	37.9	0.60	0.88	42.0	32.2	-0.51	-0.23	34.1
887.05	270.37	-3.67	37.6	0.63	0.91	42.3	31.6	-0.53	-0.25	34.0
889.14	271.01	-3.94	38.2	0.48	0.76	41.1	32.1	-0.72	-0.44	32.6
890.96	271.56	-3.69	37.4	0.58	0.86	41.9	32.2	-0.44	-0.16	34.6
895.14	272.84	-3.89	37.8	0.45	0.73	40.9	32.7	-0.55	-0.27	33.8

Table 14

Mean depth, ft	Mean depth, m	*Subbotina* spp.		Using temperatures from TEX^{H}_{86}			Using temperatures from TEX^{L}_{86}			
		$\delta^{18}O$ PDB, ‰	T, °C	$\delta^{18}O_{water}$ PDB, ‰	$\delta^{18}O_{water}$ SMOW, ‰	Salinity, psu	T, °C	$\delta^{18}O_{water}$ PDB, ‰	$\delta^{18}O_{water}$ SMOW, ‰	Salinity, psu
857.05	261.23	-1.78	30.7	1.17	1.45	46.1	24.0	-0.23	0.05	36.1
859.00	261.82	-2.34	31.5	0.77	1.05	43.2	25.3	-0.51	-0.23	34.1
861.15	262.48	-2.50	33.1	0.93	1.21	44.4	26.8	-0.34	-0.06	35.3
863.08	263.07	-2.80	33.0	0.61	0.89	42.0	28.9	-0.22	0.06	36.2
865.14	263.69	-2.78	32.9	0.62	0.90	42.1	31.0	0.23	0.51	39.3
867.08	264.28	-2.79	32.3	0.48	0.76	41.2	28.4	-0.31	-0.03	35.5
869.05	264.89	-2.49	33.6	1.03	1.31	45.1	28.4	-0.01	0.27	37.7
870.94	265.46	-2.77	31.2	0.29	0.57	39.8	26.5	-0.68	-0.40	32.8
873.08	266.11	-2.97	32.0	0.24	0.52	39.4	28.5	-0.46	-0.18	34.4
875.05	266.72	-3.06	34.0	0.54	0.82	41.6	27.8	-0.70	-0.42	32.7
877.01	267.31	-2.94	33.4	0.54	0.82	41.6	29.7	-0.20	0.08	36.3
879.14	267.96	-2.97	34.5	0.73	1.01	42.9	28.4	-0.48	-0.20	34.3
881.15	268.57	-3.20	35.1	0.62	0.90	42.1	28.3	-0.73	-0.45	32.5
883.11	269.17	-3.39	34.8	0.37	0.65	40.4	29.9	-0.60	-0.32	33.4
885.12	269.78	-2.98	35.4	0.90	1.18	44.1	29.7	-0.23	0.05	36.1
887.05	270.37	-3.33	35.1	0.49	0.77	41.2	29.1	-0.70	-0.42	32.7
889.14	271.01	-3.07	35.7	0.87	1.15	43.9	29.6	-0.35	-0.07	35.2
890.96	271.56	-3.11	34.9	0.67	0.95	42.5	29.7	-0.36	-0.08	35.1
893.10	272.22	-3.45	35.5	0.45	0.73	40.9	29.1	-0.83	-0.55	31.8
895.14	272.84	-2.98	35.3	0.88	1.16	44.0	30.2	-0.14	0.14	36.7
899.26	274.09	-1.95	30.1	0.88	1.16	44.0	23.0	-0.59	-0.31	33.5
901.94	274.91	-1.19	29.6	1.54	1.82	48.7	22.6	0.08	0.36	38.3
903.74	275.46	-1.28	29.7	1.47	1.75	48.2	22.4	-0.07	0.21	37.2

Table 15

Mean depth, ft	Mean depth, m	$\delta^{18}O_{PF}$ PDB, ‰	Using Anand et al. (2003) calibration and 2.5 mmol/mol Mg/Ca ratio for the PETM from Cramer et al. (2011)			
			T, °C	$\delta^{18}O_{water}$ PDB, ‰	$\delta^{18}O_{water}$ SMOW, ‰	Salinity, psu
				Morozovella spp.		
857.05	261.23	-3.11	32.8	0.26	0.54	39.6
859.00	261.82	-3.21	32.5	0.10	0.38	38.4
861.15	262.48	-3.63	33.9	-0.05	0.23	37.4
865.14	263.69	-3.79	32.3	-0.51	-0.23	34.1
867.08	264.28	-3.30	33.1	0.12	0.40	38.6
873.08	266.11	-3.50	34.7	0.23	0.51	39.4
877.01	267.31	-3.43	33.4	0.05	0.33	38.1
881.15	268.57	-3.98	32.0	-0.77	-0.49	32.2
				Acarinina spp.		
859.00	261.82	-2.68	33.4	0.81	1.09	43.5
873.08	266.11	-2.86	33.3	0.62	0.90	42.2
881.15	268.57	-3.33	33.8	0.25	0.53	39.5
890.96	271.56	-3.14	32.6	0.18	0.46	39.0
893.10	272.22	-3.53	30.9	-0.54	-0.26	33.9
896.49	273.25	-3.39	30.8	-0.42	-0.14	34.7
				Subbotina spp.		
861.15	262.48	-2.50	28.1	-0.07	0.21	37.2
863.08	263.07	-2.80	29.8	-0.03	0.25	37.5
865.14	263.69	-2.78	31.1	0.26	0.54	39.5
867.08	264.28	-2.79	31.3	0.27	0.55	39.7
870.94	265.46	-2.77	31.2	0.28	0.56	39.7
873.08	266.11	-2.97	31.9	0.21	0.49	39.2
875.05	266.72	-3.06	31.8	0.10	0.38	38.4
877.01	267.31	-2.94	33.3	0.53	0.81	41.5
879.14	267.96	-2.97	32.1	0.26	0.54	39.6
881.15	268.57	-3.20	33.6	0.32	0.60	40.0
883.11	269.17	-3.39	33.6	0.14	0.42	38.7
890.96	271.56	-3.11	34.5	0.60	0.88	42.0
893.10	272.22	-3.45	33.6	0.09	0.37	38.3
895.14	272.84	-2.98	34.3	0.70	0.98	42.7
899.26	274.09	-1.95	31.3	1.12	1.40	45.7
901.94	274.91	-1.19	29.5	1.51	1.79	48.5

FIGURE CAPTIONS

1. Bulk carbonate $\delta^{13}C$, dinocysts $\delta^{13}C$, *Apectodinium* acme, and TEX_{86} records across the PETM at Bass River and Wilson Lake Hole A, NJ (figure from Sluijs et al., 2007, using data of Zachos et al., 2006, 2007; Sluijs et al., 2007). CIE = Carbon isotope excursion; SST = sea surface temperature.

2. Location map of New Jersey coreholes: Millville (this study), Clayton, Wilson Lake, and Bass River. Black lines represent projection of coreholes onto the shelf dip-profile (the line perpendicular to Cenozoic outcrop). Gray lines indicate the depth to the K/Pg boundary (base map after New Jersey Geological Survey (NJGS) that is used to project sites to dip profile).

3. Paleoshelf reconstruction across the New Jersey coastal plain and paleodepths of USGS corehole Wilson Lake and two ODP Leg 174AX drilling sites, i.e. Millville (this study) and Bass River, based on a 1:1000 gradient (Steckler et al., 1999). Planktonic foraminifera are shown at depths of their habitats: *Morozovella* (mixed layer dweller), *Acarinina* (deep mixed/intermediate layer dweller), and *Subbotina* (intermediate dweller). Diagrams at the right show changes in temperature, $\delta^{13}C$, oxygen concentration, and amount of nutrients with depth (modified after Esmeray-Senlet et al., in review).

4. Photographs of 2 ft (61 cm) segments of the uppermost Paleocene-lower Eocene section of Millville core, NJ. White labels indicate the points and depths of sampling.

5. Percent lithology, biostratigraphy, and $\delta^{13}C_{org}$ records of the uppermost Paleocene-lower Eocene section at Millville, NJ (Harris et al., 2010) with grain size and bulk carbonate $\delta^{13}C$ data from this study.

6. Photographs of Millville core displaying the lower and upper contacts between Marlboro (M) and Vincentown (VT) Formations (Sugarman, Miller, Browning et al., 2005).

7. The set of membrane lipids of marine Thaumarchaeota, glycerol dibiphytanyl glycerol tetraethers (GDGTs), used for TEX_{86} (Kim et al., 2008).

8. The set of glycerol dibiphytanyl glycerol tetraethers (GDGTs) used for the BIT index: I-III – non-isoprenoid soil-derived GDGTs; IV – crenarchaeol, isoprenoid GDGT of Marine Thaumarchaeota (Hopmans et al., 2004).

9. The BIT values for open marine surface sediments in upper graph and surface soil samples in lower graph (Schouten et al., 2013).

10. Stable isotopic records ($\delta^{13}C$ and $\delta^{18}O$) of planktonic foraminifera (*Morozovella* spp., *Acarinina* spp., *Subbotina* spp.) and bulk carbonate of the uppermost Paleocene-lower Eocene section at Millville, NJ.

11. Mg/Ca ratio of planktonic foraminifera (*Morozovella* spp., *Acarinina* spp., and *Subbotina* spp.) and bulk carbonate of the uppermost Paleocene-lower Eocene section at Millville, NJ. Rejected data is indicated by empty symbols: empty squares and dimonds indicate possible diagenetic alterations in *Subbotina* spp. and *Morozovella* spp.; empty circles show *Acarinina* spp. with very low calcium concentrations. Yellow area represents intervals of high iron concentration.

12. TEX_{86} results: values of the original TEX_{86} (Schouten et al., 2002); TEX^{H}_{86} and TEX^{L}_{86} (Kim et al., 2010) at Millville, NJ. Carbon isotopic records are shown as stratigraphic control.

13. The BIT values of the uppermost Paleocene-lower Eocene section at Millville, NJ. Carbon isotopic records are shown as stratigraphic control.

14. The chromatogram of the sample from the depth 907.60 ft (276.64 m) at Millville, NJ. Zoomed section shows the distribution of alkenones in the standard and absence of alkenones in the analyzed sample.

15. Calibrated TEX^{H}_{86} and TEX^{L}_{86} values into temperatures using Kim et al. (2010) equations at Millville, NJ. Carbon isotopic records are shown as stratigraphic control.

16. Temperature records the uppermost Paleocene-lower Eocene sections in New Jersey cores Millville (this study) and Wilson Lake (data from Zachos et al., 2006 and Sluijs et al., 2007), according to TEX^{H}_{86} and TEX^{L}_{86} values calibrated with Kim et al. (2010) equations. See figure 1 for core locations. Cores are aligned at the initiation of the carbon isotope excursion (CIE).

17. Temperature records of the uppermost Paleocene-lower Eocene sections in New Jersey cores Millville (this study) and Bass River (data from Sluijs et al., 2007), according to TEX^{H}_{86} and TEX^{L}_{86} results calibrated with Kim et al. (2010) equations. See figure 1 for core locations. Cores are aligned at the initiation of the carbon isotope excursion (CIE).

18. GDGT ratios proposed by Kim et al. (2010): GDGT ratio-1 and GDGT ratio-2 (original TEX_{86}) at Millville, NJ. Carbon isotopic records are shown as stratigraphic control.

19. Mg/Ca values of planktonic foraminifera (*Morozovella* spp., *Acarinina* spp., and *Subbotina* spp.) calibrated into temperatures using Anand et al. (2003) multispecies

calibration and assuming that Mg/Ca ratio of the seawater was 2.5 mmol/mol during the PETM (Cramer et al., 2011) at Millville, NJ. Right plot shows temperature anomalies for each genus of planktonic foraminifera. Carbon isotopic records are shown as stratigraphic control.

20. Compilation of temperature records at Millville, NJ, obtained from TEX^{L}_{86} and TEX^{H}_{86} calibrations (Kim et al., 2010), Mg/Ca ratio calibrations (Anand et al., 2003) using seawater Mg/Ca ratio of 1.5 mmol/mol and 2.5 mmol/mol.

21. Paleosalinity estimations at Millville, NJ: left - using $\delta^{18}O$ of planktonic foraminifera (*Morozovella* spp. and *Subbotina* spp.) and temperatures obtained from TEX^{L}_{86}; center - using $\delta^{18}O$ of planktonic foraminifera (*Morozovella* spp. and *Subbotina* spp.) and temperatures obtained from TEX^{H}_{86}; and right - using $\delta^{18}O$ of planktonic foraminifera (*Morozovella* spp., *Acarinina* spp., and *Subbotina* spp.) and temperatures obtained from Mg/Ca ratio of *Morozovella* spp., *Acarinina* spp., and *Subbotina* spp. using Anand et al. (2003) equation.

22. Compilation of records at Millville, NJ: % $CaCO_3$; organic (Harris et al., 2010) and bulk carbonate $\delta^{13}C$; planktonic foraminifera (*Morozovella* spp., *Acarinina* spp., and *Subbotina* spp.) and bulk carbonate $\delta^{18}O$; temperature calibrated from TEX^{L}_{86}; and Mg/Ca ratio of planktonic foraminifera (*Morozovella* spp., *Acarinina* spp., and *Subbotina* spp.).

23. Thermocline variations during the PETM. Upper plots show data from Millville, NJ: (1) organic (Harris et al., 2010) and bulk carbonate $\delta^{13}C$; (2) planktonic foraminifera (*Morozovella* spp., *Acarinina* spp., and *Subbotina* spp.) and bulk carbonate $\delta^{18}O$; (3) planktonic foraminifera (*Morozovella* spp., *Acarinina* spp., and

Subbotina spp.) $\delta^{13}C$; (4) temperature calibrated from TEX^{L}_{86}; and (5) Mg/Ca ratio of planktonic foraminifera (*Morozovella* spp., *Acarinina* spp., and *Subbotina* spp.). Lower schemes represent three intervals during the PETM: (1) before the CIE onset representing normal thermocline, (2) CIE "core" representing water mixing and a breakdown in the thermocline, and (3) CIE "recovery" representing redevelopment of the thermocline.

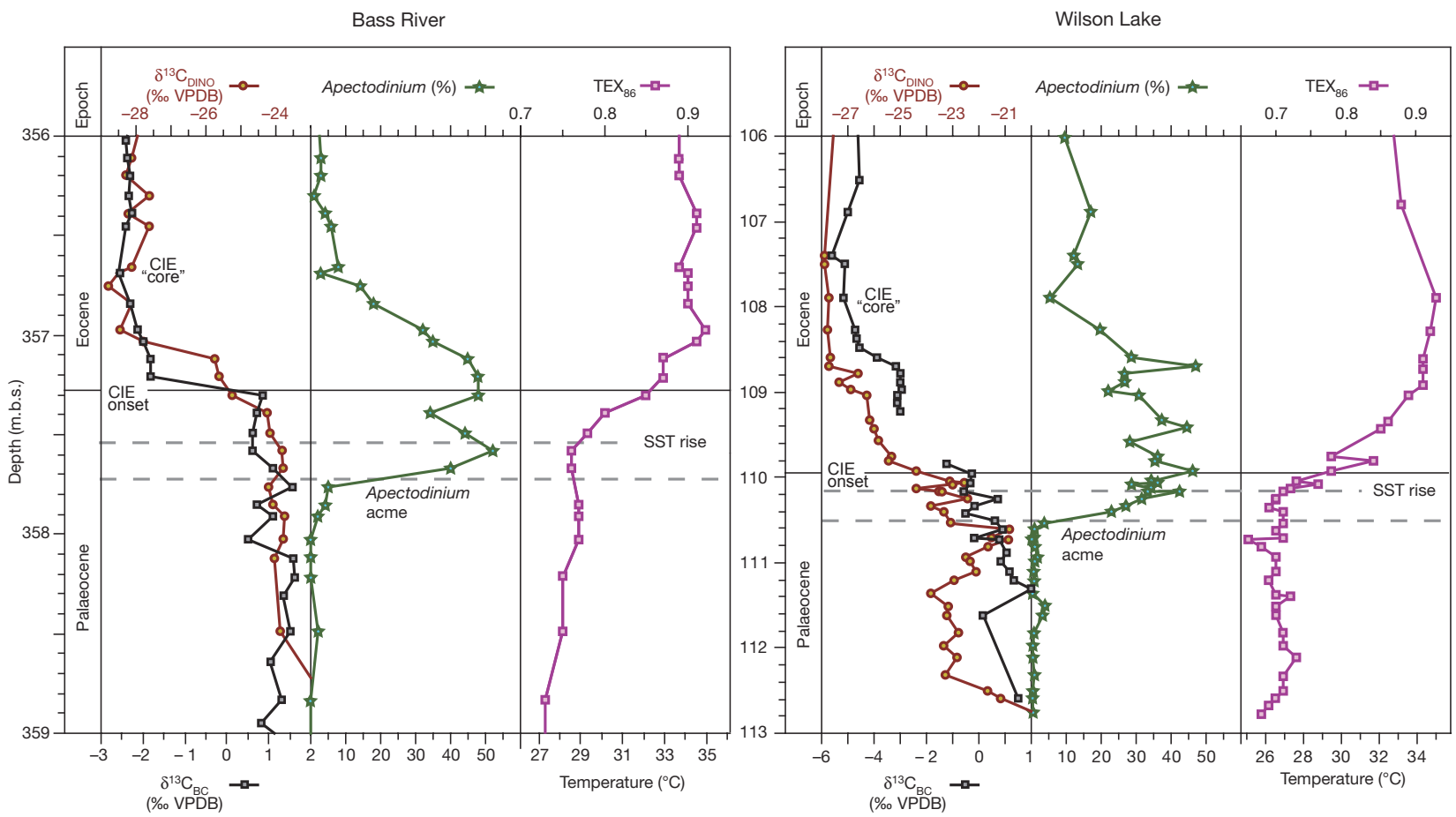
Bass River
Wilson Lake
Epoch
Eocene
Palaeocene
Depth (m.b.s.)
δ13CDINO (‰ VPDB)
Apectodinium (%)
TEX86
CIE "core"
CIE onset
SST rise
Apectodinium acme
δ13CBC (‰ VPDB)
Temperature (°C)

Figure 1

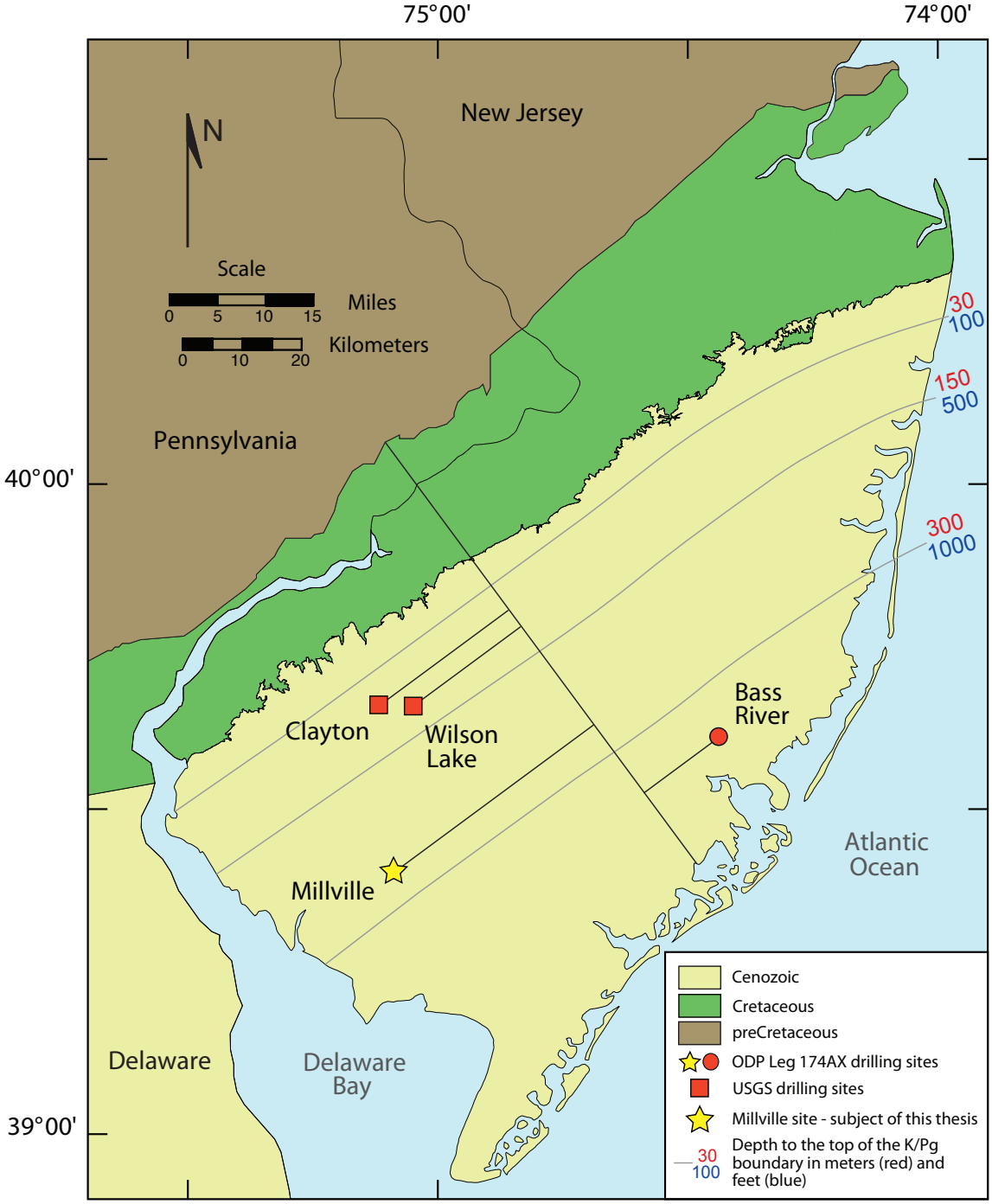
75°00'
74°00'
40°00'
39°00'
N
New Jersey
Scale
0 5 10 15 Miles
0 10 20 Kilometers
Pennsylvania
30
100
150
500
300
1000
Clayton
Wilson Lake
Bass River
Millville
Atlantic Ocean
Delaware
Delaware Bay
Cenozoic
Cretaceous
preCretaceous
ODP Leg 174AX drilling sites
USGS drilling sites
Millville site - subject of this thesis
30
100
Depth to the top of the K/Pg boundary in meters (red) and feet (blue)

Figure 2

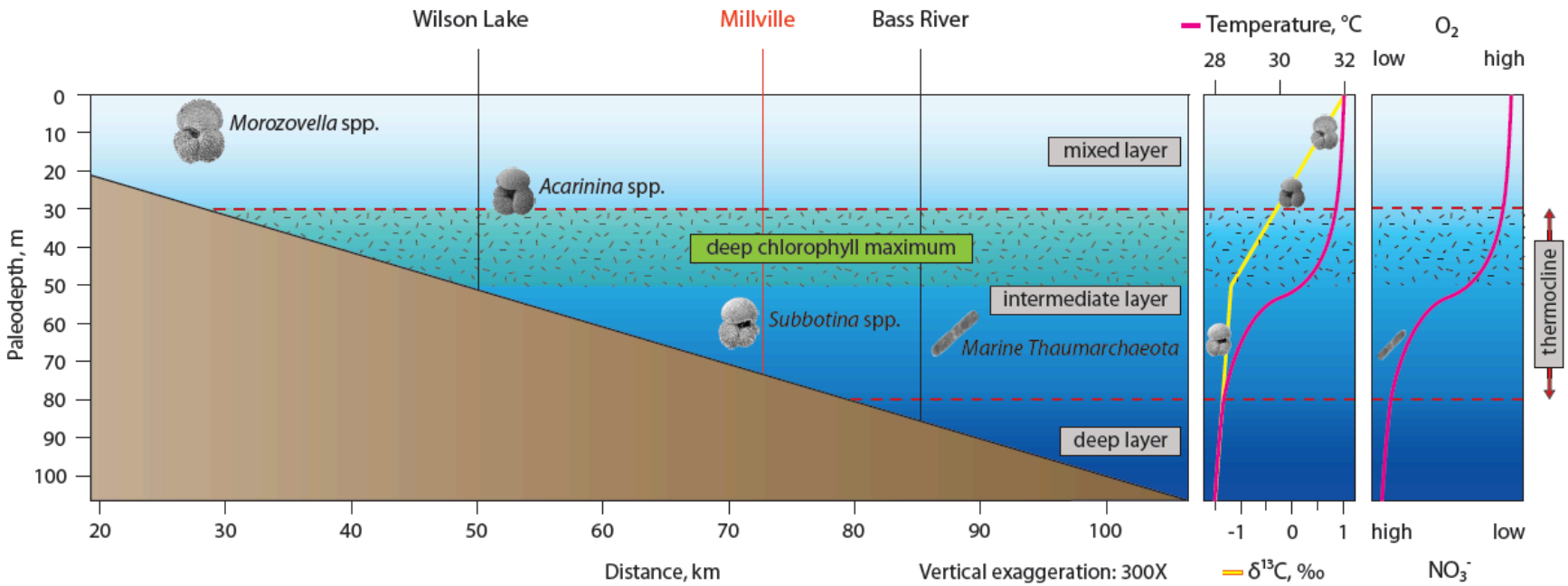
Wilson Lake
Millville
Bass River
Temperature, °C
28
30
32
O2
low
high
Morozovella spp.
Acarinina spp.
mixed layer
deep chlorophyll maximum
intermediate layer
Subbotina spp.
Marine Thaumarchaeota
deep layer
thermocline
Paleodepth, m
0
10
20
30
40
50
60
70
80
90
100
20
30
40
50
60
70
80
90
100
Distance, km
Vertical exaggeration: 300X
-1
0
1
δ13C, ‰
high
low
NO3-

Figure 3


USGS WRD
857.00-
.10
858.92-
859.07
861.10-
.20
"863.00-
.15"
865.10-
.18
867.00-
.15

Figure 4

Figure 4 Cont.

Figure 4 Cont.

Figure 4 Cont.

Figure 4 Cont.

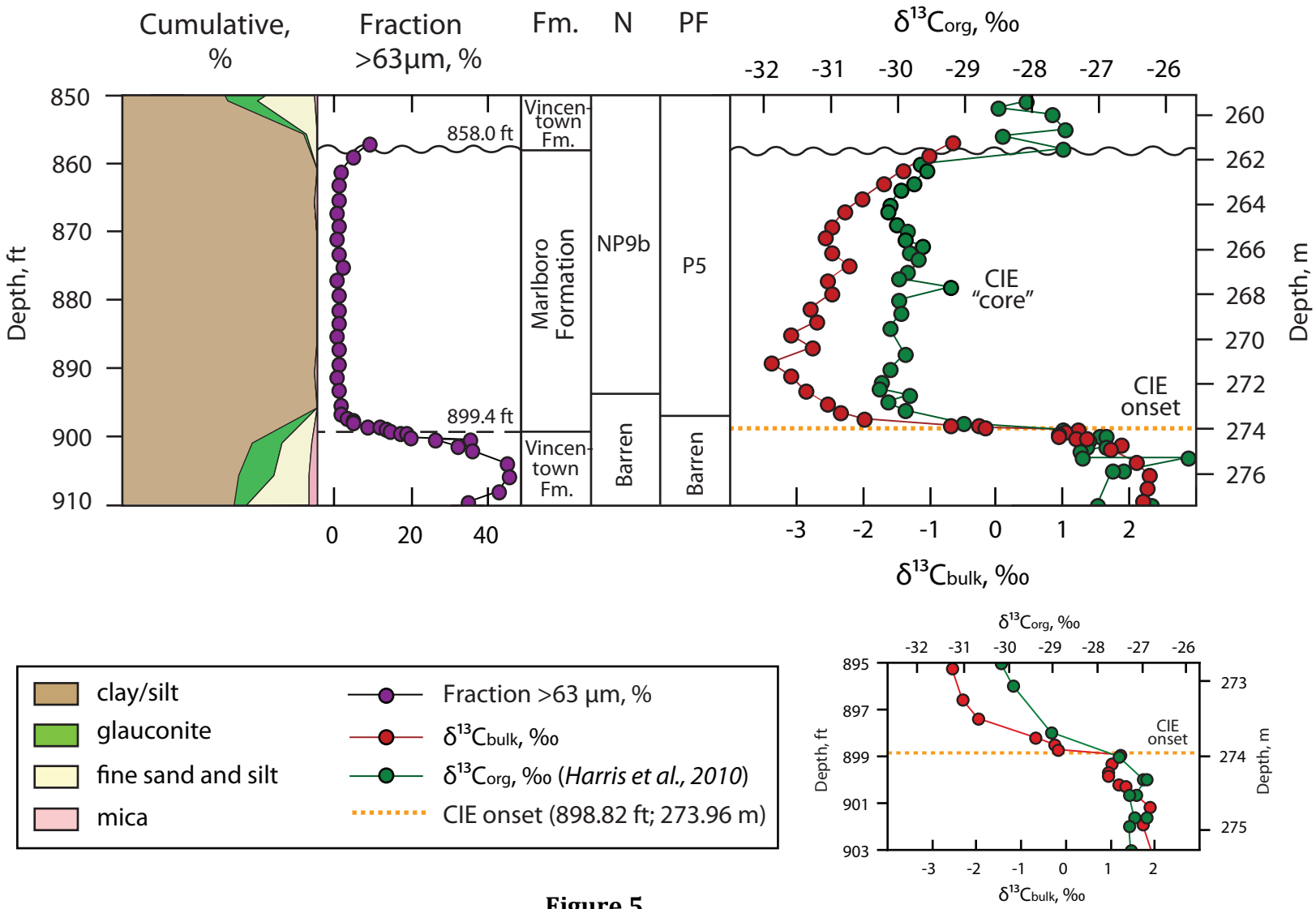
Cumulative, %
Fraction >63µm, %
Fm.
N
PF
δ13Corg, ‰
Depth, ft
Depth, m
858.0 ft
899.4 ft
Vincen-town Fm.
Marlboro Formation
NP9b
P5
Barren
CIE "core"
CIE onset
δ13Cbulk, ‰
clay/silt
glauconite
fine sand and silt
mica
Fraction >63 µm, %
δ13Cbulk, ‰
δ13Corg, ‰ (Harris et al., 2010)
CIE onset (898.82 ft; 273.96 m)

Figure 5

The lower contact between Vincentown and Marlboro Formations

The upper contact between Vincentown and Marlboro Formations

Figure 6

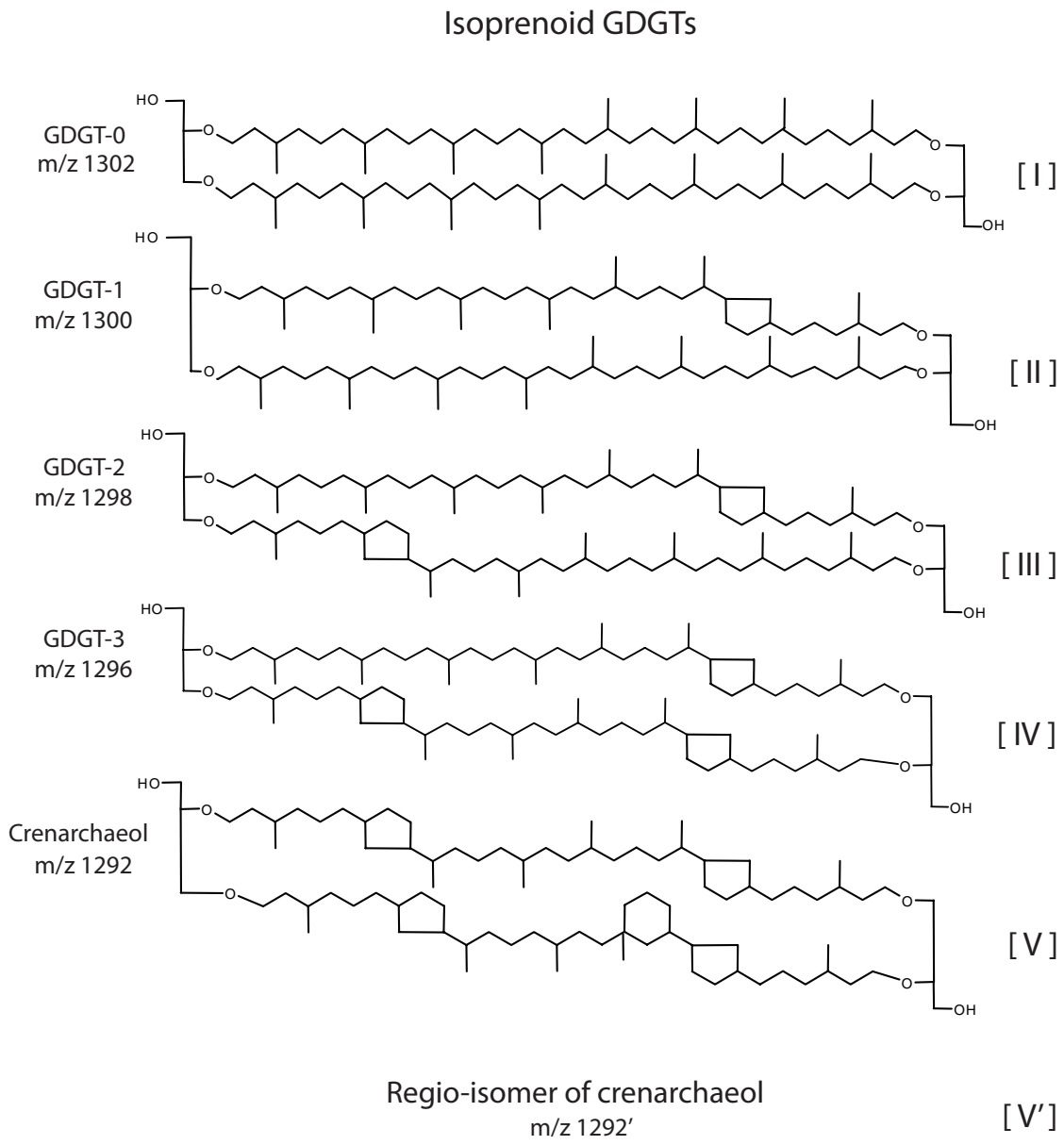
Isoprenoid GDGTs
GDGT-0
m/z 1302
[I]
GDGT-1
m/z 1300
[II]
GDGT-2
m/z 1298
[III]
GDGT-3
m/z 1296
[IV]
Crenarchaeol
m/z 1292
[V]
Regio-isomer of crenarchaeol
m/z 1292'
[V']
HO
O
OH

Figure 7

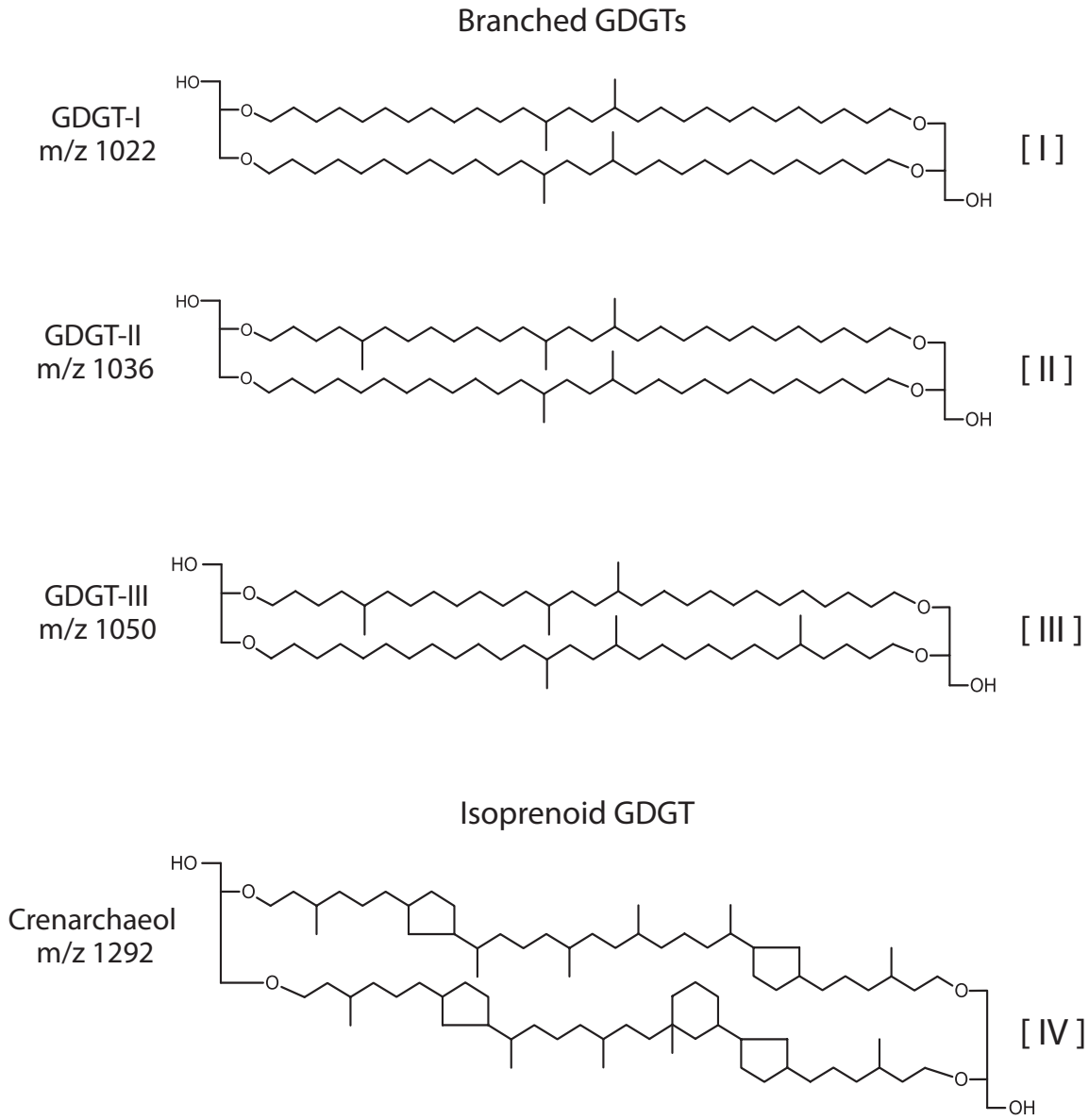
Branched GDGTs
GDGT-I
m/z 1022
[I]
GDGT-II
m/z 1036
[II]
GDGT-III
m/z 1050
[III]
Isoprenoid GDGT
Crenarchaeol
m/z 1292
[IV]
HO
O
OH

Figure 8

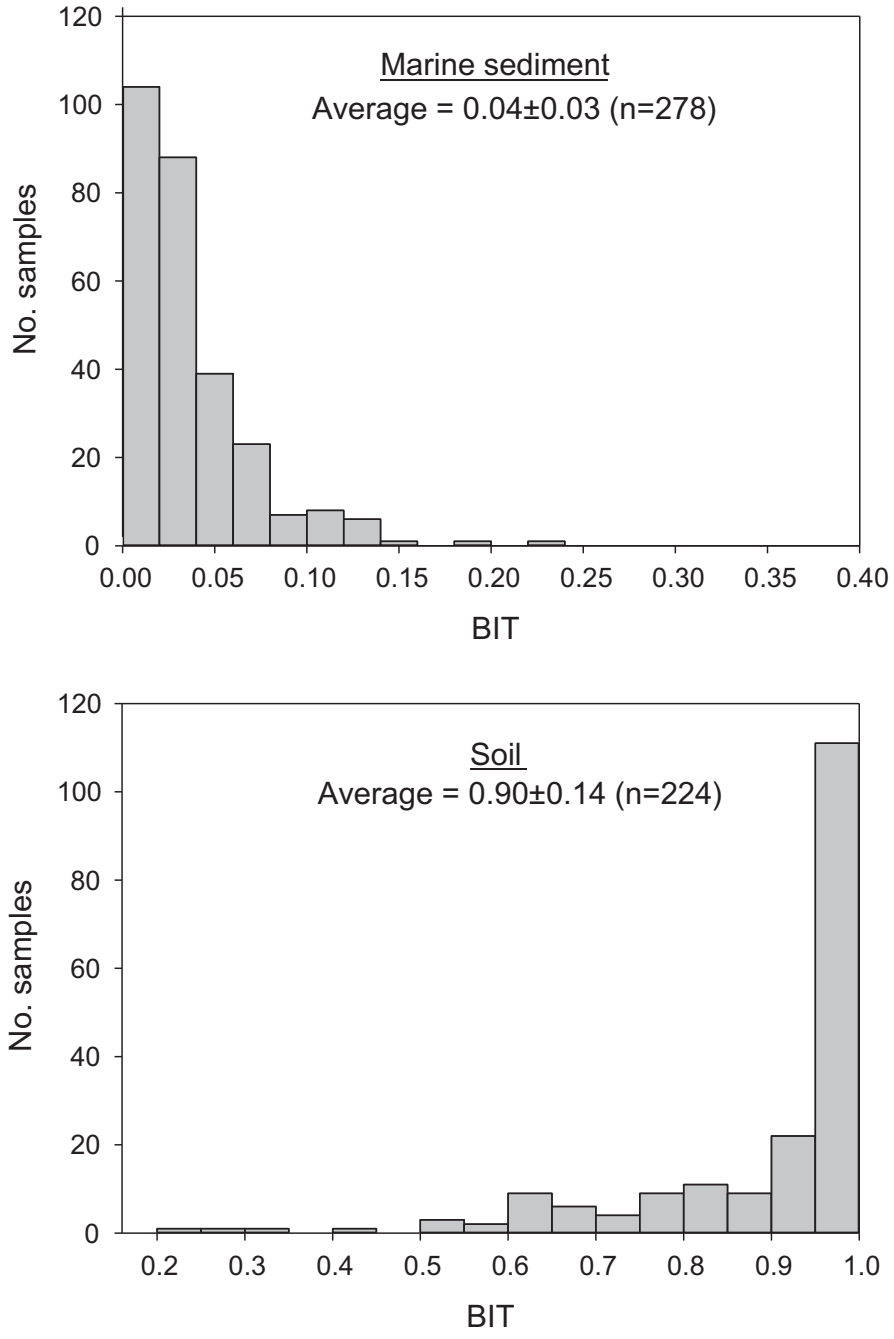
Marine sediment
Average = 0.04±0.03 (n=278)
No. samples
BIT
0
20
40
60
80
100
120
0.00
0.05
0.10
0.15
0.20
0.25
0.30
0.35
0.40
Soil
Average = 0.90±0.14 (n=224)
No. samples
BIT
0
20
40
60
80
100
120
0.2
0.3
0.4
0.5
0.6
0.7
0.8
0.9
1.0

Figure 9

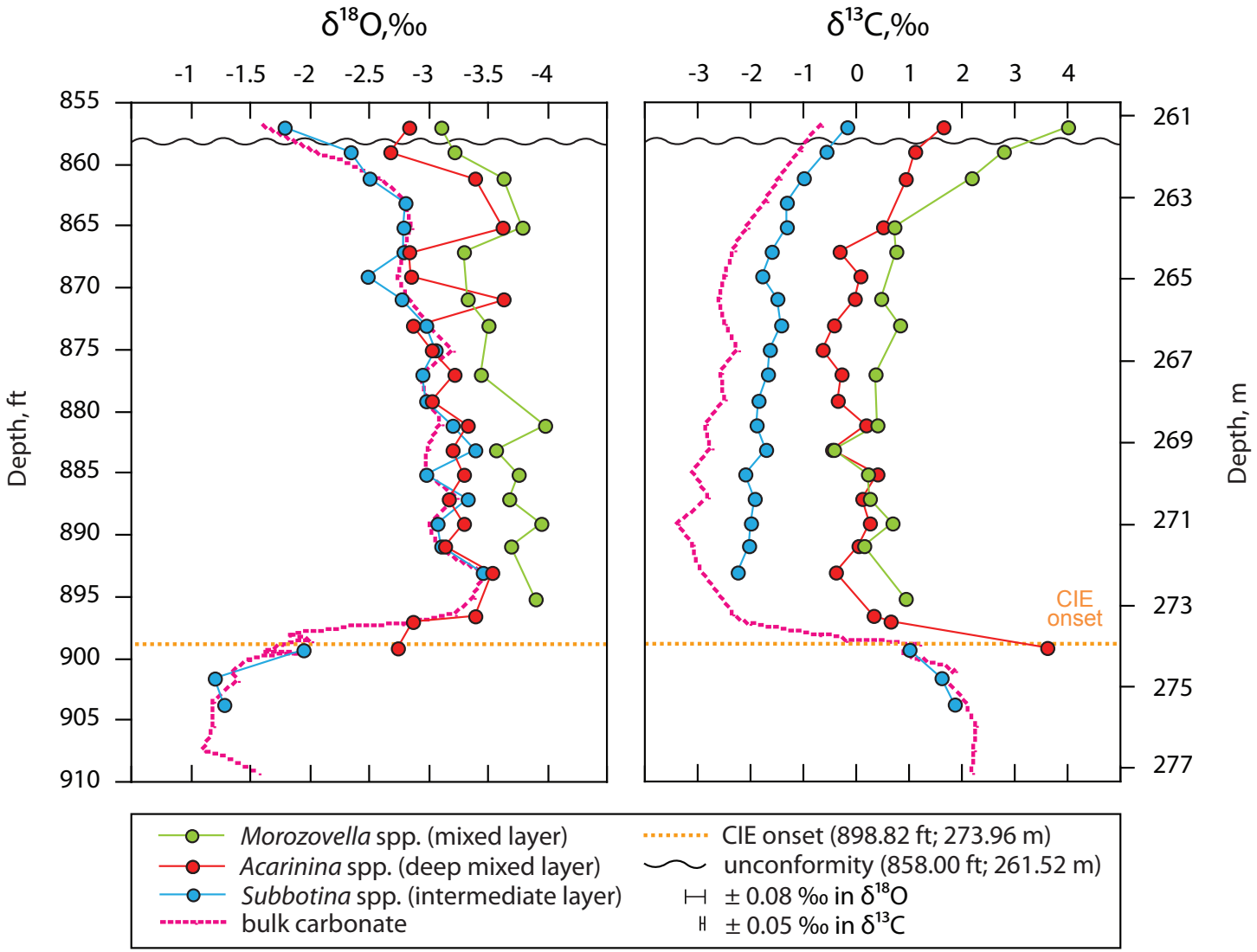
δ18O,‰
-1
-1.5
-2
-2.5
-3
-3.5
-4
δ13C,‰
-3
-2
-1
0
1
2
3
4
Depth, ft
855
860
865
870
875
880
885
890
895
900
905
910
Depth, m
261
263
265
267
269
271
273
275
277
CIE onset
Morozovella spp. (mixed layer)
Acarinina spp. (deep mixed layer)
Subbotina spp. (intermediate layer)
bulk carbonate
CIE onset (898.82 ft; 273.96 m)
unconformity (858.00 ft; 261.52 m)
± 0.08 ‰ in δ18O
± 0.05 ‰ in δ13C

Figure 10

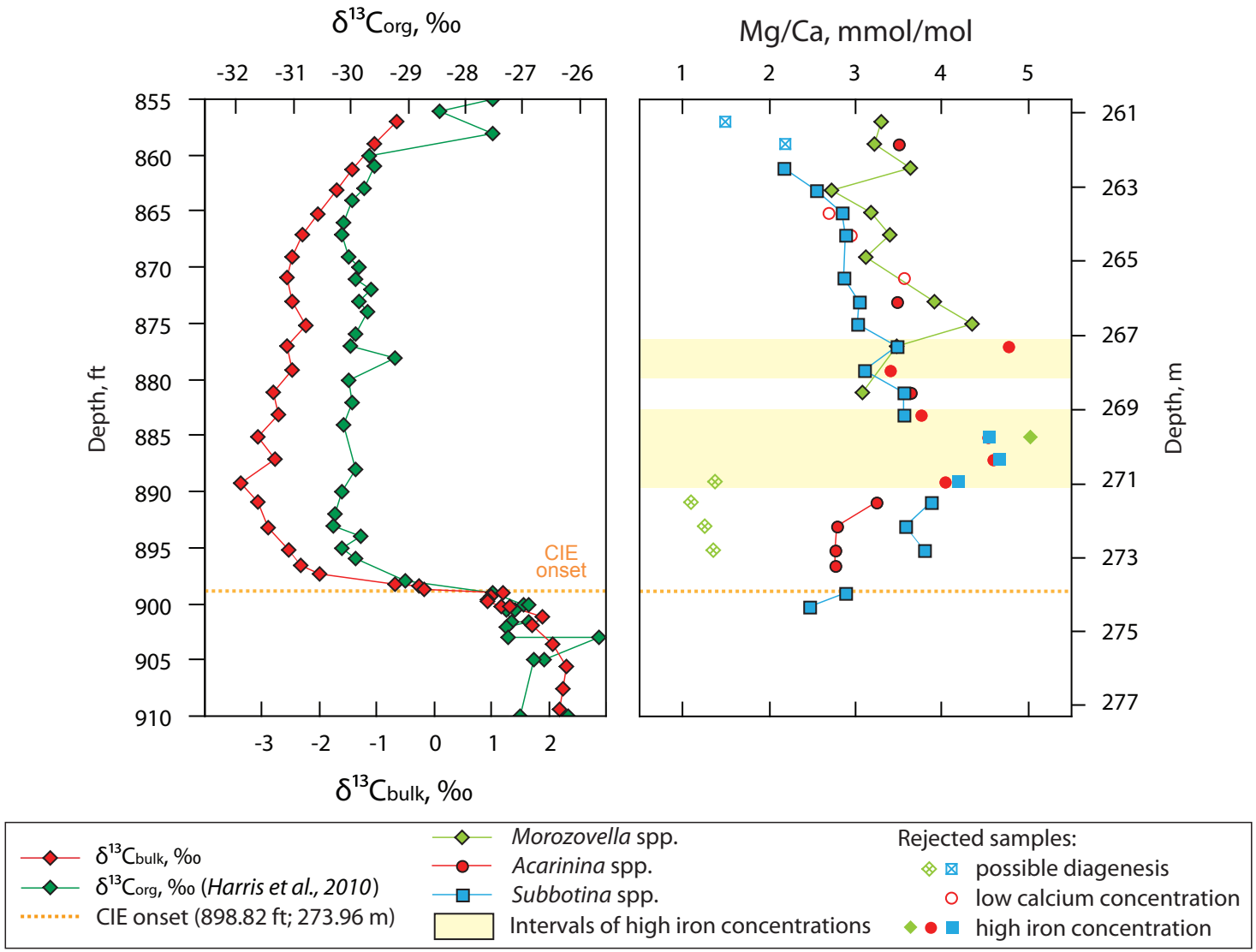
δ13Corg, ‰
-32 -31 -30 -29 -28 -27 -26
Mg/Ca, mmol/mol
1 2 3 4 5
Depth, ft
855 860 865 870 875 880 885 890 895 900 905 910
Depth, m
261 263 265 267 269 271 273 275 277
CIE onset
-3 -2 -1 0 1 2
δ13Cbulk, ‰
δ13Cbulk, ‰
δ13Corg, ‰ (Harris et al., 2010)
CIE onset (898.82 ft; 273.96 m)
Morozovella spp.
Acarinina spp.
Subbotina spp.
Intervals of high iron concentrations
Rejected samples:
possible diagenesis
low calcium concentration
high iron concentration

Figure 11

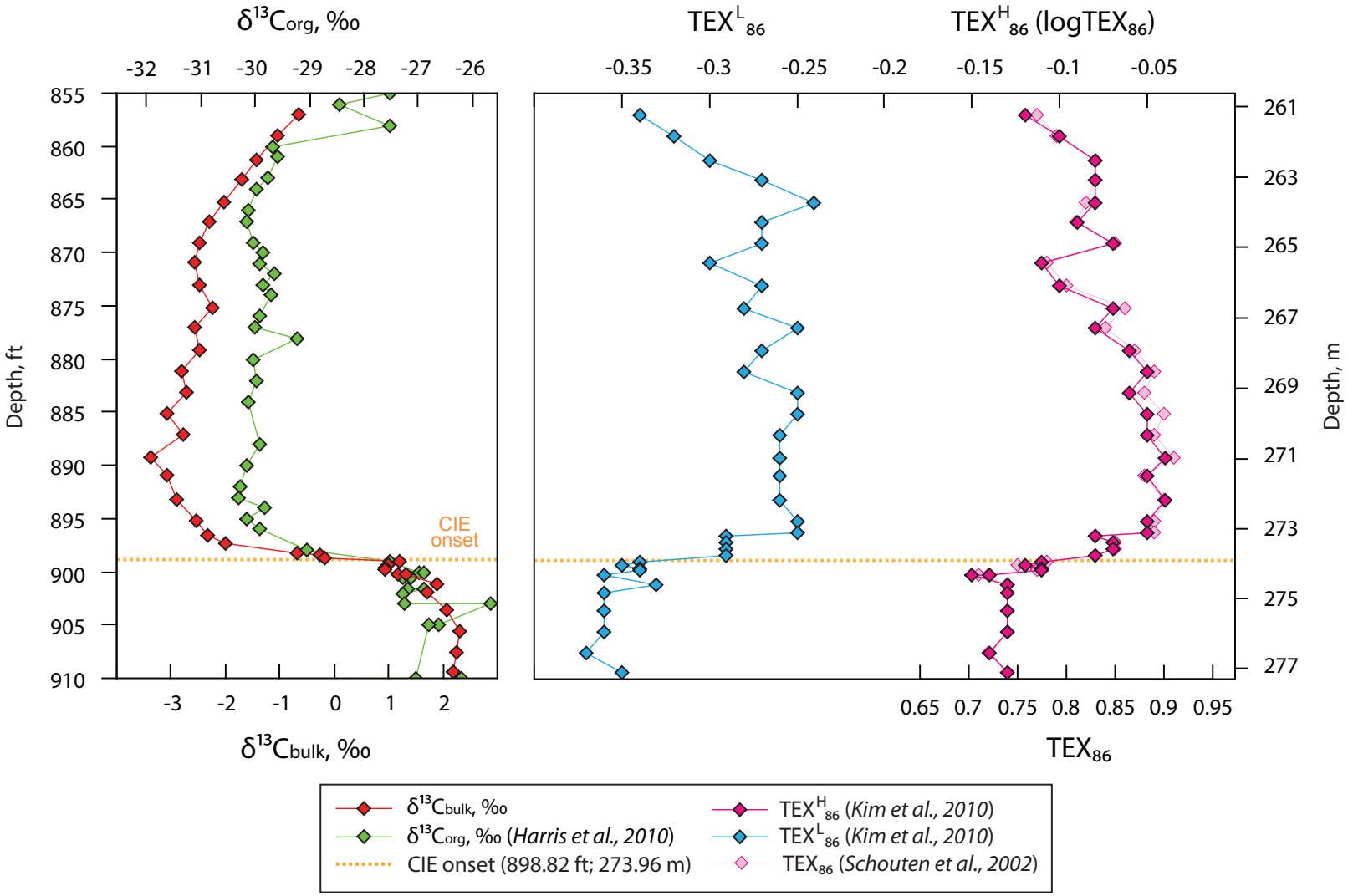
δ13Corg, ‰
-32 -31 -30 -29 -28 -27 -26
TEXL86
-0.35 -0.3 -0.25 -0.2 -0.15 -0.1 -0.05
TEXH86 (logTEX86)
Depth, ft
855 860 865 870 875 880 885 890 895 900 905 910
Depth, m
261 263 265 267 269 271 273 275 277
CIE onset
-3 -2 -1 0 1 2
δ13Cbulk, ‰
0.65 0.7 0.75 0.8 0.85 0.9 0.95
TEX86
δ13Cbulk, ‰
δ13Corg, ‰ (Harris et al., 2010)
CIE onset (898.82 ft; 273.96 m)
TEXH86 (Kim et al., 2010)
TEXL86 (Kim et al., 2010)
TEX86 (Schouten et al., 2002)

Figure 12

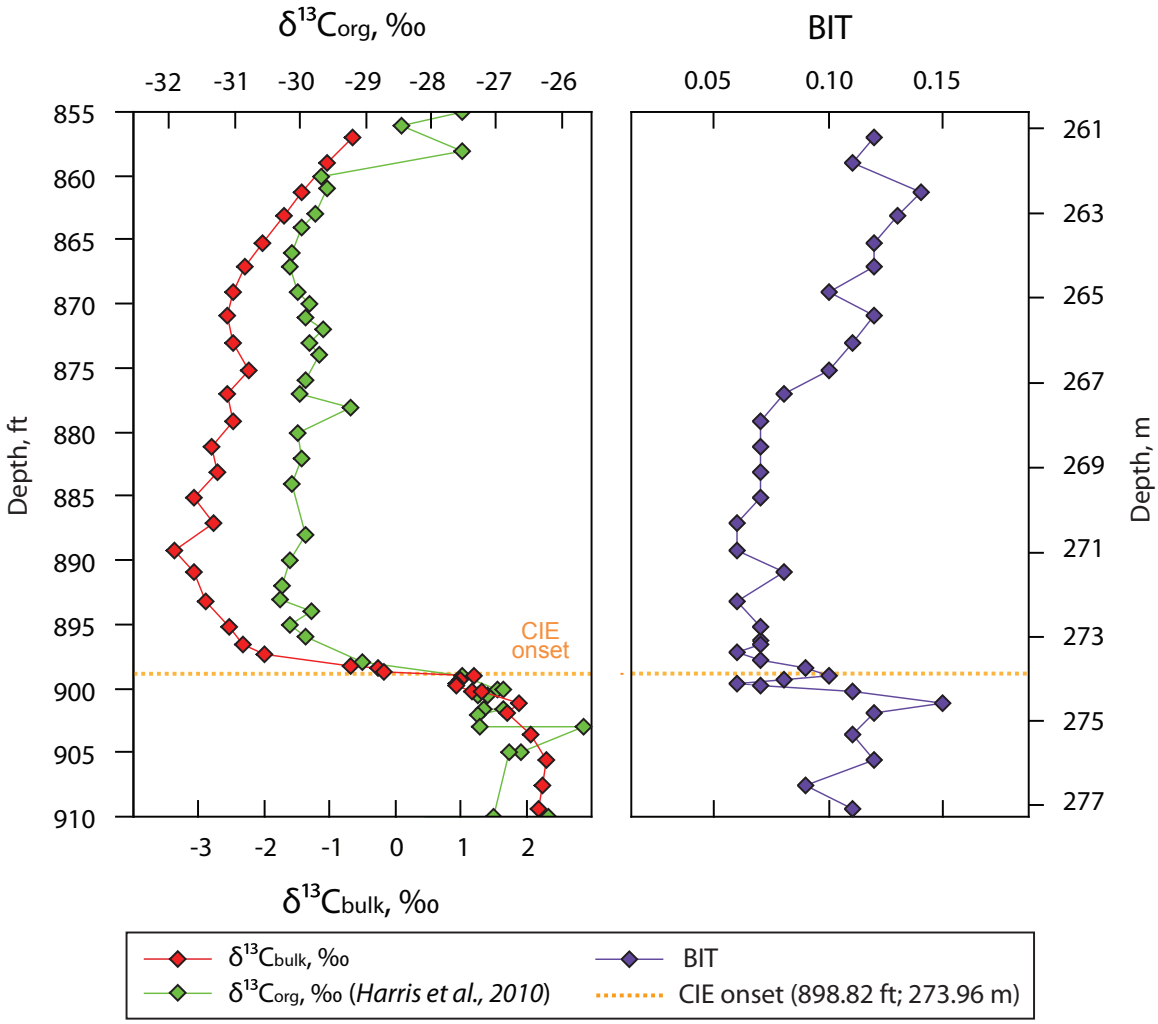
δ13Corg, ‰
-32 -31 -30 -29 -28 -27 -26
BIT
0.05 0.10 0.15
855 860 865 870 875 880 885 890 895 900 905 910
Depth, ft
261 263 265 267 269 271 273 275 277
Depth, m
CIE onset
-3 -2 -1 0 1 2
δ13Cbulk, ‰
δ13Cbulk, ‰
δ13Corg, ‰ (Harris et al., 2010)
BIT
CIE onset (898.82 ft; 273.96 m)

Figure 13

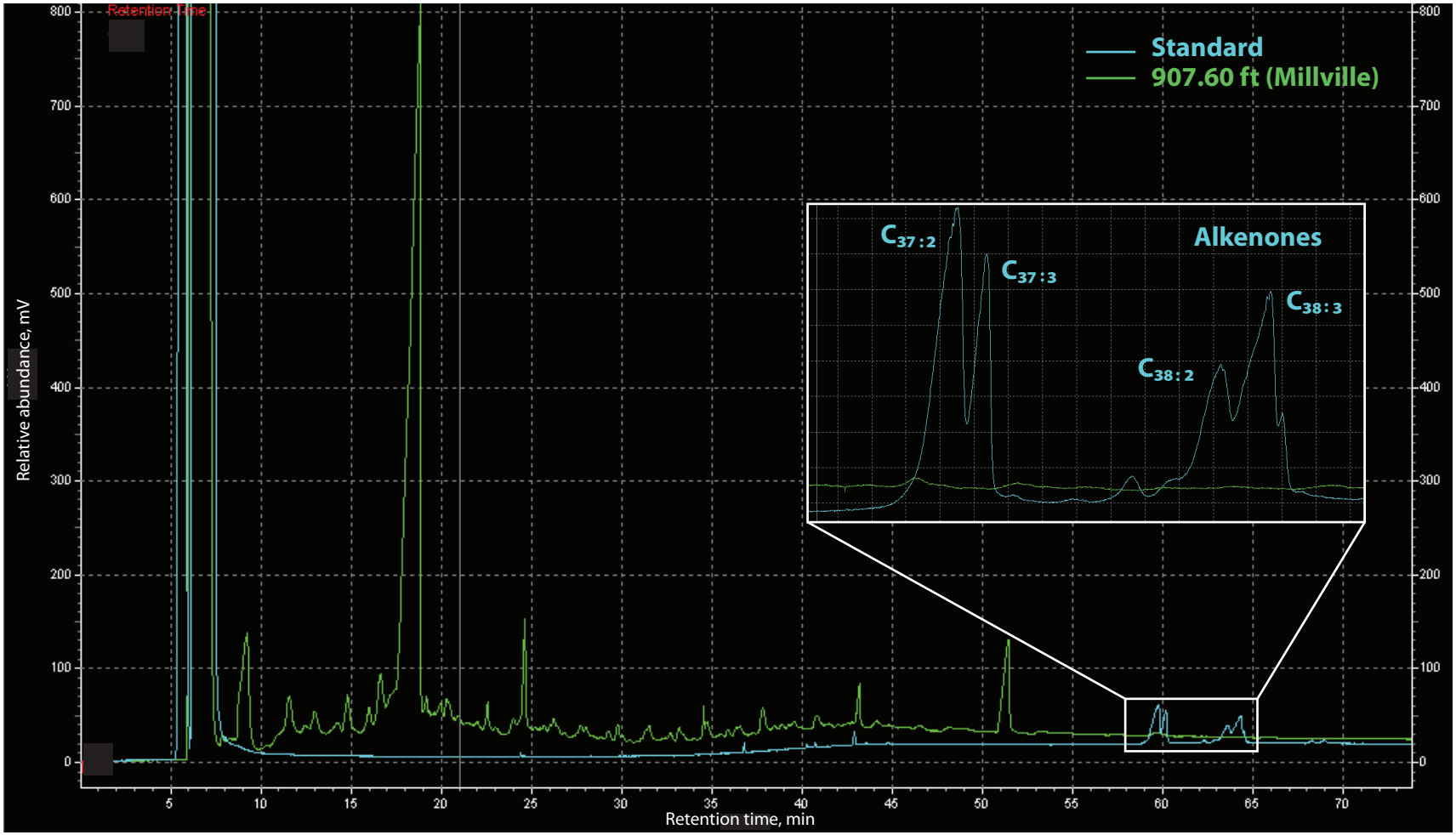
Standard
907.60 ft (Millville)
Alkenones
$C_{37:2}$
$C_{37:3}$
$C_{38:2}$
$C_{38:3}$
Relative abundance, mV
Retention time, min

Figure 14

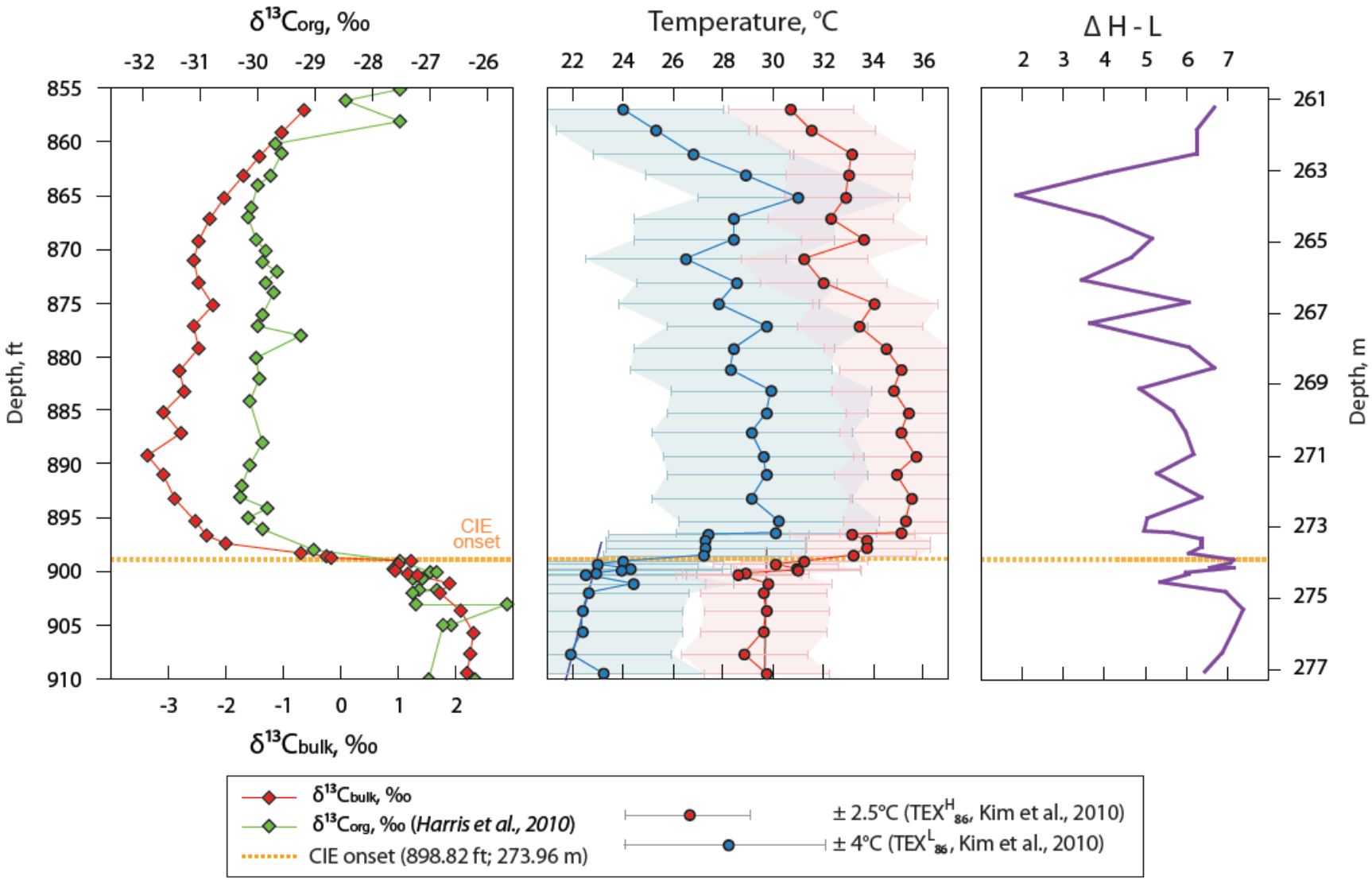
δ13Corg, ‰
-32 -31 -30 -29 -28 -27 -26
Temperature, °C
22 24 26 28 30 32 34 36
Δ H - L
2 3 4 5 6 7
Depth, ft
855 860 865 870 875 880 885 890 895 900 905 910
Depth, m
261 263 265 267 269 271 273 275 277
CIE onset
-3 -2 -1 0 1 2
δ13Cbulk, ‰
δ13Cbulk, ‰
δ13Corg, ‰ (Harris et al., 2010)
CIE onset (898.82 ft; 273.96 m)
± 2.5°C (TEXH86, Kim et al., 2010)
± 4°C (TEXL86, Kim et al., 2010)

Figure 15

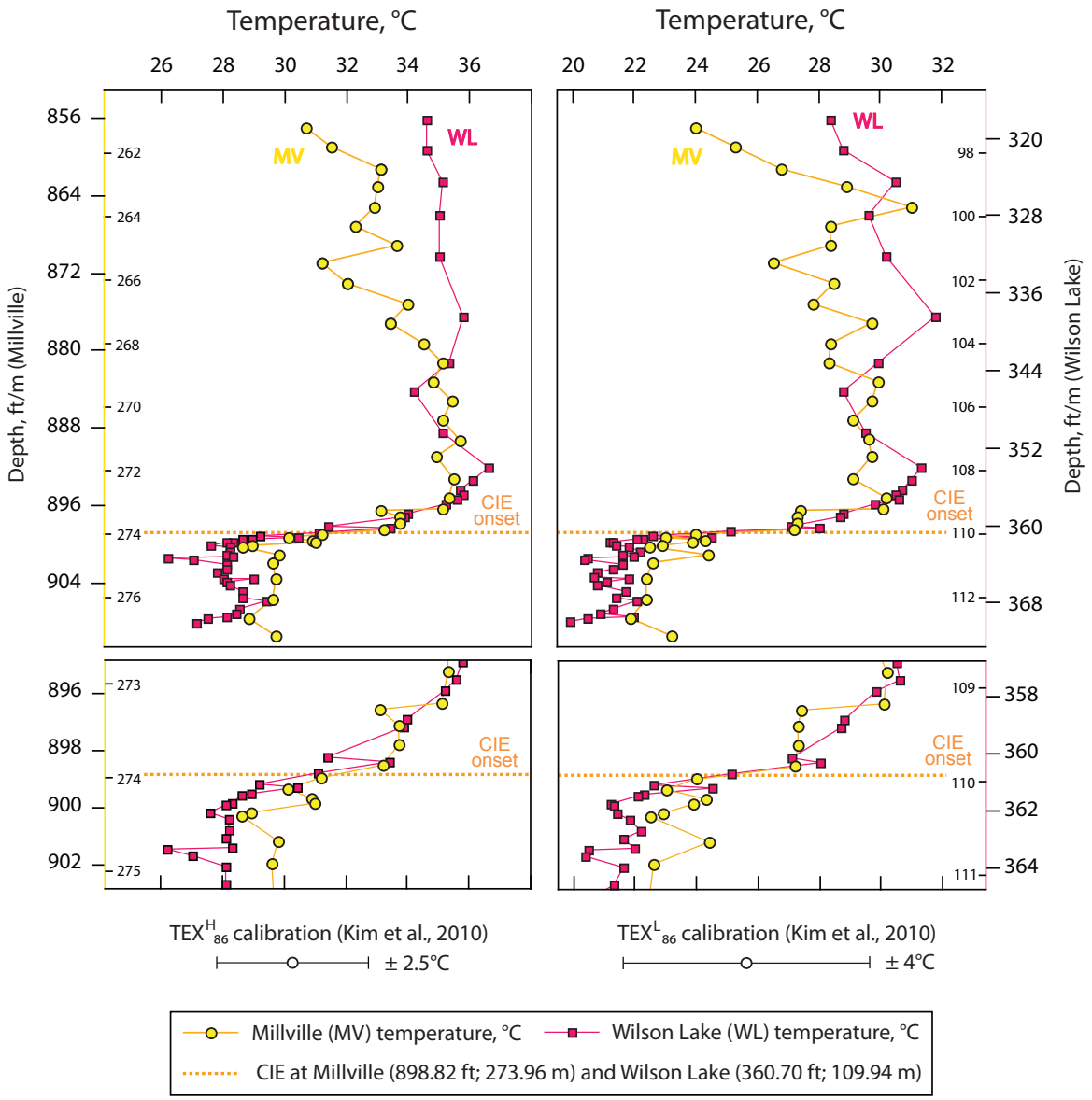
Temperature, °C
Temperature, °C
MV
WL
CIE onset
Depth, ft/m (Millville)
Depth, ft/m (Wilson Lake)
TEX$^{H}_{86}$ calibration (Kim et al., 2010)
± 2.5°C
TEX$^{L}_{86}$ calibration (Kim et al., 2010)
± 4°C
Millville (MV) temperature, °C
Wilson Lake (WL) temperature, °C
CIE at Millville (898.82 ft; 273.96 m) and Wilson Lake (360.70 ft; 109.94 m)

Figure 16

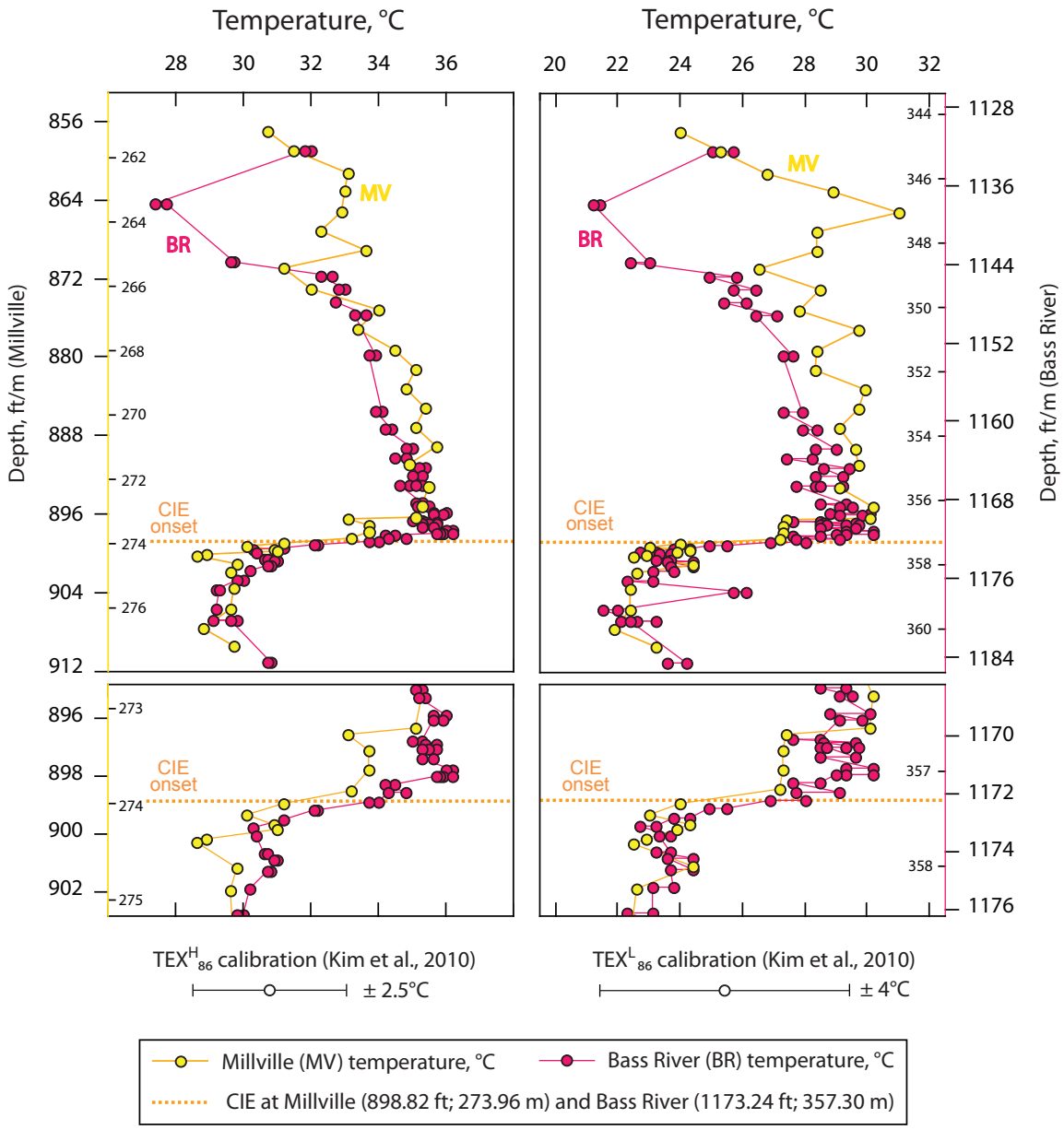
Temperature, °C
28
30
32
34
36
Temperature, °C
20
22
24
26
28
30
32
Depth, ft/m (Millville)
856
864
872
880
888
896
904
912
262
264
266
268
270
272
274
276
MV
BR
CIE onset
896
898
900
902
273
274
275
CIE onset
Depth, ft/m (Bass River)
1128
1136
1144
1152
1160
1168
1176
1184
344
346
348
350
352
354
356
358
360
MV
BR
CIE onset
1170
1172
1174
1176
357
358
CIE onset
TEX$^{H}_{86}$ calibration (Kim et al., 2010)
± 2.5°C
TEX$^{L}_{86}$ calibration (Kim et al., 2010)
± 4°C
Millville (MV) temperature, °C
Bass River (BR) temperature, °C
CIE at Millville (898.82 ft; 273.96 m) and Bass River (1173.24 ft; 357.30 m)

Figure 17

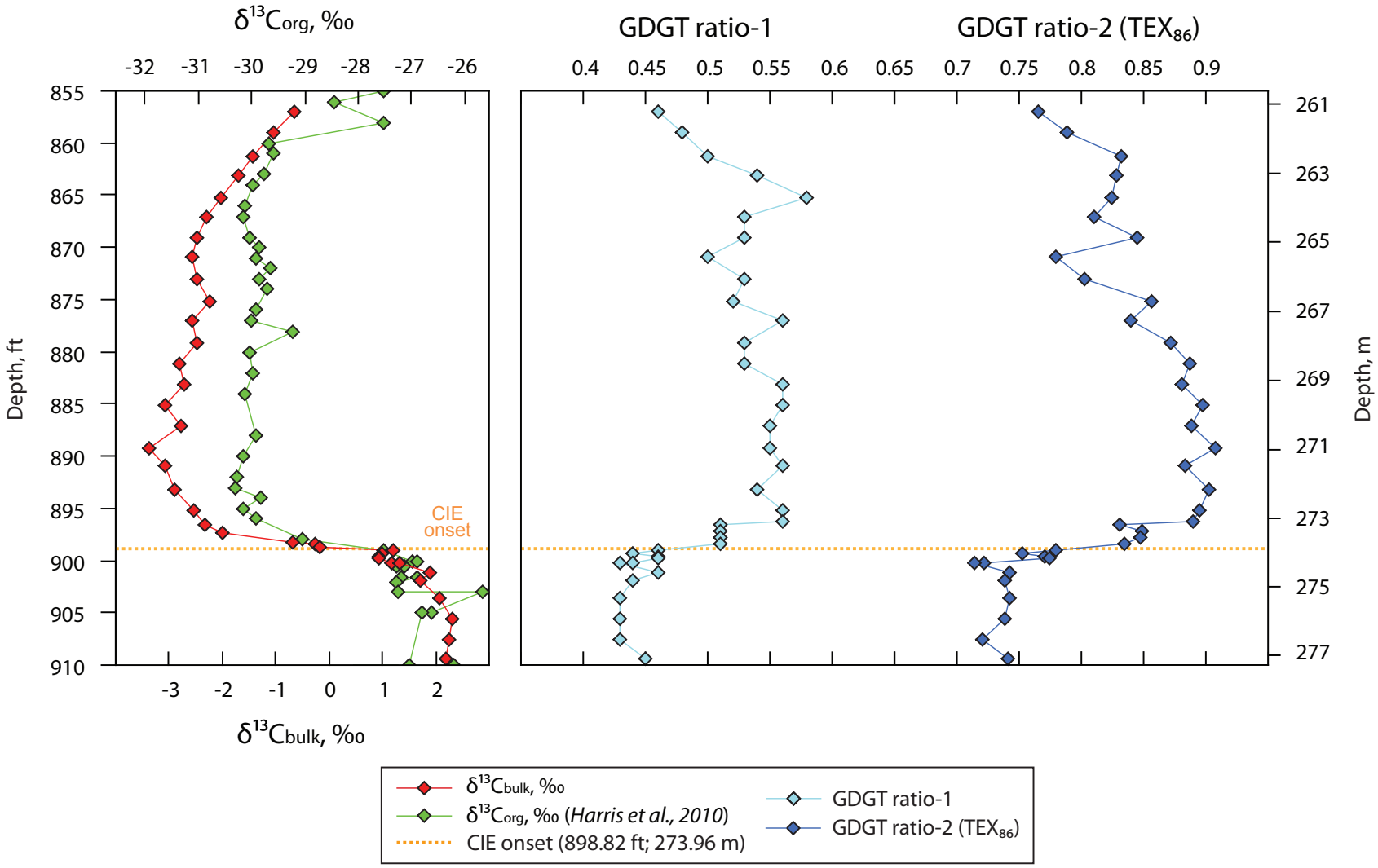
δ13Corg, ‰
-32 -31 -30 -29 -28 -27 -26
GDGT ratio-1
0.4 0.45 0.5 0.55 0.6 0.65 0.7
GDGT ratio-2 (TEX86)
0.75 0.8 0.85 0.9
Depth, ft
855 860 865 870 875 880 885 890 895 900 905 910
Depth, m
261 263 265 267 269 271 273 275 277
CIE onset
-3 -2 -1 0 1 2
δ13Cbulk, ‰
δ13Cbulk, ‰
δ13Corg, ‰ (Harris et al., 2010)
CIE onset (898.82 ft; 273.96 m)
GDGT ratio-1
GDGT ratio-2 (TEX86)

Figure 18

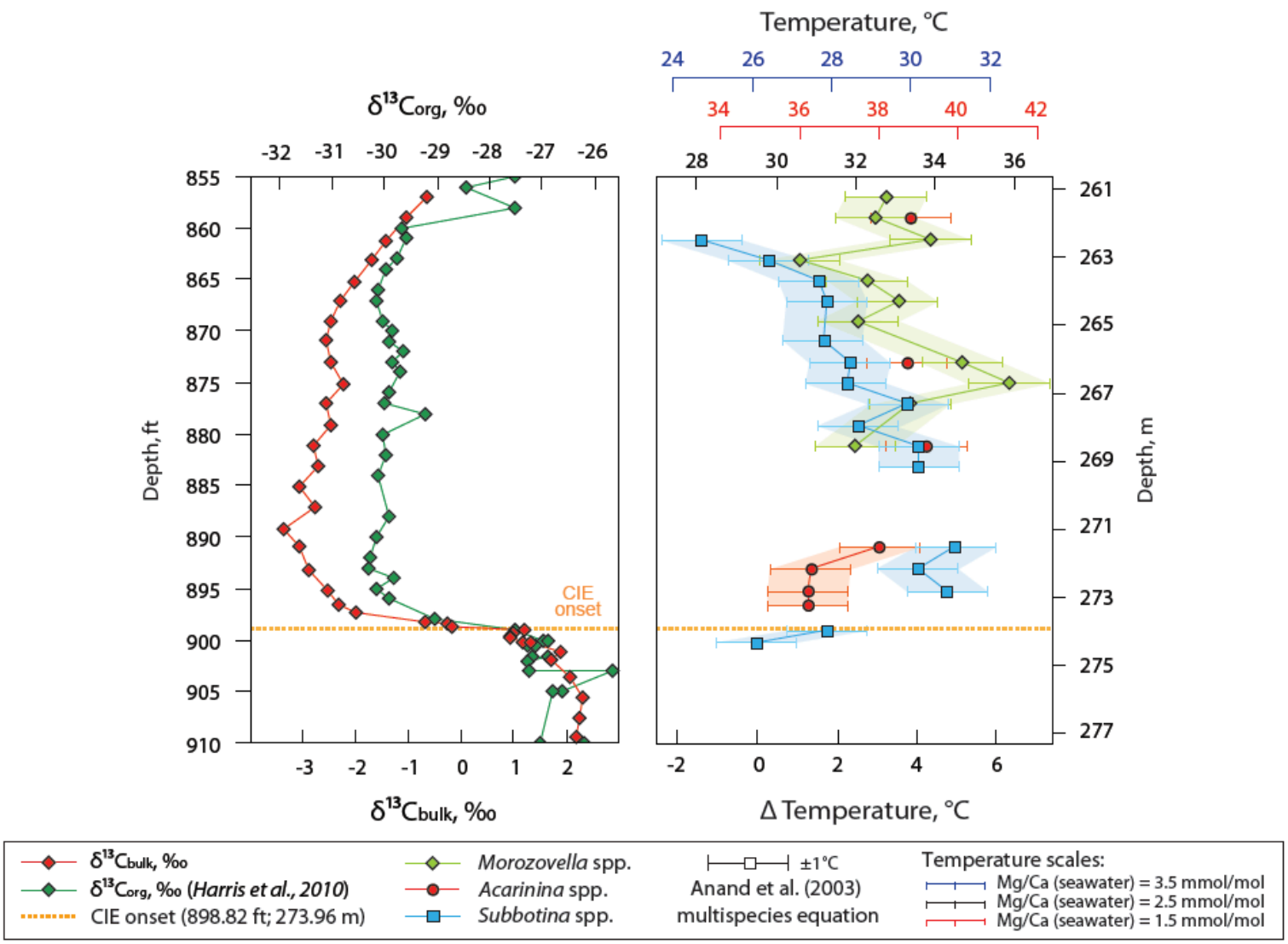
Temperature, °C
24 26 28 30 32
34 36 38 40 42
δ13Corg, ‰
-32 -31 -30 -29 -28 -27 -26
28 30 32 34 36
855 860 865 870 875 880 885 890 895 900 905 910
Depth, ft
CIE onset
261 263 265 267 269 271 273 275 277
Depth, m
-3 -2 -1 0 1 2
δ13Cbulk, ‰
-2 0 2 4 6
Δ Temperature, °C
δ13Cbulk, ‰
δ13Corg, ‰ (Harris et al., 2010)
CIE onset (898.82 ft; 273.96 m)
Morozovella spp.
Acarinina spp.
Subbotina spp.
±1°C
Anand et al. (2003)
multispecies equation
Temperature scales:
Mg/Ca (seawater) = 3.5 mmol/mol
Mg/Ca (seawater) = 2.5 mmol/mol
Mg/Ca (seawater) = 1.5 mmol/mol

Figure 19

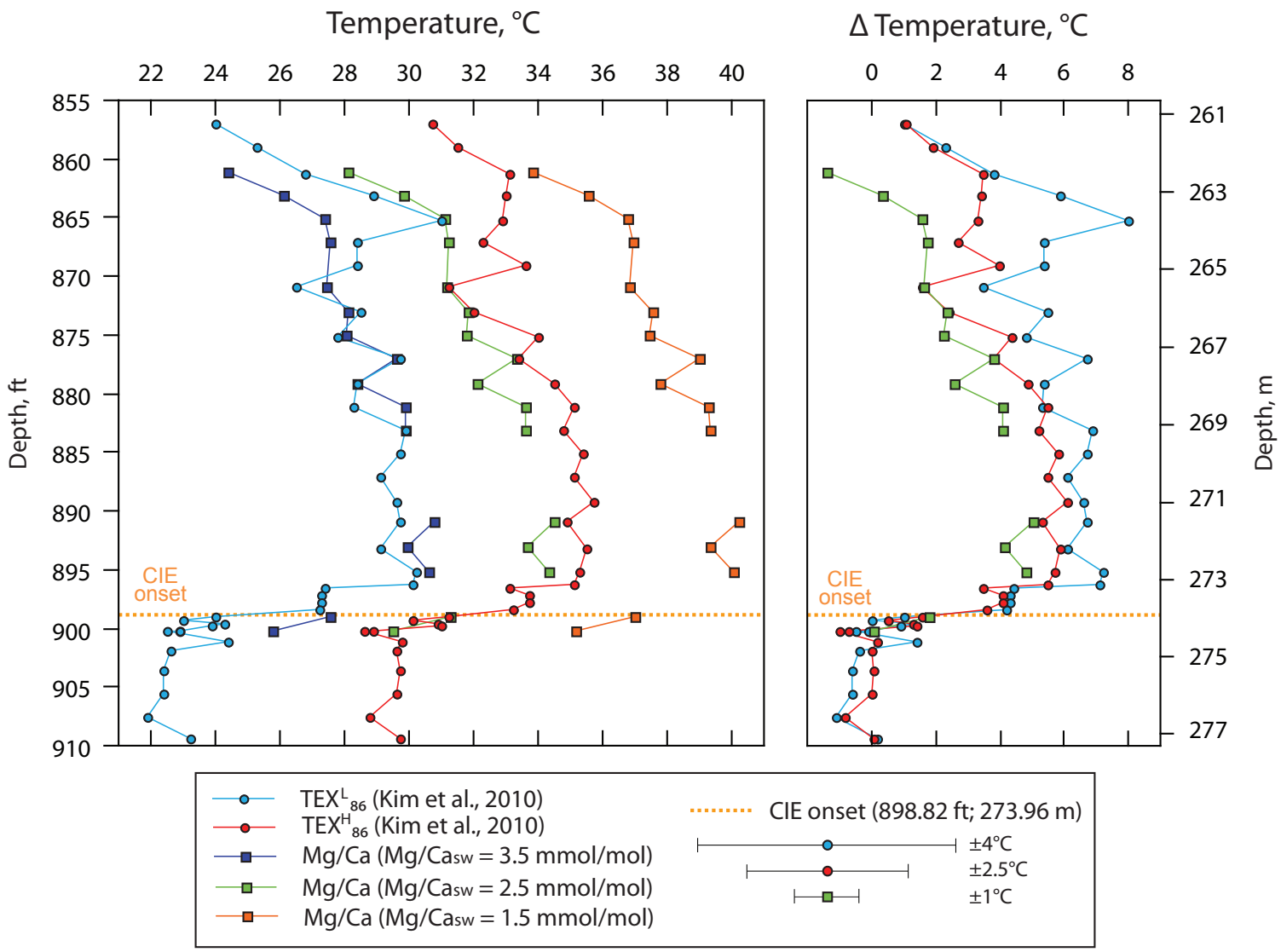
Temperature, °C
22
24
26
28
30
32
34
36
38
40
Δ Temperature, °C
0
2
4
6
8
Depth, ft
855
860
865
870
875
880
885
890
895
900
905
910
Depth, m
261
263
265
267
269
271
273
275
277
CIE onset
CIE onset
TEX$^{L}_{86}$ (Kim et al., 2010)
TEX$^{H}_{86}$ (Kim et al., 2010)
Mg/Ca (Mg/Casw = 3.5 mmol/mol)
Mg/Ca (Mg/Casw = 2.5 mmol/mol)
Mg/Ca (Mg/Casw = 1.5 mmol/mol)
CIE onset (898.82 ft; 273.96 m)
±4°C
±2.5°C
±1°C

Figure 20

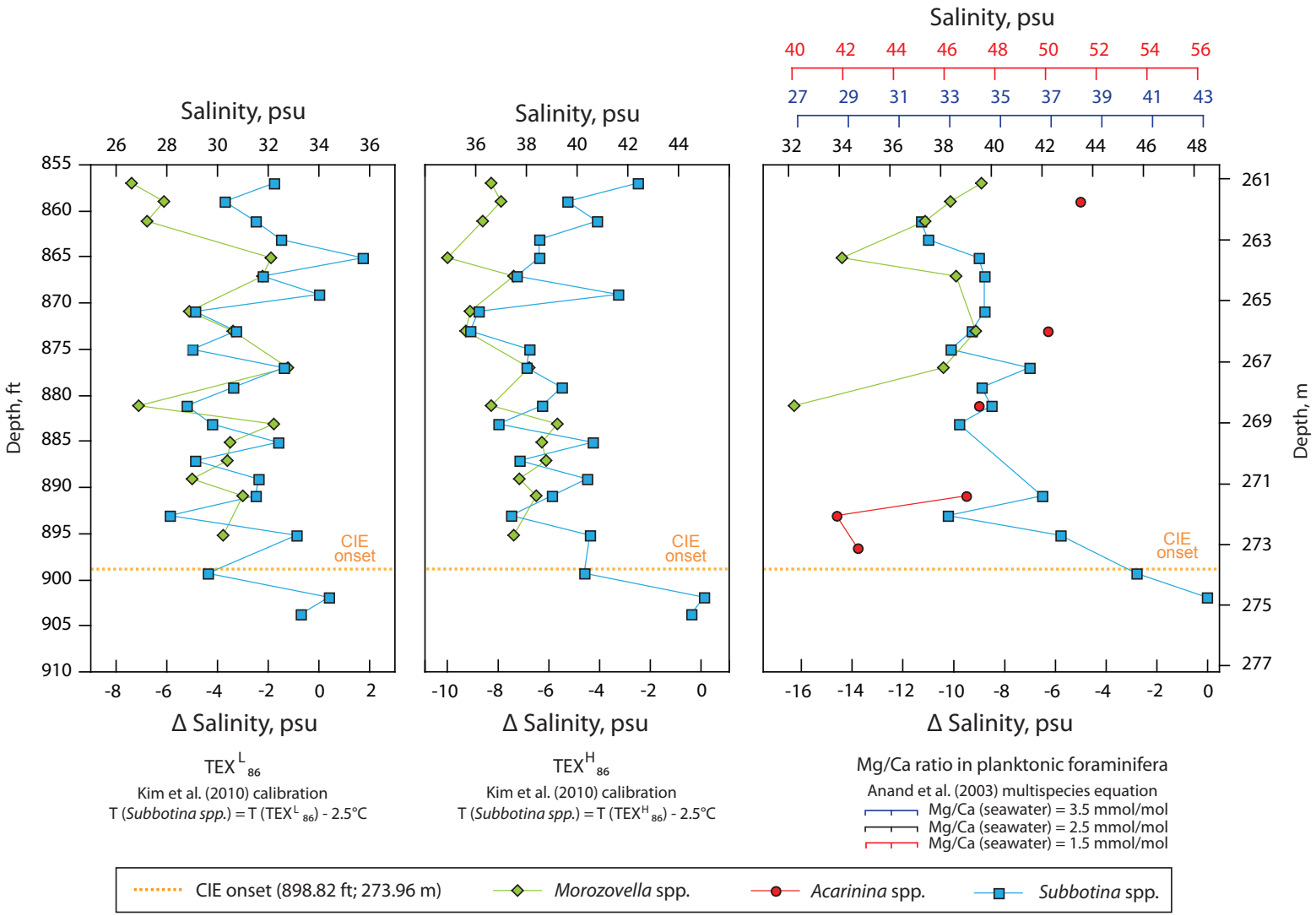
Salinity, psu
Depth, ft
Δ Salinity, psu
CIE onset
TEX L 86
Kim et al. (2010) calibration
T (Subbotina spp.) = T (TEX L 86) - 2.5°C
TEX H 86
Kim et al. (2010) calibration
T (Subbotina spp.) = T (TEX H 86) - 2.5°C
Mg/Ca ratio in planktonic foraminifera
Anand et al. (2003) multispecies equation
Mg/Ca (seawater) = 3.5 mmol/mol
Mg/Ca (seawater) = 2.5 mmol/mol
Mg/Ca (seawater) = 1.5 mmol/mol
Depth, m
CIE onset (898.82 ft; 273.96 m)
Morozovella spp.
Acarinina spp.
Subbotina spp.

Figure 21

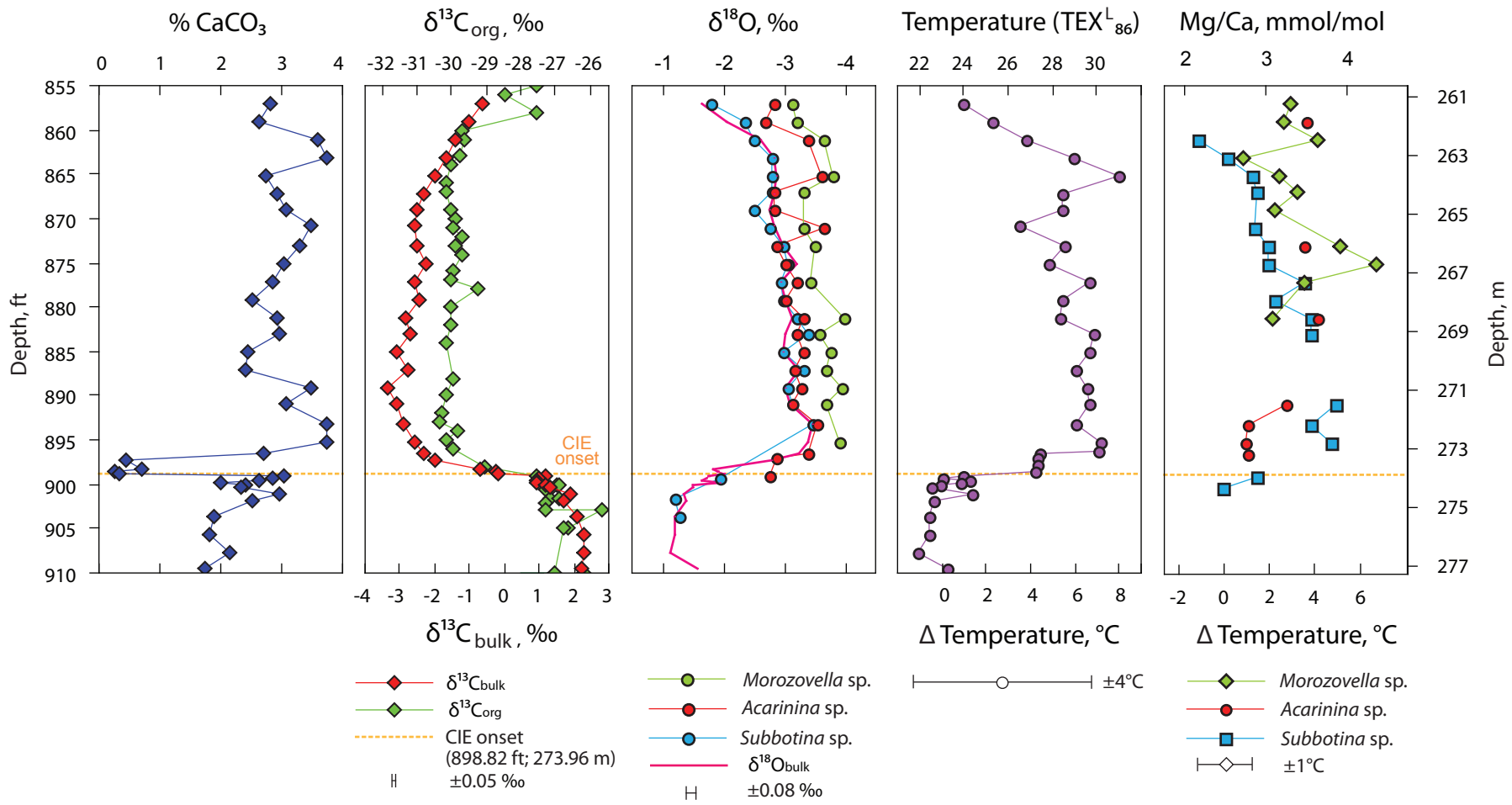
% CaCO3
δ13Corg, ‰
δ18O, ‰
Temperature (TEXL86)
Mg/Ca, mmol/mol
Depth, ft
Depth, m
CIE onset
δ13Cbulk, ‰
Δ Temperature, °C
Δ Temperature, °C
δ13Cbulk
δ13Corg
CIE onset
(898.82 ft; 273.96 m)
±0.05 ‰
Morozovella sp.
Acarinina sp.
Subbotina sp.
δ18Obulk
±0.08 ‰
±4°C
Morozovella sp.
Acarinina sp.
Subbotina sp.
±1°C

Figure 22

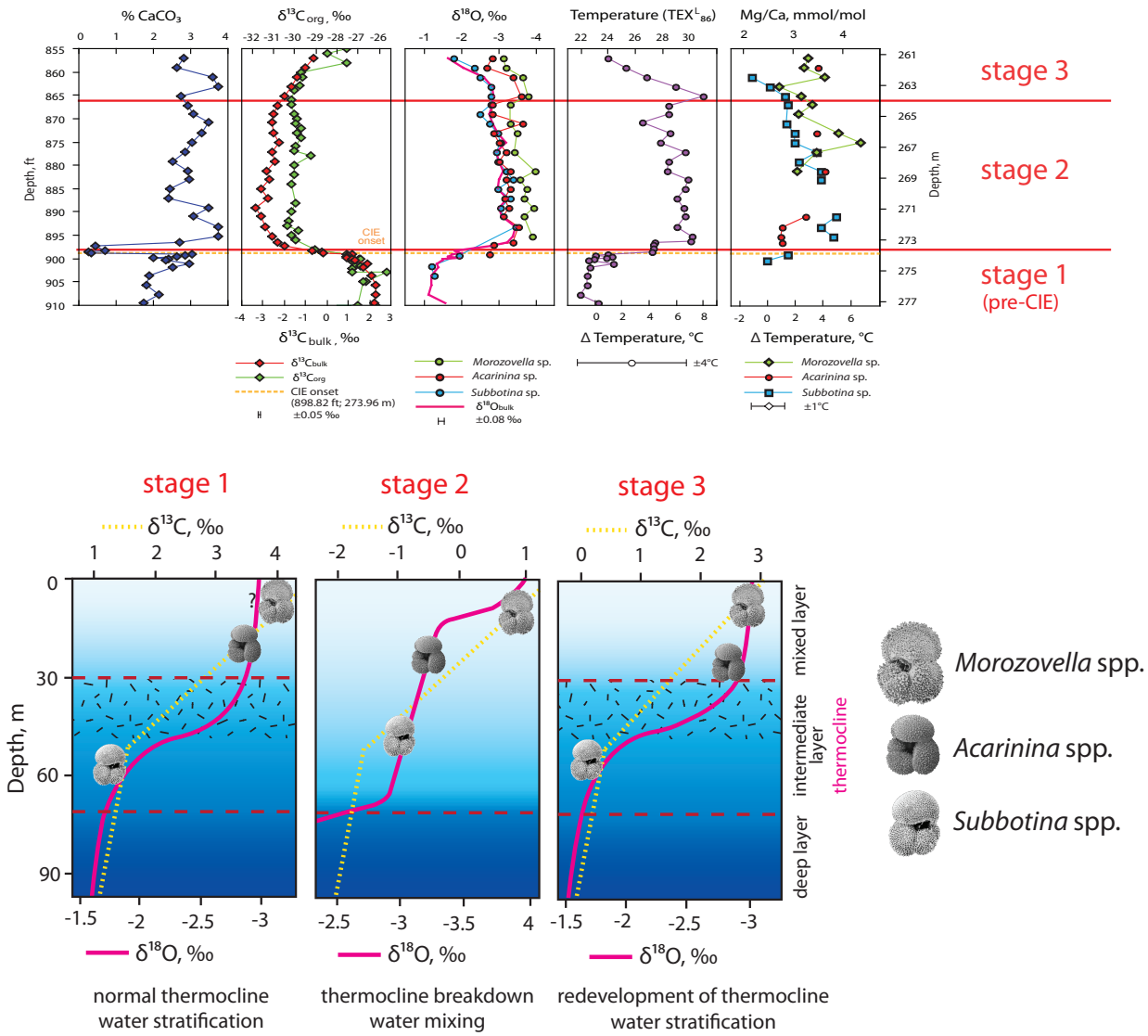
% CaCO3
δ13Corg, ‰
δ18O, ‰
Temperature (TEXL86)
Mg/Ca, mmol/mol
Depth, ft
Depth, m
stage 3
stage 2
stage 1
(pre-CIE)
CIE onset
δ13Cbulk, ‰
Δ Temperature, °C
δ13Cbulk
δ13Corg
CIE onset (898.82 ft; 273.96 m) ±0.05 ‰
Morozovella sp.
Acarinina sp.
Subbotina sp.
δ18Obulk ±0.08 ‰
±4°C
±1°C
stage 1
stage 2
stage 3
δ13C, ‰
Depth, m
mixed layer
intermediate layer
thermocline
deep layer
δ18O, ‰
normal thermocline water stratification
thermocline breakdown water mixing
redevelopment of thermocline water stratification
Morozovella spp.
Acarinina spp.
Subbotina spp.

Figure 23